

# **Some Studies of Growing Networks with Non-Linear Dynamical Elements**

**A THESIS**

**submitted for the Award of Ph.D degree of  
Mohan Lal Sukhadia University**

**in the  
Faculty of Science**

**BY  
Sarika Jalan**



**Under the Supervision of**

**Prof. R. E. Amritkar**

**THEORETICAL PHYSICS & COMPLEX SYSTEM DIVISION  
PHYSICAL RESEARCH LABORATORY, AHMEDABAD.**

**MOHANLAL SUKHADIA UNIVERSITY, UDAIPUR**

Year of submission: 2004

## CERTIFICATE

This is to certify that the thesis entitled "Some Studies of Growing Networks with Non-Linear Dynamical Elements" submitted for the award of the degree of Doctor of Philosophy of Mohanlal Sukhadia University in the faculty of Science is a record of bonafide investigations carried out by Miss. Sarika Jalan under my supervision and guidance.

This is an original piece of work on which no one has been awarded a degree in this University or in any other University.

The literary presentation of the thesis is satisfactory and it is in a form suitable for publication. The work presented in the thesis has been done after registration in this University.

Further, the candidate has put in attendance of more than 200 days in my institution as required under rule 7(b) and thus completed the residential requirement.

Prof. R. E. Amritkar  
(SUPERVISOR)

*to my mother ...*

# Contents

<b>Acknowledgement</b>	<b>vi</b>
<b>Abstract</b>	<b>viii</b>
<b>1 Introduction</b>	<b>1</b>
1.1 Motivation . . . . .	1
1.2 Key Ingredients . . . . .	3
1.2.1 Networks : <i>They are Everywhere</i> . . . . .	3
1.2.2 Synchronization of <i>Dynamical Elements</i> . . . . .	7
1.2.3 Nonlinearity and Chaos . . . . .	9
1.3 Chaotic Dynamics on Networks: Models to Study Different Phenomena . . . . .	13
1.3.1 Coupled Maps <i>Revisited</i> . . . . .	14
1.3.2 Coupled Maps on Networks . . . . .	15
1.4 Organization of the THESIS . . . . .	16
<b>2 Synchronized Clusters on Coupled Map Networks (CMNs)</b>	<b>17</b>
2.1 Introduction . . . . .	17
2.2 Model of a Coupled Map Network . . . . .	17
2.3 Phase Synchronization and Synchronized Clusters . . . . .	18
2.4 General Properties of Synchronized Dynamics . . . . .	19
2.4.1 Behavior of Individual Nodes . . . . .	19
2.4.2 Mechanism of Cluster Formation . . . . .	19
2.4.3 Self-organized and Driven Cluster Formation in a Tree Network . . . . .	20
2.4.4 States of Synchronized Dynamics . . . . .	21
2.5 Quantitative Measures for Self-organized and Driven Behaviour . . . . .	21
2.6 Summary . . . . .	22
<b>3 Numerical Analysis And Results</b>	<b>23</b>
3.1 Introduction . . . . .	23
3.2 Coupled Maps on Scale-free Network: A Case Study . . . . .	24

3.2.1	Linear Coupling . . . . .	24
3.2.2	Nonlinear Coupling . . . . .	32
3.2.3	Dependence on the Number of Connections . . . . .	33
3.3	Coupled Maps on Other Different Networks . . . . .	38
3.3.1	One-Dimensional Networks . . . . .	38
3.3.2	Small World Networks . . . . .	42
3.3.3	Cayely Trees . . . . .	43
3.3.4	Higher Dimensional Lattices . . . . .	44
3.3.5	Random Networks . . . . .	44
3.4	Examples of Self-organized and Driven Behavior . . . . .	46
3.5	Circle Map . . . . .	47
3.6	Summary . . . . .	48
<b>4</b>	<b>Temporal Dynamics and Synchronization in CMNs: Stability Analysis</b>	<b>50</b>
4.1	Introduction . . . . .	50
4.1.1	Linear Stability Analysis . . . . .	51
4.1.2	Global Stability Analysis . . . . .	51
4.2	Stability Analysis for Self-organized Synchronization . . . . .	52
4.2.1	Coupled Network with $N = 2$ . . . . .	52
4.2.2	Globally Coupled Networks . . . . .	57
4.2.3	Lyapunov Function Analysis . . . . .	59
4.3	Stability Analysis for Driven Synchronization . . . . .	61
4.3.1	Coupled Networks with $N = 3$ . . . . .	61
4.3.2	Complete Bipartite Coupled Networks . . . . .	70
4.3.3	Lyapunov Function Analysis . . . . .	74
4.4	Self-organized and Driven Synchronization . . . . .	75
4.5	Coupled Maps on Multipartite Networks . . . . .	75
4.5.1	Model . . . . .	76
4.5.2	Linear Stability Analysis . . . . .	76
4.6	Floating nodes . . . . .	79
4.7	Summary . . . . .	80
<b>5</b>	<b>Conclusions and Future Outlook</b>	<b>82</b>
	<b>Appendix</b>	<b>84</b>
	<b>References</b>	<b>85</b>
	<b>List of Publications</b>	<b>98</b>

## Acknowledgement

*It gives me great pleasure to express my gratitude to Prof. R. E. Amritkar for his excellent guidance and valuable suggestions. I have benefited immensely from his sound intuition and deep insight in the subject. I will always be indebted to him for what I have learned from him in these five years.*

*I acknowledge Prof. C. K. Hu for his useful comments. My sincere thanks to Profs. V. B. Sheorey, J. Parikh, Dilip Angom for their suggestions and encouragements at various stages. Special thanks to Dr. Arul, for exploring the excitement of the subject to me, in my first year of joining CSCPN (now ThPhCS) division. My sincere thanks are due to academic committee for critically reviewing my work at various stages.*

*I thank all the staff members of PRL for their kind corporation at all stages. I specially acknowledge computer center staff, particularly Dholakia ji, for providing excellent computers facilities and library staff for maintaining excellent on-line journal facilities.*

*I take this opportunity to thank my class 10th Physics teacher Vanshraj Verma, who gave me the first direction towards my carrier in science.*

*It is my pleasure to acknowledge all the NLD members 'Sagar, Sankar, Jayendra, Murali, newly joined Parimal,' and other 7th floor seniors/ colleagues Sudhir, Rishi, Pattu, Sunish, Arun, Hyderabad gang (Charan, Atre), for always making lab atmosphere very lively and supportive to me. I thank to Sankar for his help during my programming and computational difficulties. My special acknowledgment to Jayendra, both of us got immensely benefited from the discussions on the subject. I will always cherish our company of more than five+1/2 years, form the first day to the last day at PRL.*

*I was fortunate to get very supportive atmosphere of PRL hostel form the beginning, I thank my all seniors for showering their affections on me, just to name a few Ratan, Kunu, Vinai, Alok, Ann and Soumen da. I also acknowledge here all my affectionate juniors. I acknowledge my hardworking and simple batchmats Jayendra, Lokesh from Raipur, Tarak from Berdhaman, Sanjay from UK(C) and Satraj from Malluland, I can not forget all the enjoyable and comfort moments shared with*

*them starting from the very first day of joining PRL.*

*Without mentioning Volley, TT and occasionally Cricket, my acknowledgment remains incomplete. I specially acknowledge all the PRL's TT players (champions !) with whom I enjoyed playing TT. These sports have always given me new energy whenever I felt tired.*

*Finally I acknowledge my parents and my Bhaiya for their unconditional love and constant support. The journey to this thesis would have not been possible without my mother's supports and constant interests in my studies. I thank to my all Chachee's and my dear Bhabhi for their love and care for me. I owe a lot to my little niece, for giving me a great happiness in the mid of this thesis writing.*

**Sarika Jalan**

## Abstract

We study the synchronization of the coupled dynamics on a variety of networks including one-d, 2-d and higher dimensional networks, small world networks, scale-free networks, random networks, tree networks, globally coupled networks, bipartite networks and multipartite networks. The dynamics is governed by a local nonlinear map for each node of the network and interaction connecting nodes via the links of the network.

Chapter 2 of my thesis introduces our model for the coupled dynamics on the networks. We define different states of coupled dynamics by considering the number and type of synchronized clusters, and also formulate a quantitative measure for synchronization.

In chapter 3 we study the *phase synchronization* of the coupled maps on the various networks. We define phase synchronization as follows; two nodes  $i$  and  $j$  are phase synchronized if all the local minima (maxima) in the time series of the dynamical variable at node  $i$ , match with that of the node  $j$ . In a phase synchronized cluster, all the pairs of the nodes are phase synchronized. We find that, for small coupling strengths nodes show turbulent behaviour but form phase synchronized clusters as coupling strength increases. We identify two different ways of cluster formation, namely *self-organized synchronization* which leads to clusters with dominant intra-cluster couplings and *driven synchronization* which leads to clusters with dominant inter-cluster couplings. We also observe ideal clusters of both self-organized and driven type. In the novel driven synchronization the nodes of one cluster are driven by those of others. Most of the time when synchronized clusters are formed, they are accompanied with the isolated nodes. Some of these nodes are of the *floating types* which show intermittent behaviour between getting attached to some clusters and evolving independently. The residence time of a floating node in a synchronized cluster shows an exponential distribution. Numerical calculations of the largest Lyapunov exponent ( $\lambda_l$ ) for coupled dynamics on the various networks show that mostly whenever ideal clusters are formed  $\lambda_l$  is negative. But for some cases, ideal clusters are formed with the positive

$\lambda_i$ .

For the local dynamics governed by the *logistic map* we study phase diagram in the plane of the coupling constant ( $\epsilon$ ) and the logistic map parameter ( $\mu$ ). For large coupling strengths and nonlinear coupling we find that the scale free networks and the Cayley tree networks lead to the better cluster formation than the other types of networks with the *same average connectivity*. For most of the our studies carried in the chapter 3, we use number of connections of the order of the number of nodes, which allows us to distinguish between the two mechanisms of cluster formation. As the number of connections increases both the number of nodes forming clusters and the size of the clusters in general increase.

Chapter 4 presents the analytical results and understandings for self-organized and driven synchronization. For the analytical studies in this chapter, we take exact synchronization. We use linear stability analysis and Lyapunov function approach to determine the stability conditions for various synchronized and periodic states in the coupled dynamics on small networks, viz. two and three nodes, and their extension to the larger networks. As an example of large networks, showing both self-organized and driven synchronized clusters, we take complete bipartite networks. The phase diagrams for the the networks studied in this chapter have features very similar to the different kinds of random networks studied in the chapter 3. Lyapunov function analysis gives the hint for the origin of the two mechanisms of synchronization.

## Chapter 1

# Introduction

---

---

### 1.1 Motivation

Complex systems have underlying structures that are described by networks or graphs. The study of such networks is emerging as one of the fastest growing subject in the physics world [1, 2]. In the past few years we have witnessed considerable advances in this direction, prompted by several parallel developments. First, the computerization of data acquisition in all fields led to the emergence of large database on the topology of various networks, second, the increased computing power allowed to investigate networks containing millions of nodes and finally, instead of considering individual element of a system there is an increasingly voiced need to understand the behaviour of the system as a whole [3]. One significant discovery in the field of the complex networks is the observation that a number of naturally occurring large and complex networks, from many diverse fields, have some similar underlying features bringing them in universal classes of small-world [5] and scale free [4] networks. Recently Barabási et. al and Strogatz et. al have provided simple algorithms to generate these networks representing the natural systems. Since their introduction, small world networks and scale free networks have received tremendous attention [6, 7, 8, 9, 10, 11, 12, 13, 14, 15, 16, 17].

Several real networks (networks representing the natural systems) consist of dynamical elements interacting with each other. The behaviour of an isolated dynamical system in the long term limit could be described by stable fixed points, limit cycles or chaotic attractor, but when many of such dynamical systems are coupled together, the details matter. Now we address a question that, how an enormous network of interacting dynamical systems will behave collectively, given their individual dynamics and coupling architecture. One of

the most fascinating phenomena observed in the behaviour of complex dynamical systems made up of many elements, is the spontaneous emergence of order and the phenomenon of collective synchronization, where a large number of the system's constituents form a common dynamical pattern, despite the intrinsic differences in their individual dynamics [18, 19, 21, 80]. This observation of patterns helps us in understanding the behaviour of the system and provides the motivation for the present thesis work. To resemble the natural situation, chaotic elements can be taken as evolving units at individual nodes which are coupled via the links of the network.

There is extensive research on coupled maps/oscillators on *one*-d lattices and globally coupled lattices [22, 23], but studies of coupled dynamics on the different random networks have just begin. Coupled maps on networks provide us a computationally simple model which displays several phenomena of scientific and technological interest relevant for such systems, such as synchronization, spatio-temporal intermittency and chaos, and periodic behaviour. Apart from it coupled maps on different networks deal with many other issues, namely whether dynamical systems coupled in the small-world and/or scale free networks would display enhanced signal propagation speed, synchronizability and computational power, as compared with lattices of the same size; how topology of a network affects the dynamics of nodes forming the network, how dynamical behaviour of a single node which is a part of a large network, gets affected by the dynamics of other nodes in the networks, both that are directly connected and that are not directly connected.

In my thesis I study the synchronization and cluster formation properties of coupled maps connected via the links of the various networks. Local dynamics being in the chaotic regime, for small coupling strengths nodes show turbulent behaviour, but form synchronized clusters as coupling strength increases. The most important finding of our investigations is that, starting from random initial conditions the asymptotic behaviours of coupled map networks (CMNs) reveal two different ways of clusters formation. First there are clusters with dominant intra-cluster couplings which are referred as *self-organized* synchronization and secondly there are clusters with dominant inter-cluster coupling which are referred as *driven* synchronization. In order to understand the relation between synchronized dynamics and topology of the underlying network, for most of the our studies we take networks with small average connectivity.

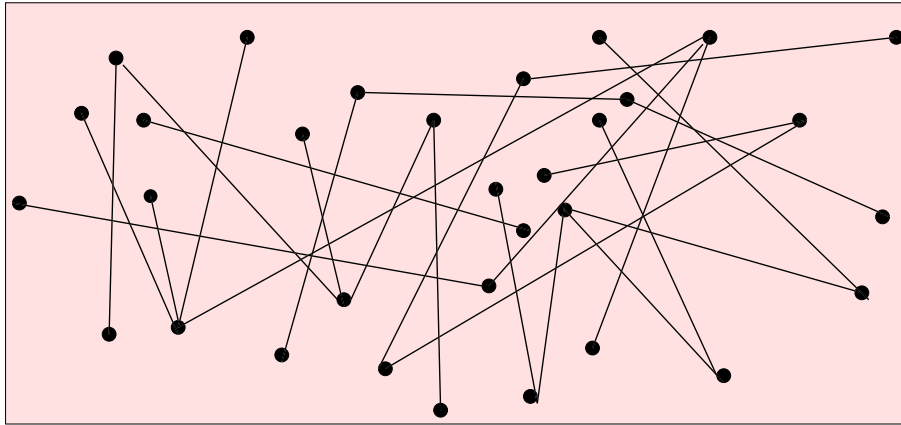


**Figure 1.1:** Figure shows a random networks (graph). Solid dots denote nodes (vertices) and solid lines denote the connection (edges) between the nodes

## 1.2 Key Ingredients

In this section I introduce and explain important key concepts used in my thesis, namely complex networks, synchronization and chaos.

### 1.2.1 Networks : *They are Everywhere*

Complex networks describe a wide range of systems, starting from biology to social sciences [1]. Some natural, scientific and technological systems where network properties are important, are given in the Table 1.1.

Mathematically networks are described in terms of graphs [24]. A graph (or network) is a pair of sets,  $G = P, E$  where  $P$  is a nonempty set of  $N$  vertices (nodes)  $p_1, p_2, \dots, p_N$  and  $E$  is a set of edges (couplings) that connect two elements of  $P$ . Following we introduce some basic tools of characterization of networks.

*Nodes degree and degree distribution* : The number of edges incident at the nodes is called the degree. Degree distribution  $P(k)$ , is the probability that a randomly selected node has exactly  $k$  edges.

*Connected graphs* : A Graph  $G$  is said to be connected if there is at least one path (edges connecting a pair) between every pair of vertices in  $G$ . Otherwise,  $G$  is disconnected. Size of a graph is the number of vertices in the graph.

*Node-Node distance* : The distance between two nodes is defined as the number of edges between two nodes. For lattices average shortest distance,  $l$  is of the order of number of

Table 1.1: Examples of some networks representing natural systems

	EXAMPLES	NODES	EDGES	REF.
1	crystal	atoms	bonds	[25]
2	electrical circuit	points	resistances, capacitors	[26]
3	polymer	atoms	bonds	[27]
4	percolation	sites	bonds	[28]
5	neural network	neurons	axons	[29]
6	cellular network	chemicals	reactions	[30]
7	protein folding	conformations	differ by one fold	[31]
8	food webs	species	predator-pray	[32]
9	power grid	generators / transformers	high voltage links	[33]
10	citation network	papers	citations	[34]
11	co-authorship net.	authors	co-authors	[35]
12	world-wide-web	web pages	hyperlinks	[36]
13	internet network	computers	physical/wireless links	[12]
14	social network	people	social relationship	[37]
15	election network	candidates	votes	[38]
16	actor network	actors	acted in same movie	[39]
17	disease network	people	contact with infected person	[40]
18	phone call network	phone no.	completed calls	[41]
19	linguistic network	words	synonyms	[42]
20	railway network	stations	rail lines	[43]
21	airport network	airports	flights	[44]

nodes in the graph,  $l \sim N$ . The diameter of a graph is the maximal distance between any pair of its nodes.

*Clustering coefficient* : Complex systems exhibit clustering, and tendency of a network to cluster is quantified by the clustering coefficients. Consider any node  $i$  with  $k_i$  edges connecting  $i$  to  $k_i$  other nodes. If any of these  $k_i$  nodes are connected to each other then, triangles are formed. If  $E_i$  is the number of edges between the  $k_i$  nodes, then the ratio of number of actual triangles to the maximum possible number is given as the clustering coefficient  $C_i$  and average clustering coefficient  $C = \frac{1}{N} \sum_{i=1}^N C_i$ .

Now I give introductions of some different types of graph/networks, we have used for our studies.

### Random graphs/networks

The theory of random graphs was introduced by *Erdős and Rényi* (ER) in 1959. They define a random graph as  $N$  labeled nodes connected by  $k$  edges, which are chosen randomly from the  $N(N - 2)/2$  possible edges [45]. Generation of a random network according to ER model is as follows.

*Generation* : Starting with  $N$  nodes, connect every pair of nodes with probability  $p$ . It creates a graph with approximately  $k = pN(N - 1)/2$  edges/connections distributed randomly.

In a random graph, with connection probability  $p$ , the degree  $k_i$  of a node  $i$  follows a binomial distribution,

$$P(k_i = k) = C_{N-1}^k p^k (1 - p)^{N-1-k}$$

which for large  $N$  can be replaced by a Poisson distribution. Clustering coefficient of a random graph is,  $C_{rand} = \frac{\langle k \rangle}{N}$ . For all random graphs with  $N$  nodes and connection probability  $p$ , the range of values for which diameters vary is concentrated around,  $\ln(N)/\ln(pN)$ . It shows that random networks tend to have small diameters, provided  $p$  is not too small. Average (node-node) distances of networks representing the natural systems are close to the average distance of random graph with the same size.

### Small World Networks

Networks representing natural systems (real networks) have small diameter like random networks but they have large clustering coefficients, appearing to be independent of network size [5, 11, 12]. The latter property is characteristic of lattice, whose clustering coefficient is size independent and depends only on coordination number. For a  $d$ -dimensional hypercubic lattice the average node-node distance scales as  $N^{1/d}$ , which increases much faster with  $N$  than the logarithmic increase observed for random graphs and real graphs. In 1998 *Watts and Strogatz* (WS) proposed a model to generate the small world networks [46] which have high clustering coefficients and small average node-node distance [5]. Generation of a small world network according to WS model is following.

*Generation* : (1) Start with order : Start with a ring lattices with  $N$  nodes in which every node is connected to its first  $k$  neighbours ( $k/2$  on either side).

(2) Randomize : Randomly rewire each edge of the lattice with probability  $p$  such that self-connections (connection of a node to itself) and duplicate connections (two connec-

tions between a same pair of nodes) are excluded. By varying  $p$  one can go from an order network ( $p = 0$ ) to a random network ( $p = 1$ ).

This model shows that for small  $p$ , average distance ( $l$ ) scales linearly with the system size, while for large  $p$  the scaling is logarithmic i.e average node-node distance grows as  $\ln N$ . These networks have mostly local edges and long distance edges are fewer. These long distance edges play an important role in reducing average shortest distance. In addition to a short average distance, small-world networks have a relatively high clustering coefficient. The results obtained from simulated small world networks can not be directly compared to most real networks because the rewiring probability  $p$  is not known. Note that rewiring does not change the average degree, it only modifies the degree distribution.

### Scale Free Networks

In real networks, nodes with small degrees are most frequent and the number of nodes having high connections is few [29, 30, 32, 34, 12, 37, 16]. These networks are scale free, i.e. the probability that a node in the network is connected to  $k$  other nodes of the network decays as a power law [15].

$$P(k) \sim k^{-\lambda} \quad (1.1)$$

where  $\lambda$  is a constant. In 1999, *A.-L. Barabási and Reka Albert* (BA) gave the mechanism responsible for the emergence of networks with power law degree distributions [4]. Their approach to model the networks with power law degree distribution is different from the approach to model random networks and small worlds networks. Model of scale free networks put the emphasis on capturing the network evolution. The algorithm of the BA model is following [14].

*Generation* : (1) Growth : Starting with a small number ( $m_0$ ) of nodes, at every time step, add a new node with  $m(\leq m_0)$  edges that link the new node to  $m$  different nodes already present in the system.

(2) Preferential attachment : Probability that a new node is connected to node  $i$  depends on the degree  $k_i$  of node  $i$ , such that

$$\pi(k_i) = \frac{k_i}{\sum_j k_j} \quad (1.2)$$

After  $t$  time steps this procedure results in a network with  $N = t + m_0$  nodes and  $mt$  edges.

One of the most important properties of the scale-free networks is that they display a topological robustness against random node failure because a few hubs (highly connected nodes) dominate their topology. But these scale-free networks are fragile to the removal of the highly connected nodes or hubs. [13].

After introducing the topologies of various networks, the next step is to study networks having dynamical elements at the nodes, coupled on the networks. One important property shown by the coupled dynamical systems is the synchronization and phenomena of cluster formation, so in the next section we introduce synchronization in the dynamical systems.

### 1.2.2 Synchronization of *Dynamical Elements*

Synchronization phenomenon [18, 19, 20] was discovered in 1665 by Christiaan Huygenes, the famous Dutch mathematician, astronomer and physicists [47]. The pendulum clocks mounted on a wall were the first example of spontaneous synchronization [48]. He observed that as each pendulum swings, it transfers energy to the housing, some of which will reach to the other pendulum [49].

**Definition :** Synchronization refers to a process wherein two (or many) systems adjust a given property of their motion to a common behaviour due to a coupling or to a forcing (periodical or noisy) [19, 20, 117]. Synchronization in literature is defined in various ways.

(1) Exact synchronization corresponds to the dynamical variables for different nodes having identical values.

$$x_i(t) = x_j(t); \text{ for all time } t > 0, i, j \in N \quad (1.3)$$

(2) The phase synchronization [19, 50, 51, 52, 53, 54] corresponds to the dynamical variables for different nodes having some definite relation between the phase. In coupled oscillators, for the weak coupling strength only phases of the subsystems are locked, while the amplitude can be highly uncorrelated (see example).

(3) For large coupling strength, there exists a regime of lag synchronization where the state of two oscillators are nearly identical, but one system lags in time to the other. The system states may remain almost identical but with a time lag  $\tau$ ,

$$x_i(t + \tau) \approx x_i(t); \text{ for all time } t > 0, i, j \in N \quad (1.4)$$

where  $x(t)$  is the value of dynamical variable at time  $t$ .

**Example. A Model to study Synchronization :** Collective synchronization in terms of a huge population of interacting limit-cycle oscillators was studied mathematically by Winfree [55],

$$\dot{\theta}_i = \omega_i + \left( \sum_{j=1}^N X(\theta_j) \right) Z(\theta_i). \quad i = 1 \dots N \quad (1.5)$$

where  $\theta_i$  denotes the phase of oscillator  $i$  and  $\omega_i$  its natural frequency. Each oscillator  $j$  exerts a phase-dependent influence  $X(\theta_j)$  on all the others; the corresponding response of oscillator  $i$  depends on its phase  $\theta_i$ , through the sensitivity function  $Z(\theta_i)$ . When the spread of natural frequencies is large compared to the coupling, the system behaves incoherently. As the spread decreases then at a certain threshold small cluster of oscillators suddenly freezes into synchrony. Motivated by this phenomena Kuramoto introduced the famous Kuramoto model [56],

$$\dot{\theta}_i = \omega_i + \frac{\epsilon}{N} \sum_{j=1}^N \sin(\theta_j - \theta_i). \quad i = 1 \dots N \quad (1.6)$$

Oscillators are desynchronized completely until the coupling strength  $\epsilon$  exceeds a critical value  $\epsilon_c$ . After this coupling strength oscillators start getting phase synchronized. As a result of phase synchronization frequencies  $\omega_i = \dot{\theta}_i$  are locked, i.e.  $n\omega_i - m\omega_j = 0$ . These coupled oscillator models are very well studied in the physics literature [23, 57, 58, 59, 60]. Although, the model was originally motivated by biological oscillators, it has appeared in many diverse systems, such as the flavour evolution of neutrinos [61], arrays of Josephson junctions [62], semiconductor lasers [63] etc.

**Synchronization in the Natural Systems :** There are several examples of synchronization in the natural systems. In the biological sciences, for instance, one of the challenging problems is to understand how a group/cluster of cells or functional units, each displaying complicated nonlinear dynamic phenomena, can interact with one another to produce a coherent response on a higher organizational level. Desperate features of a face, each analyzed by specific cerebral areas that receive visual input and respond specifically to movement, angles, color, etc., associated with incidental aspects of background, despite complex concurrent changes in the visual stimulus. Neurophysiology indicates that it may be because of the brain's use of a phenomenon termed synchronous oscillation to correlate

spatially separated responses to a stimulus. Clusters of neurons exhibit synchronous oscillations of neural firing rates [64]. Other biological examples include networks of pacemaker cells in the heart [65]; circadian pacemaker cells in the suprachiasmatic nucleus of the brain (where the individual cellular frequencies are also measured), synchronization and rhythmic processes in physiology [66]; metabolic synchrony in yeast cell suspensions [67]; congregation of synchronously flashing fireflies [68]; and crickets that chirp in unison [69]. Examples in physics and engineering start from array of lasers [70] and microwave oscillators to superconducting Josephson junction [62]. The particles in superconducting materials, and the orbits of moons around planets, show similar behaviour. Social examples include crowd behaviour, the behaviour of audience at a concert or ball game, where everyone starts clapping in unison, even though no one person is the leader [71].

Collective synchronization in the natural systems can be understood by using some simple mathematical models of coupled systems which we will discuss in section 1.3. The dynamics of the individual system can be described by nonlinear element. In the next section we briefly discuss chaos in nonlinear systems.

### 1.2.3 Nonlinearity and Chaos

Nonlinearity and chaos are widely spread in fields as different as physics, engineering, biology and even in economics [74, 75, 77, 78, 80, 81, 82, 83]. A nonlinear system is a system whose time evolution equations are nonlinear. More elaborately, if  $g(x, t)$  and  $h(x, t)$  are linearly independent solutions of the time evolution equation of a nonlinear system; then  $cg(x, t) + dh(x, t)$  would not be a solution for that system ( $c$  and  $d$  are any numbers). The basic idea of nonlinearity is following: if a parameter that describes a *linear* system, such as the spring constant  $k$  in the evolution equation  $d^2x/dt^2 = -(k/m)x$  for the position of the particle subject to the force from an ideal spring, is changed, then the frequency and amplitude of the resulting oscillations will change. But the qualitative nature of the behaviour (simple harmonic oscillation in this example) remains the same. In fact by appropriately rescaling the length and time axes, we can make the behaviour for any value of  $k$  look just like that for some other value of  $k$ . For *nonlinear* system, a small change in a parameter can lead to sudden changes in both the qualitative and quantitative behaviour of the system. For one value, the behaviour might be periodic, for another value only slightly different from the first, the behaviour might be completely aperiodic. Chaos is the term used to de-

scribe the *apparently* complex behaviour of a deterministic system [73]. There are many possible definitions of chaos, ranging from measure theoretic notions of randomness in ergodic theory to the topological approach [76, 78, 80].

**Definition :** We give here the definition adopted in famous book of Robert L. Devaney [76]. Let  $J$  be a set.  $f : J \rightarrow J$  is said to be chaotic on  $J$  if,

1.  $f$  is Topological Transitive :  $f : J \rightarrow J$  is said to be topologically transitive if for any pair of open sets  $U, V \in J$ , there exists  $k > 0$  such that  $f^k(U) \cap V \neq \emptyset$ .
2. Periodic points are dense in  $V$  : A subset  $U$  of  $J$  is dense in  $J$  if  $\bar{U} = J$ .
3.  $f$  has sensitive dependence on initial conditions :  $f : J \rightarrow J$  has sensitive dependence on initial conditions if there exists  $\delta > 0$  such that, for any  $x \in J$  and any neighbourhood  $\delta$  of  $x$ , there exists  $y \in \delta$  and  $n \geq 0$  such that  $|f^n(x) - f^n(y)| > \delta$ .

The 'sensitive dependence' condition captures the idea that in chaotic systems minute errors in the experiments can eventually lead to large scale divergences. As a function of time, the "separation" (suitable defined) between two nearby trajectories increases exponentially, at least for short times. Among all the definitions of chaos, sensitive to initial condition is the most important and most applicable for general characterization of chaos in natural systems and it is thus widely understood as the central idea in chaos.

**Measure :** Lyapunov exponent gives the quantitative test of chaotic behaviour and degree or measure of chaoticity. In the course of time, two orbits of a given system that had started out close together will depart exponentially from each other (note that this divergence cannot go on forever in a bounded space). There distance grows as  $e^{\lambda t}$ , where  $\lambda$  is called the Lyapunov exponent. More elaborately, Lyapunov exponents measure the mean rate of exponential separation of neighbouring trajectories, starting with two different initial conditions  $\mathbf{x}_0$  and  $\mathbf{x}_0 + \Delta\mathbf{x}_0$ . Lyapunov exponent for this system would be [77],

$$\lambda = \lim_{\substack{t \rightarrow \infty \\ \Delta\mathbf{x}_0 \rightarrow 0}} \left( \frac{1}{t} \right) \ln \frac{|\Delta\mathbf{x}_0(t)|}{|\Delta\mathbf{x}_0(0)|} \quad (1.7)$$

Lyapunov exponents of a  $N$  dimensional map,

$$\mathbf{x}_{t+1} = \mathbf{F}(\mathbf{x}_t)$$

where  $\mathbf{x}$  and  $\mathbf{F}$  are  $N$ -dimensional vectors, will be a set of  $N$  characteristic exponents corresponding to the  $N$  eigenvalues of the associated tangent map. Lyapunov exponents for

this  $N$  dimensional system can be calculated as following. Evolution of tangent vector  $\Delta \mathbf{x}_t = [\Delta x_t^1, \Delta x_t^2 \dots, \Delta x_t^N]^T$  along a trajectory can be written as,

$$\Delta \mathbf{x}_{t+1} = \mathbf{J}_t \Delta \mathbf{x}_t$$

where  $\mathbf{J}(\mathbf{x}_t)$  is the Jacobian matrix at a time  $t$ , given by  $(J(\mathbf{x}_t))_{ij} = \delta x_{t+1}^i / \delta x_t^j$ . Eigenvalues  $\Lambda_i, i = 1, \dots, N$ , of the matrix,

$$(\mathbf{J})_t = (\mathbf{J}(\mathbf{x}_t) \mathbf{J}(\mathbf{x}_{t-1}) \dots \mathbf{J}(\mathbf{x}_1))$$

, gives the Lyapunov exponents as,

$$\lambda_i = \lim_{\tau \rightarrow \infty} \frac{1}{\tau} \ln |\Lambda_i(\tau)|, \quad i = 1, \dots, N \quad (1.8)$$

For numerical calculation of Lyapunov exponents in the Chapter 3 and Chapter 4, we follow Benettin *et al.* method [72, 77, 84].

Few examples where chaotic behaviour is observed, are fluids [85], plasma [86], solid state devices [87], circuits [88], lasers [89], mechanical devices [90], biology (chaotic phenomena and nonlinear dynamics in biology are dealt in [48]), chemistry [91], acoustics [92], celestial mechanics [93], atmospheric physics [94]. More importantly, chaotic behaviour shows qualitative and quantitative universal features, which are independent of the details of the particular system. Following I describe logistic map, a most studied and widely used mathematical model exhibiting chaotic dynamics in biological population growth.

**Logistic Map.** *A Mathematical Model of Biological Population Growth :*

In 1976, Sir Robert May gave a very simple mathematical model to describe the growth of biological population as following [95]: let  $x_t$  denotes a population at time  $t$ , and  $x_{t+1}$  the same one year later, then assume  $x_{t+1} = \mu x_t$ , where  $\mu$  represents the rate of growth. Population at time  $t + 1$  is given by,

$$x_{t+1} = f(x_t) \quad (1.9)$$

$$= \mu x_t (1 - x_t) \quad (1.10)$$

It is known as the non-linear logistic difference equation or logistic map. Here population is treated as a fraction of maximum population between zero and one. *Zero* represents extinction, *one* the maximum population. Fixed point of the above map is given by

$$x_\mu^* = f_\mu(x_\mu^*)$$

The subscript  $\mu$  indicates that  $x^*$  depends on the value of  $\mu$ . For one-d map. Following Eq.( 1.8), criteria for the stability of a fixed point ( $x^*$ ) can be written as,  $x^*$  is a stable fixed point if  $|df/dx|_* < 1$ , it is a unstable fixed point if  $|df/dx|_* > 1$ .

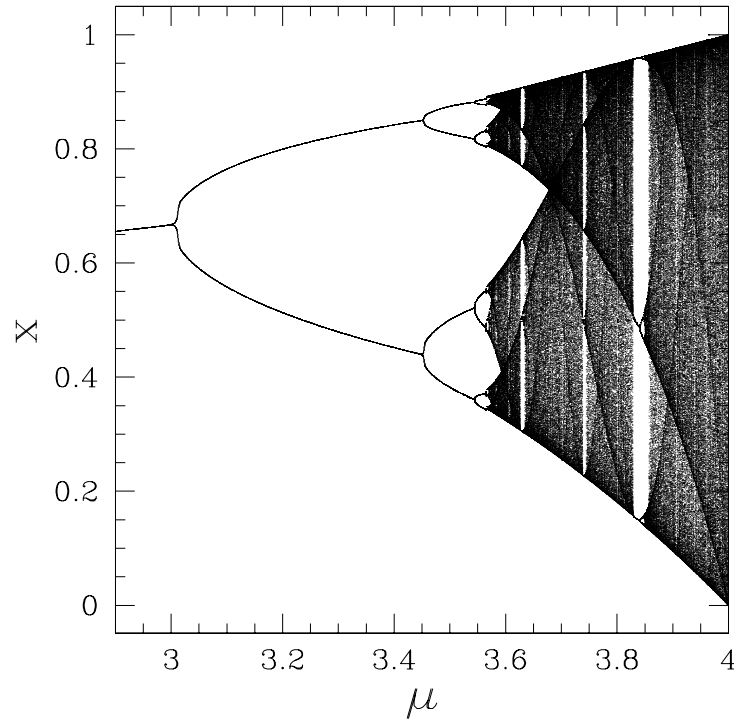


**Figure 1.2:** Figure shows the bifurcation diagram for the logistic map. Trajectories of Logistic map's variable,  $x$ , is plotted as the function of the parameter  $\mu$ . For  $\mu < 3$ , trajectories lie on stable fixed point.

The sequence of  $x$  values generated by the iteration Eq. (1.10) is called trajectory or orbit. Fig. 1.2 shows the bifurcation diagram for logistic map [80, 79]. For  $\mu < 1$ ,  $x = 0$  is the stable attractor, i.e. all trajectories approach this value. For  $1 < \mu < 3$ , the attractor consists of a single point  $x = 1 - 1/\mu$ , at  $\mu = 3$  this fixed point become unstable and period doubling bifurcation occurs. For  $\mu = 1 + \sqrt{6}$ , trajectories settle into 4-cycle. Further increase in  $\mu$  leads higher periods. Between region  $\mu = 3.569\dots$  and  $\mu = 3.68$ , there are multiple chaotic bands. Within each band are periodic windows, with period-3 occurring to the right (large  $\mu$  value) of period-5, which occurs right of period-7 and so on. As  $\mu$  increases, a particular periodic window, which begins with period- $n$ , disappears through a sequence of period doublings. Then a set of  $n$  chaotic bands is formed. Finally, the chaotic bands suddenly merge, the periodic orbits still exist, but they are unstable. Fig. 1.3 plots

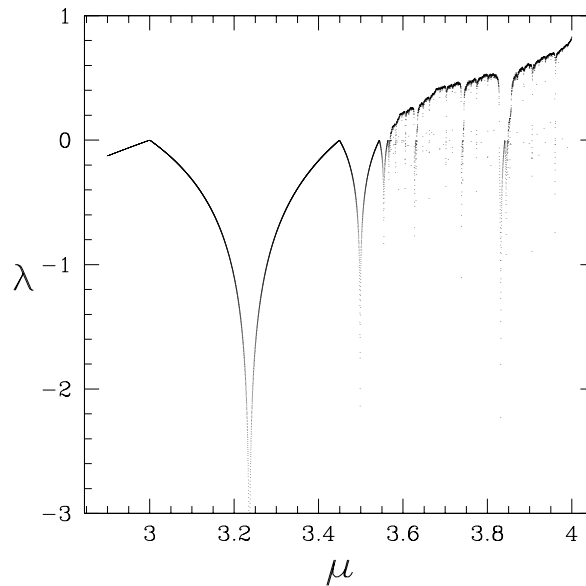


**Figure 1.3:** Figure shows average Lyapunov exponent of logistic map, as a function of logistic map parameter  $\mu$ .

the average Lyapunov exponent ( $\lambda$ ) as a function of logistic map parameter  $\mu$ . Average Lyapunov exponent is positive for the logistic map in the chaotic region.

As we have already seen in the section 1.2.1 that the structural complexity of many biological, social, technological systems are described by the networks having some particular probability distributions. Models of coupled nonlinear elements on these networks might shed light on spatiotemporal dynamics of the natural systems where nonlinearity and spatial complexity coexist.

### 1.3 Chaotic Dynamics on Networks: Models to Study Different Phenomena

The spatiotemporal dynamics of the natural systems are often very complicated and difficult to handle both experimentally and theoretically. To develop some understanding of spatiotemporal nonlinearities, simple models are used whose behaviours are relatively easy to simulate on computers. However the model does not have any direct connections with actual physical or biological systems, but general results given by these models give the proper direction to our thinking as they show some universal features. For the descrip-

tion of complex dynamics and chaos in extended systems of different nature, a number of model classes may be used : two- and three-dimensional fluid flow, coupled-oscillator models, cellular automata, transport models, reaction-diffusion systems and coupled map models. Some times for qualitative understanding of the complex spatio-temporal dynamics, it is preferable to deal not with a continuous medium, but with lattice models.

### 1.3.1 Coupled Maps *Revisited*

Coupled maps on lattices [96, 97] are one of the very important and efficient tool to study many space and time varying processes of physical interest. Lattice system may be constructed, e.g. in electronics and optics, to realize devices with novel operational possibilities. (One of the first works where the model of CML type was suggested had arisen from analysis of electronic delay-feedback generator.) Coupled maps have been found to be useful in several practical situations. These include fluid dynamics [98], nonstatistical behavior in optical systems [99], Rayleigh-Benard convection [100], convection [101], stock market [102], ecological systems [103], logic gates [104], solitons [105] and c-elegans [106]. Coupled map lattice - CML were introduced in the beginning of eighties with the pioneering works of K. Kaneko and others [107, 108, 109, 110, 111, 112, 113]. Kaneko studied a one-dimensional coupled map system,

$$x_{t+1}(i) = (1 - \epsilon)f(x_t(i)) + \frac{\epsilon}{2}(f_t(i - 1) + f_t(i + 1)) \quad (1.11)$$

This expression tells us the that numerical value at location  $i$  at the time step  $(t + 1)$  is determined by the value at  $i$  at the  $t$ th time step and by the values at the neighbouring sites  $i - 1$  and  $i + 1$ . The parameter  $\epsilon$  determines the strength of the coupling to the neighbours. The function  $f$  might be any function like the logistic map function. The factor  $\epsilon/2$  is normalization factor which assures that the  $x$  values stay between 0 and 1. In general we can use many different map functions and we might also allow for coupling among more than just nearest neighbour. This simple coupled map model shows a rich variety of novel phenomenon such as; clustering, hierarchical clusterings, partial order in relationship with spin glass, chaotic itinerancy, collective chaos and interesting synchronized behavior. The initial work on CML, shows two phenomena [110], namely **spatio-temporal chaos** and **coherent or synchronized structures** which opened the rigorous investigation in this direction. Synchronization and cluster formation lead to rich spatio-temporal pat-

terns when opposing tendencies compete; the nonlinear dynamics of the maps which in the chaotic regime tends to separate the orbits of different elements, and the couplings that tend to synchronize them [107]. There are several numerical as well as analytical studies on coupled maps on lattices as well as globally coupled networks. Here I am only referring few earlier works and few very recent works on coupled maps on lattices. These works include very first work on analytical stability analysis by H. Fujisaka and T. Yamada [97]. It deals with the stability of synchronized motion in dynamical systems on nearest neighbour coupled networks and globally coupled networks. Formation of two synchronized clusters or coherent behaviour and then loss of coherence in globally coupled maps are described analytically as well as numerically at different places with different point of view [115, 116, 117, 118, 119, 120, 121, 122, 123, 124, 125, 126]. Chaotic coupled maps on 1-d lattices show beautiful phase ordering of nodes [127, 128, 129, 130, 131, 132].

### 1.3.2 Coupled Maps on Networks

Studies of coupled maps have usually been done under the assumption of certain regularity in the connection topology, where nodes are coupled to their nearest neighbours, or to the all other nodes. Lately, more general networks with random, small-world, scale-free, and hierarchical architectures have been emphasized as appropriate models of interaction. Refs. [5, 59, 133, 134, 135, 136] shed some light on the collective behaviour of coupled maps/oscillators with local and non-local connections. Random networks with large number of connections also show synchronized behavior for large coupling strengths [137, 138, 139]. There are also some studies on synchronization of coupled maps on other networks viz. Cayley tree [140], small-world networks [5, 141, 142, 143] hierarchal organization [144] and, fractional networks [145]. Mostly these studies have considered networks with large number of connections. For my thesis mostly we have considered the networks with the connections of the order of the size of the network. This small number of connections allows us to study the mechanism of formation of synchronized clusters and the role that different connections play in synchronizing the nodes.

## 1.4 Organization of the THESIS

In chapter I, first we give the motivation and main objective for my thesis work, then we introduce and discuss all the key concepts of my PhD thesis viz. complex networks, synchronization, and coupled maps.

In chapter 2, we introduce our model for coupled map network (CMN). We define phase synchronization which we use in our numerical studies. We also define general properties of CMN's which include characterization of different mechanisms of cluster formation, different states of synchronized clusters based on number and behaviour of nodes forming clusters and quantitative measures for the synchronization.

In chapter 3, we present the detailed numerical results of coupled maps on various networks. First I discuss coupled maps on scale-free networks using phase diagram, various node-node plots and different quantitative measures, for both linear and nonlinear couplings, and then other networks are briefly discussed. We also give some examples of self-organized and driven synchronization in physical and social systems.

In chapter 4, we study the dynamics of coupled maps on some simple networks using linear stability analysis and Lyapunov function approach. Mainly we study the asymptotic stability of self-organized and driven synchronization in networks with small number of nodes viz. 2 and 3 nodes networks and extension of these small networks to networks with the large number of the nodes.

In chapter 5, I conclude my thesis with the future directions.

## Chapter 2

# Synchronized Clusters on Coupled Map Networks (CMNs)

---

---

### 2.1 Introduction

In this chapter we introduce different properties of the synchronized clusters and coupled dynamics on networks. For local dynamics being in the chaotic regime, for small coupling strength there is no cluster formation, as coupling strength increases nodes form synchronized clusters. Through different case studies mechanisms of the synchronized cluster formation and behaviour of the coupled dynamics on various networks will be extensively explored in the next chapters.

Whole chapter is organized as follows. In section 2.2, we introduce our model for coupled dynamics. Section 2.3 define phase synchronization and synchronized clusters. Section 2.4 discusses the general properties of synchronized dynamics on networks, which include behaviour of a single node in coupled dynamics, mechanism of cluster formation and different synchronized states. In section 2.5, we provide a qualitative measure for different mechanism, these measures are based on the number of intra-cluster and inter-cluster connections. Section 2.6 summarizes the chapter.

### 2.2 Model of a Coupled Map Network

Consider a network of  $N$  nodes and  $N_c$  connections (or couplings) between the nodes. Let each node of the network be assigned a dynamical variable  $x^i, i = 1, 2, \dots, N$ . The

evolution of the dynamical variables can be written as

$$x_{t+1}^i = (1 - \epsilon)f(x_t^i) + \frac{\epsilon}{k_i} \sum_{j+1}^N C_{ij}g(x_t^j) \quad (2.1)$$

where  $x_t^i$  is the dynamical variable of the  $i$ -th node at the  $t$ -th time step and  $\epsilon$  is the coupling constant. The topology of the network is introduced through the adjacency matrix  $C$  with elements  $C_{ij}$  taking values 1 or 0 depending upon whether  $i$  and  $j$  are connected or not.  $C$  is a symmetric matrix with diagonal elements zero.  $k_i = \sum C_{ij}$  is the degree of node  $i$ . The factors  $(1 - \epsilon)$  in the first term and  $k_i$  in the second term are introduced for normalization. The function  $f(x)$  defines the local nonlinear map and the function  $g(x)$  defines the nature of coupling between the nodes. We present the detailed results for logistic map

$$f(x) = \mu x(1 - x) \quad (2.2)$$

governing the local dynamics. We have also considered sine maps for the local dynamics. We discuss the results for the following two types of coupling functions.

$$g(x) = x \quad (2.3a)$$

$$g(x) = f(x) \quad (2.3b)$$

We refer to the first type of coupling function as linear coupling later as nonlinear coupling.

### 2.3 Phase Synchronization and Synchronized Clusters

For our numerical investigations (in the chapter 3), mainly we consider networks with the connections of the order of  $N$ . With this small number of connections, local dynamics (i.e. function  $f(x)$ ) of the nodes being in the chaotic zone, only few clusters with small number of nodes show exact synchronization. However, clusters with larger number of nodes are obtained when we study phase synchronization. For the further study of cluster formation in coupled map networks we define the phase synchronization as follows [146].

Let  $\nu_i$  and  $\nu_j$  denote the number of times the dynamical variables  $x_t^i$  and  $x_t^j$ ,  $t = t_0, t_0 + 1, 2, \dots, t_0 + T - 1$ , for the nodes  $i$  and  $j$  show local minima during the time interval  $T$  starting from some time  $t_0$ . Let  $\nu_{ij}$  denote the number of times these local minima match with each other. We define the phase distance,  $d_{ij}$ , between the nodes  $i$  and  $j$  by the

following relation,

$$d_{ij} = 1 - \frac{\nu_{ij}}{\max(\nu_i, \nu_j)}. \quad (2.4)$$

Clearly,  $d_{ij} = d_{ji}$ . Also,  $d_{ij} = 0$  when all minima of variables  $x^i$  and  $x^j$  match with each other and  $d_{ij} = 1$  when none of the minima match. In the Appendix, we show that the above definition of phase distance satisfies metric properties. We say that nodes  $i$  and  $j$  are phase synchronized if  $d_{ij} = 0$ , and a cluster of nodes is (phase) synchronized if all pairs of nodes belonging to that cluster are (phase) synchronized.

## 2.4 General Properties of Synchronized Dynamics

We consider some general properties of synchronized dynamics. They are valid for any coupled discrete and continuous dynamical systems. Also, these properties are applicable for exact as well as phase synchronization and are independent of the type of network.

### 2.4.1 Behavior of Individual Nodes

As the network evolves, it splits into several synchronized clusters. Depending on their asymptotic dynamical behaviour the nodes of the network can be divided into three types.

- (a) *Cluster nodes*: A node of this type synchronizes with other nodes and forms a synchronized cluster. Once this node enters a synchronized cluster it remains in that cluster afterwards.
- (b) *Isolated nodes*: A node of this type does not synchronize with any other node and remains isolated for all time.
- (c) *Floating Nodes*: A node of this type keeps on switching intermittently between an independent evolution and a synchronized evolution attached to some cluster.

Of particular interest are the floating nodes and we will discuss some of their properties in the next two chapters.

### 2.4.2 Mechanism of Cluster Formation

The study of the relation between the synchronized clusters and the couplings between the nodes represented by the adjacency matrix  $C$  shows two different mechanisms of cluster formation.

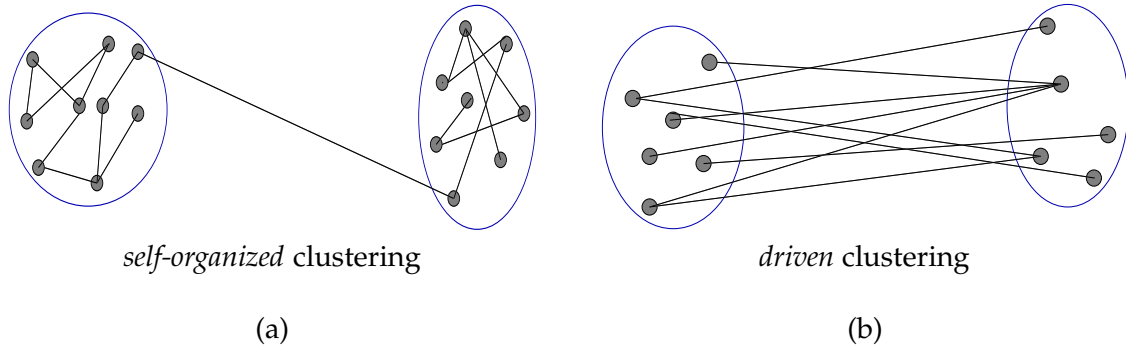


**Figure 2.1:** Figure represents (a) self-organized clustering and (b) driven clustering. Two big circles in each figure represent two synchronized clusters in the network, (a) representing ideal self-organized clustering, where all the nodes in a circle are connected with the other nodes within the same circle and (b) representing ideal driven clustering, where all the nodes in a circle are connected with the nodes of the other circle and there is no connection within the nodes of the same circle. Note in the ideal self-organized clustering (Fig. (a)), there is one connection which is of inter-cluster type. This connection is necessary for a connected graph/network.

(i) Self-organized clusters: The nodes of a cluster can be synchronized because of intra-cluster couplings (see e.g. Fig. 2.1 (a)). We refer to this as the self-organized synchronization and the corresponding synchronized clusters as self-organized clusters.

(ii) Driven clusters: The nodes of a cluster can be synchronized because of inter-cluster couplings (see e.g. Fig. 2.1 (b)). Here the nodes of one cluster are driven by those of the others. We refer to this as the driven synchronization and the corresponding clusters as driven clusters.

In our numerical studies we have been able to identify ideal clusters of both the types, as well as clusters of the mixed type where both ways of synchronization contribute to cluster formation. We will discuss several examples to illustrate both types of clusters.

### 2.4.3 Self-organized and Driven Cluster Formation in a Tree Network

Geometrically the two mechanisms of cluster formation can be easily understood by considering a tree type network. A tree can be broken into different clusters in different ways.

(a) A tree can be broken into two or more disjoint clusters with only intra-cluster couplings by breaking one or more connections. It leads to self-organized clusters. This splitting is not unique and there could be several ways to organize nodes to form self-organized clusters. (b) A tree can also be divided into two clusters by putting connected nodes into different clusters. This division is unique and leads to two clusters with only inter-cluster couplings, i.e. driven clusters.

(c) Several other ways of splitting a tree are possible. E.g. it is easy to see that a tree can be broken into three clusters of the driven type.

#### 2.4.4 States of Synchronized Dynamics

Normally, the states of coupled dynamical systems are classified on the basis of the number of clusters as in Ref. [147]. Our finding of two mechanisms of cluster formation allow us to redefine this classification.

(a) Turbulent state (I-T): All nodes behave chaotically with no cluster formation.

(b) Partially ordered state (III): Nodes form a few clusters with some isolated nodes not attached to any cluster. We can further subdivide the clusters of the partially ordered state into subcategories depending on the type of clusters i.e. self-organized (S), driven (D) or mixed type (M).

(c) Ordered state (IV): Nodes form two or more clusters with no isolated nodes. The ordered state can be further divided into 3 substates based on the nature of dynamics of the synchronized clusters as chaotic ordered state (C), quasi-periodic ordered state (Q), and periodic ordered state (P). Also, as for partially ordered state we can have subcategories as self-organized (S), driven (D) or mixed type (M).

(d) Coherent state (V): Nodes form a single synchronized cluster. The dynamical behavior is usually periodic (P) or of a fixed point (F).

(e) Variable state (II): Nodes form different states, partially ordered or ordered state depending on the initial conditions.

For local dynamics in the chaotic range, initially for small coupling strength all nodes behave in turbulent manner with no cluster formation at all. As coupling strength increases, after a critical coupling strength value coupled dynamics starts forming clusters.

## 2.5 Quantitative Measures for Self-organized and Driven Behaviour

To get a clear picture of self-organized and driven behaviour we define two quantities  $f_{\text{intra}}$  and  $f_{\text{inter}}$  as measures for the intra-cluster couplings and the inter-cluster couplings

as follows:

$$f_{\text{intra}} = \frac{N_{\text{intra}}}{N_c} \quad (2.5a)$$

$$f_{\text{inter}} = \frac{N_{\text{inter}}}{N_c} \quad (2.5b)$$

where  $N_{\text{intra}}$  and  $N_{\text{inter}}$  are the numbers of intra- and inter-cluster couplings respectively. In  $N_{\text{inter}}$ , couplings between two isolated nodes are not included. Clearly for ideal driven clusters  $f_{\text{intra}} = 0$  and  $f_{\text{inter}} = 1$  and for ideal self-organized clusters reverse is true.

## 2.6 Summary

In this chapter I introduce the model for coupled dynamics and define the qualitative and quantitative characterization of synchronized clusters. We characterize different states of clusters, first based on the number of clusters and nature of coupled dynamics and second based on the number of inter- and intra-cluster connections. By considering the number of inter- and intra-cluster couplings we can identify phase synchronized clusters with dominant self-organized behavior (S), dominant driven behavior (D) and mixed behavior (M) where both mechanisms contribute. Final attractor may consist of coherent state, ordered state or turbulent state.

## Chapter 3

# Numerical Analysis And Results

---

---

### 3.1 Introduction

In this chapter we present the detailed numerical analysis for the dynamics of the coupled maps on the various networks. Mainly we study the phase synchronization and cluster formation properties of the coupled dynamics. We explore the temporal behaviour of individual nodes, and study the role of different connections in the formation of the synchronized clusters. For most of the our studies we have taken networks with number of connections of the order of  $N$  because a large number of natural systems fall under this category of small connections. More importantly, this small number of connections allows us to study the mechanism of the formation of synchronized clusters and the role that different connections play in synchronizing different nodes.

Whole chapter is organized as follows. In section 3.2, we present the detailed numerical results for phase synchronization in coupled dynamics on scale-free networks. We present the results for both linear and nonlinear coupling functions. Section 3.3 consists brief descriptions of coupled dynamics on other networks viz., 1-d nearest neighbour coupled network, small world network, higher dimensional (2-d and 3-d) nearest neighbour coupled network, tree networks and random networks. In these sections, coupled map networks are studied with the help of phase diagrams (for local dynamics governed by logistic map), Lyapunov exponents results and different quantitative measurements, all describing the nature of dynamics, the mechanisms of synchronized cluster formation and the behaviour of individual dynamical elements. In section 3.4, We discuss some examples of self-organized and driven synchronization in various physical and social systems. Sec-

tion 3.5 considers coupled dynamics with circle map as a local function. In section 3.6, We summarize the whole chapter and state some important results.

## 3.2 Coupled Maps on Scale-free Network: A Case Study

The evolution of the dynamical variables can be written as,

$$x_{t+1}^i = (1 - \epsilon)f(x_t^i) + \frac{\epsilon}{k_i} \sum_{j+1}^N C_{ij}g(x_t^j) \quad (3.1)$$

where all the terms have their usual meaning (see Eq. (1) of the chapter 2). The scale free network of  $N$  nodes is generated by using the model of Barabasi et.al. [14], given in the first chapter (see section 1.2.1). For the type of probability law  $\pi(k)$  that we have used,  $\lambda = 3$ . Other forms for the probability  $\pi(k)$  are possible which give different values of  $\lambda$ . However, the results reported here do not depend on the exact form of  $\pi(k)$  except that it should lead to a scale-free network. In the following sections we discuss the coupled maps on the scale-free network with two types of coupling functions. Note that for the scale free network we generated using above algorithm, number of connections,  $N_c = m_0 \times (N - 1)$ , where  $m_0$  is the number of nodes at the starting and  $N$  is the total number of nodes in the network.

### 3.2.1 Linear Coupling

*Phase diagram:* For linear coupling  $g(x) = x$ , Fig. 3.1 shows the phase diagram in the two parameter space defined by  $\mu$  and  $\epsilon$  for the scale-free network with  $m = m_0 = 1, N = 50, T = 100$ . For  $\mu < 3$ , coupled dynamics lies on a stable coherent region (region V-F). To understand the remaining phase diagram, consider the line  $\mu = 4$ . Fig. 3.2 shows the largest Lyapunov exponent  $\lambda$  as a function of the coupling strength  $\epsilon$  for  $\mu = 4$ . We identify four different regions as  $\epsilon$  increases from 0 to 1; as shown by regions I to IV in Figs. 3.1 and 3.2. For small values of  $\epsilon$ , we observe a turbulent behavior with all nodes evolving chaotically and there is no phase synchronization (region I-T). There is a critical value of coupling strength  $\epsilon_c$  beyond which synchronized clusters can be observed. This is a general property of all coupled map networks and the exact value of  $\epsilon_c$  depends on the type of network, the type of coupling function and the parameter  $\mu$ . As  $\epsilon$  increases beyond

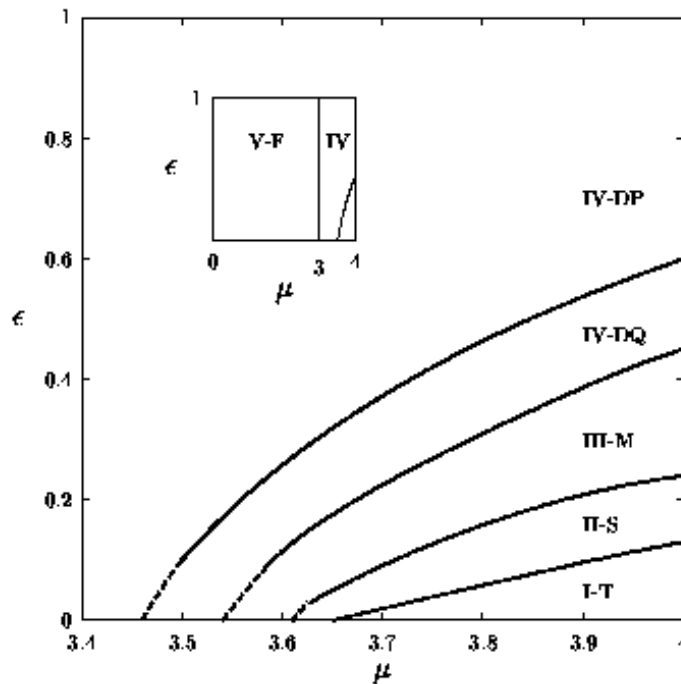


**Figure 3.1:** Phase diagram showing different regions in the two parameter space of  $\mu$  and  $\epsilon$  for scale free network for  $f(x) = \mu x(1 - x)$  and  $g(x) = x$ . Different regions based on number of clusters (as characterized in the chapter 2) are I. Turbulent region, II. region with varying behaviour, III. Partially ordered region, IV. Ordered region, V. Coherent region. The symbols T, S, M, D, P, Q and F respectively correspond to turbulent behaviour, self-organized synchronization, mixed synchronization, driven synchronization, periodic, quasiperiodic and fixed behaviour. Region boundaries are determined based on the asymptotic behaviour using several initial conditions, number of clusters and isolated nodes, synchronization behaviour and also the behaviour of the largest Lyapunov exponent. The dashed lines indicate uncertainties in determining the boundaries. Calculations are for  $N = 50, m = 1, T = 100$ . The inset shows the phase diagram for the entire range of parameter  $\mu$  i.e. from 0 to 4.

$\epsilon_c$  we get into a variable region (region II-S) which shows variety of phase synchronized behavior, namely ordered chaotic, ordered quasiperiodic, ordered periodic and partially ordered, depending on the initial conditions.

Next region (region III-M) shows partially ordered chaotic behavior. Here, the number of clusters as well as the number of nodes in the clusters depend on the initial conditions and also they change with time. In this region there are several isolated nodes not belonging to any cluster. Many of these nodes are of the floating type (for definition of floating nodes, see Chapter 2, section 2.4.1). Last two regions (IV-DQ and IV-DP) are ordered quasiperiodic and ordered periodic regions showing driven synchronization. In these regions, the network always splits into two clusters. The two clusters are perfectly anti-phase synchronized with each other, i.e. when the nodes belonging to one cluster

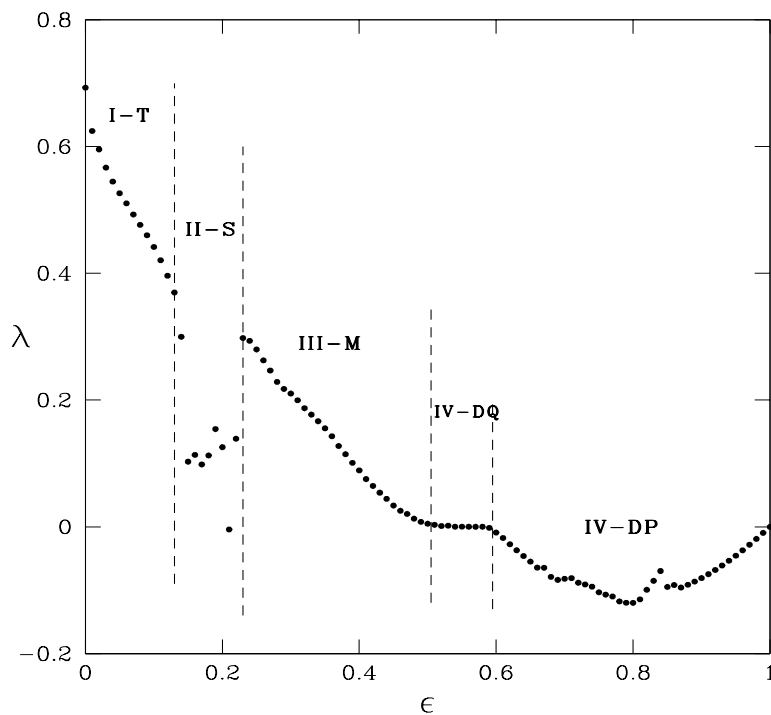


**Figure 3.2:** Largest Lyapunov exponent,  $\lambda$ , is plotted as a function of  $\epsilon$  for scale free network and  $f(x) = 4x(1-x)$  and  $g(x) = x$ . Different regions are labeled as in Fig. 3.1.

show minima those belonging to the other cluster show maxima.

*Mechanism of cluster formation:* To investigate the nature of phase synchronization in different regions of the phase diagram first, we discuss the Fig. 3.3. This figure shows node-node plots of the synchronized clusters. Any two nodes belonging to the same cluster are denoted with the open circles and the couplings between the nodes ( $C_{ij} = 1$ ) are denoted with the solid circles. Fig. 3.3(a), which is plotted in the region I-T, shows turbulent behaviour. Fig. 3.3(b) shows an ideal self-organized synchronization, with two clusters observed in the middle of region II-S. Exactly opposite behavior is observed for the region IV-DQ, this driven synchronization is further stabilized in the region IV-DP with two perfectly anti-phase synchronized driven clusters. Fig. 3.3(d) shows an ideal driven synchronization obtained in the middle of region IV-DP. The phenomena of driven synchronization in this region is a very robust one in the sense that it is obtained for almost all initial conditions, the transient time is very small, the nodes belonging to the two clusters are uniquely determined and we get a stable solution. In region III-M, we get clusters

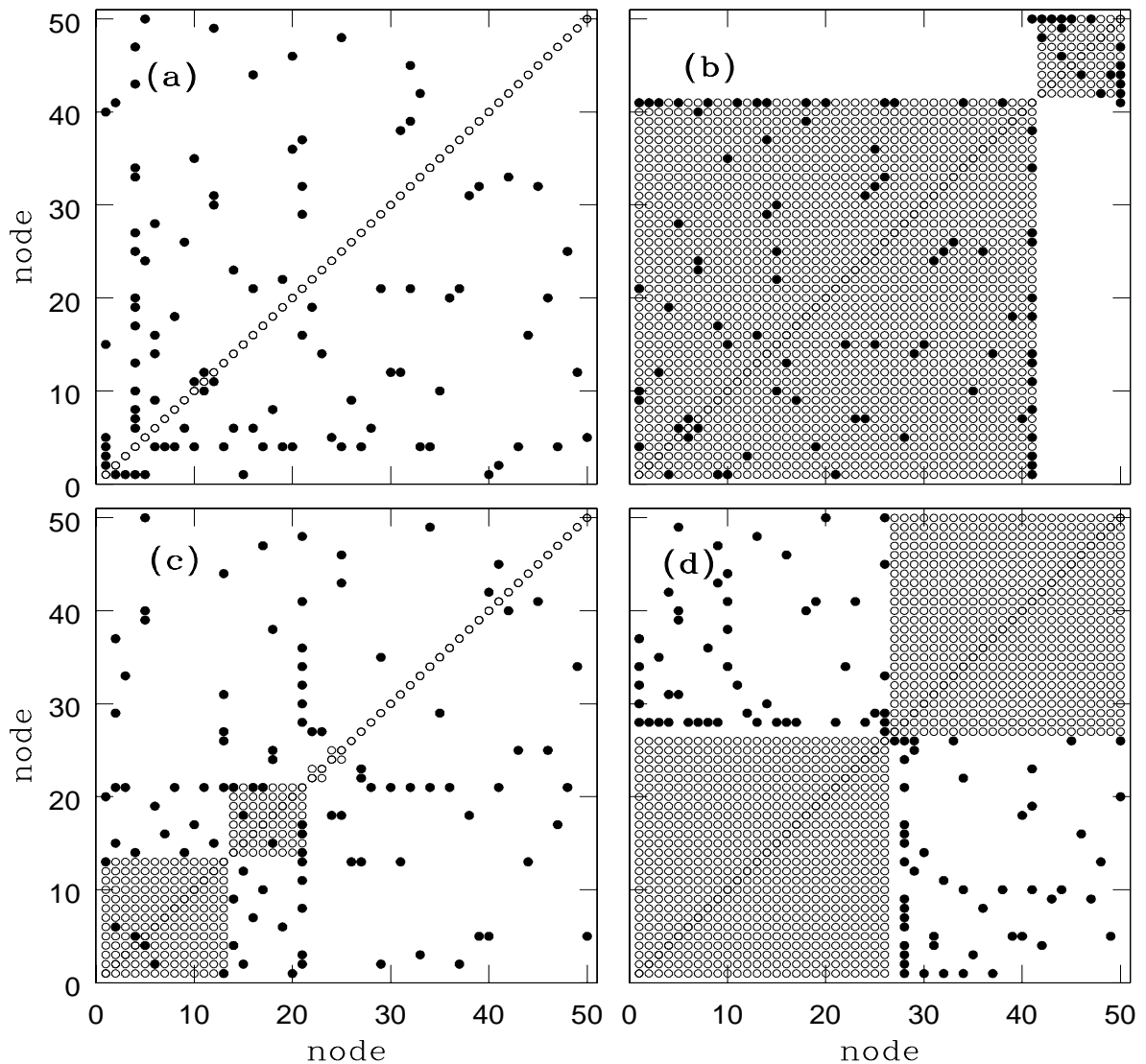


**Figure 3.3:** The figure shows several examples illustrating the self-organized and driven phase synchronization. The examples are chosen to demonstrate two different ways of obtaining synchronized clusters and the variety of clusters that are formed. All the figures show node versus node diagram for  $N = N_c = 50$ . After an initial transient (about 2000 iterates) phase synchronized clusters are studied for  $T = 100$ . The logistic map parameter  $\mu = 4$  and coupling function  $g(x) = x$ . The solid circles show that the two corresponding nodes are coupled and the open circles show that the corresponding nodes are phase synchronized. In each case the node numbers are reorganized so that nodes belonging to the same cluster are numbered consecutively and the clusters get displayed in decreasing sizes. (a) Figure shows turbulent phase for  $\epsilon = 0.10$ . (b) An ideal self-organized phase synchronization for  $\epsilon = 0.15$ . (c) Mixed behavior for  $\epsilon = 0.32$ . (d) A ideal driven phase synchronization for  $\epsilon = 0.85$ . The scale free networks were generated with  $N_0 = 1$  and  $m = 1$ .

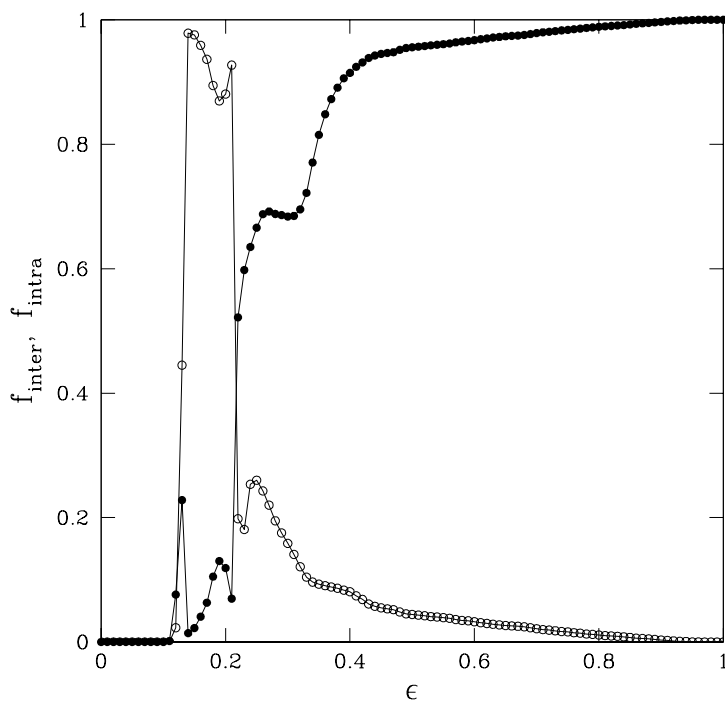


**Figure 3.4:** The fraction of intra-cluster and inter-cluster couplings,  $f_{inter}$  (solid circles) and  $f_{intra}$  (open circle) are shown as a function of the coupling strength  $\epsilon$  for the scale-free networks with  $f(x) = 4x(1-x)$  and  $g(x) = x$ . The figure is obtained by averaging over 20 realizations of the network and 50 random initial conditions for each realization.

of mixed type (Fig. 3.3(c)), here inter-cluster connections and intra-cluster connections are almost equal in numbers.

*Quantitative measures for self-organized and driven behaviour:* Fig. 3.4 shows the plot of  $f_{intra}$  and  $f_{inter}$  as a function of the coupling strength  $\epsilon$ . The figure clearly shows that for small coupling strength (region I-T), both  $f_{intra}$  and  $f_{inter}$  are zero indicating that there is no cluster formation at all. As the coupling strength increases ( $\epsilon$  greater than some critical value  $\epsilon_c$ ) we get  $f_{intra}$  nearly one at  $\epsilon \sim 0.2$  (region II-S). As coupling strength increases further  $f_{intra}$  decreases and  $f_{inter}$  increases i.e. there is a crossover from self-organized to driven behavior (regions III-M). As coupling strength enters into regions IV-DQ and IV-DP, we find that  $f_{inter}$  is large and in region IV-DP we get  $f_{inter}$  almost one corresponding to an ideal driven synchronized behaviour.

*Behaviour of cluster nodes, isolated nodes and floating nodes:* Figs. 3.5 (a) and (b) show plot of time evolution of some typical nodes. Fig. 3.5(a) is for nodes in self-organized region

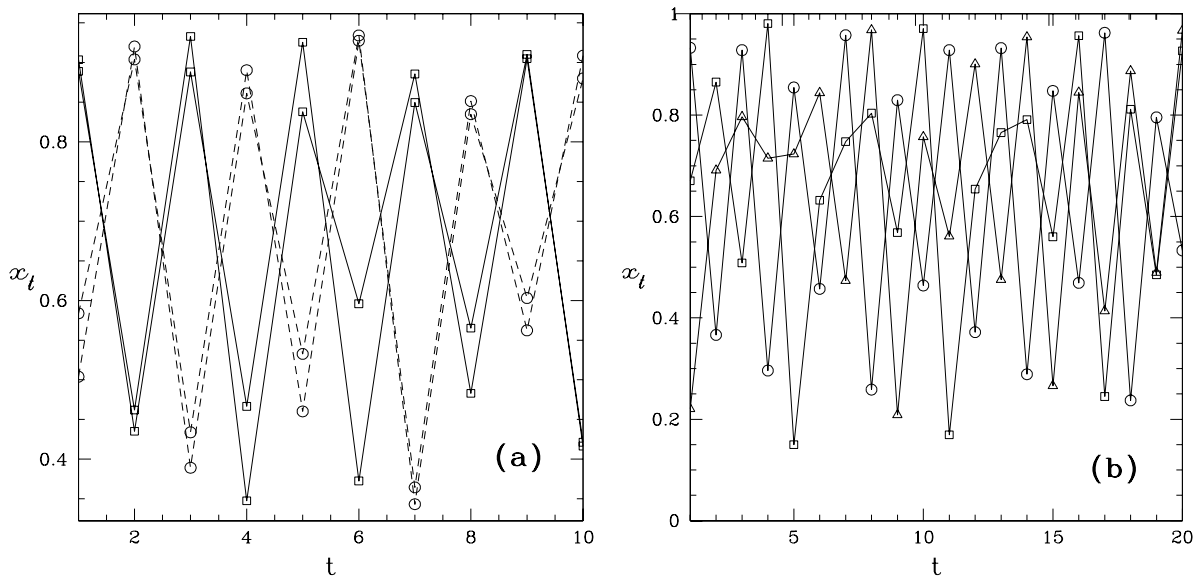


**Figure 3.5:** Figures show time evolution of nodes belonging to different clusters. This figure is plotted for scale-free network with 50 nodes coupled with  $g(x) = x$ . (a) A few nodes belonging to two phase synchronized clusters are shown. Nodes denoted by circles belong to one cluster and nodes denoted by squares to another cluster. Here  $\epsilon = 0.15$ . (b) Time series of three nodes which are not phase synchronized with each other are shown with three different symbols. Here,  $\epsilon = 0.35$ .

( $\epsilon = 0.15$ ), where nodes belonging to the same cluster are marked with the same symbols. It is clearly seen that nodes with the same symbols i.e. belonging to the same cluster are phase synchronized and those belonging to different clusters are completely anti-phase synchronized, i.e. when the nodes in one cluster are showing minima, the nodes in other cluster are showing maxima. (This behaviour is observed for driven behaviour where two clusters are formed, i.e. nodes belonging to different clusters are anti-phase synchronized with each other.) Fig. 3.5(b) plots the time evolution of three nodes in the partially ordered region ( $\epsilon = 0.35$ ). We see that these nodes are not phase synchronized with each other.

Now we explore different regions further to understand time evolution of individual nodes attached to some specific cluster. Fig. 3.6 plots all the nodes belonging to a cluster as a function of time, symbols indicate the time for which a given node belongs to a cluster. Fig. 3.6(a) shows a set of nodes (crosses) belonging to a cluster in the mixed region (region II S) for  $\epsilon = 0.19$  and another set of nodes (open circle) belonging to another cluster for the same  $\epsilon$  but obtained with different initial conditions. For this  $\epsilon$  value all the nodes form self-organized clusters with no isolated nodes and nodes in the individual cluster are

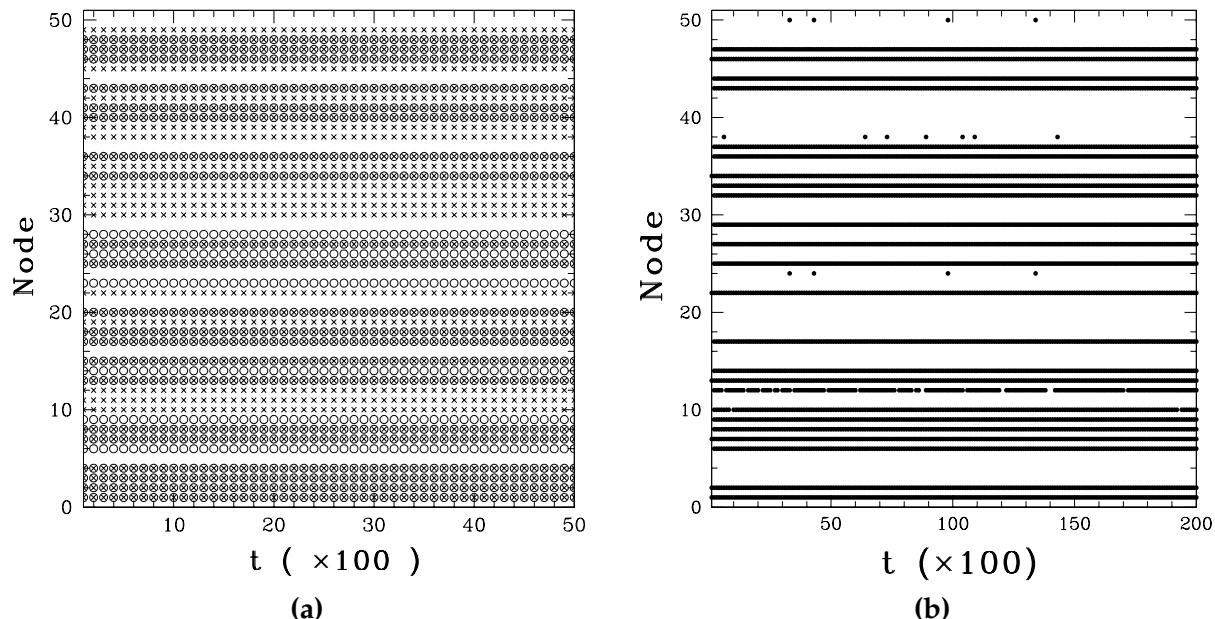


**Figure 3.6:** Figure shows the time evolution of nodes in a cluster for scale-free network. (a) shows two stationary clusters of self-organized type for  $\epsilon = 0.19$  and  $g(x) = x$ . The two clusters are for the same  $\epsilon$  value but for two different initial conditions. The nodes belonging to the two clusters are denoted by open circles and crosses. Note that some nodes are common to both the clusters while some are different. This illustrates the nonuniqueness of nodes belonging self-organized clusters depending on the initial conditions. (b) shows a cluster with some permanent nodes and some floating nodes. Here  $\epsilon = 0.4$  and  $g(x) = x$ . Node number 12, 24, 38 and 50 are of floating type. They spend some time intermittently in a synchronized evolution with the given cluster and the remaining time in either a synchronized evolution with other clusters or in an independent evolution as an isolated node.

permanent members of that cluster. Comparing the members of two clusters which are obtained from different initial conditions we see that there are some common nodes while some are different. For both the initial conditions coupled dynamics from self-organized clusters but organization of the nodes in the clusters are different. We have already describe in the chapter 2 (Section 2.4.3) that for the networks generated for  $m = 1$ , self-organized splitting is not unique. While ideal driven synchronization observed in region IV-DP, leads to a unique cluster formation and does not depend on the initial conditions.

Next we look at  $\epsilon = 0.4$  (region III-M) where we get several clusters with some isolated nodes. In Fig. 3.6(b), nodes belonging to a cluster are plotted as a function of time. We observe that there are some nodes which are attached to this cluster, intermittently leave the cluster, evolve independently or get attached with some other cluster and after

some time again come back to the same cluster. These nodes are floating nodes. For example, node number 12 in Fig. (tseries-clus)(b), which forms phase synchronized cluster with other nodes, in between leaves the cluster and evolve independently for some time. Time it spends with the cluster is about 90%. On the other hand node number 24 evolves independently for almost 90% of the time and evolves in phase synchronization with the cluster for the re

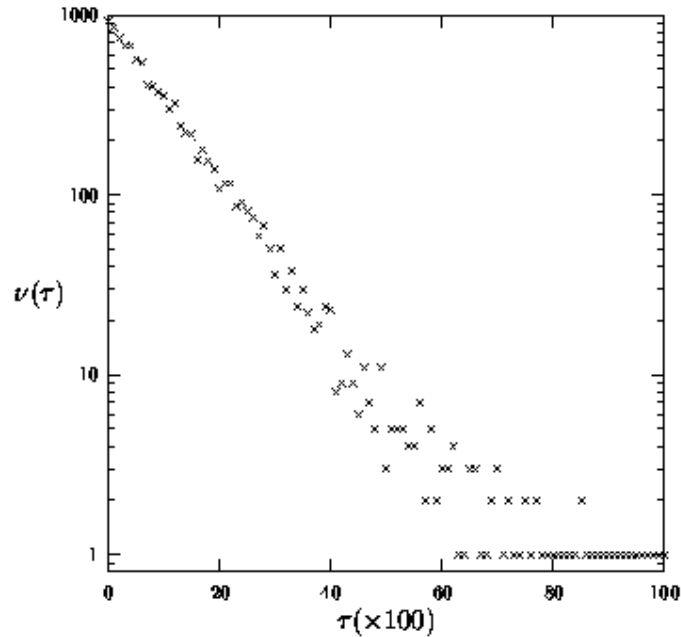


**Figure 3.7:** The figure plots the frequency of residence time  $f(\tau)$  of a floating node in a cluster as a function of the residence time  $\tau$ . The data is for node no 12 in Fig. 3.6(b). A good straight line fit on log-linear plot shows exponential dependence.

Let  $\tau$  denote the residence time of a floating node in a cluster (i.e. the continuous time interval that the node is in a cluster). Fig. 3.7 plots the frequency of residence time  $f(\tau)$  of a floating node as a function of the residence time  $\tau$ . A good straight line fit on log-linear plot shows exponential dependence,

$$f(\tau) \sim \exp(-\tau/\tau_r) \quad (3.2)$$

where  $\tau_r$  is the typical residence time for a given node. We have also studied the distribution of the time intervals for which a floating node is not synchronized with a given cluster. This also shows an exponential distribution.

### 3.2.2 Nonlinear Coupling

Now I discuss results for the nonlinear coupling of the type  $g(x) = f(x)$ . This is equivalent to a diffusive type of coupling. Phase space diagram in the  $\mu - \epsilon$  plane is plotted in Fig. 3.8. Again the phase diagram is divided into different regions I to VI, based on the criteria given in the previous chapter. For  $\mu < 3.5$ , we get coherent behaviour (regions V-P and VI-F). To describe the remaining phase diagram first consider  $\mu = 4$  line. Fig. 3.9 shows the largest Lyapunov exponent as a function of the coupling strength  $\epsilon$  for  $\mu = 4$  and Figs. 3.10 are node-node plots showing different clusters and couplings (as in Figs. 3.3) for different values belonging to the different regions. For small coupling strengths no cluster is formed and we get the turbulent region (I-T). As the coupling strength increases we get into the variable region (II-D). In this region we get partially ordered and ordered chaotic state, depending on the initial conditions. In a small portion in the middle of region II-D, all nodes form two ideal driven clusters (Fig. 3.10(a)). These two clusters are perfectly anti-phase synchronized with each other. Interestingly the dynamics still remains chaotic (Fig. 3.9). In region III-T, we get almost turbulent behaviour with very few nodes forming synchronized clusters. Regions III-M and III-D are partially ordered chaotic regions with few nodes forming clusters and several isolated or of floating type nodes. Fig. 3.10(b) is plotted for  $\epsilon$  in region III-M and it shows clusters of different types. The largest two clusters have approximately equal number of inter-cluster and intra-cluster couplings (mixed type), the next two clusters have dominant intra-cluster couplings (self-organized type) while the remaining three clusters have dominant inter-cluster couplings (driven type). Fig. 3.10(c) shows clusters in the region III-D.

Fig. 3.11 shows the plot of  $f_{\text{intra}}$  and  $f_{\text{inter}}$  as a function of the coupling strength  $\epsilon$  for  $\mu = 4$ . For small coupling strength both quantities are *zero* showing turbulent region.  $f_{\text{inter}}$  is *one* at  $\epsilon \approx 0.13$ , which shows clusters of the ideal driven type (Fig. 3.10(a)). As coupling strength increases further,  $f_{\text{inter}}$  and  $f_{\text{intra}}$  become almost *zero* (region III-T) and subsequently start increasing slowly (region III-M) but we see that  $f_{\text{inter}}$  is always greater than  $f_{\text{intra}}$  leading to the dominant driven phase synchronized clusters. For  $\epsilon > 0.7$ ,  $f_{\text{intra}}$  starts decreasing and for  $\epsilon > 0.8$ , driven behaviour becomes more prominent (region III-D and Fig. 3.10(c)).

For regions III-M and III-D, we get phase synchronized clusters but the size of clusters as well as number of nodes forming clusters both are small. We will see later that for some

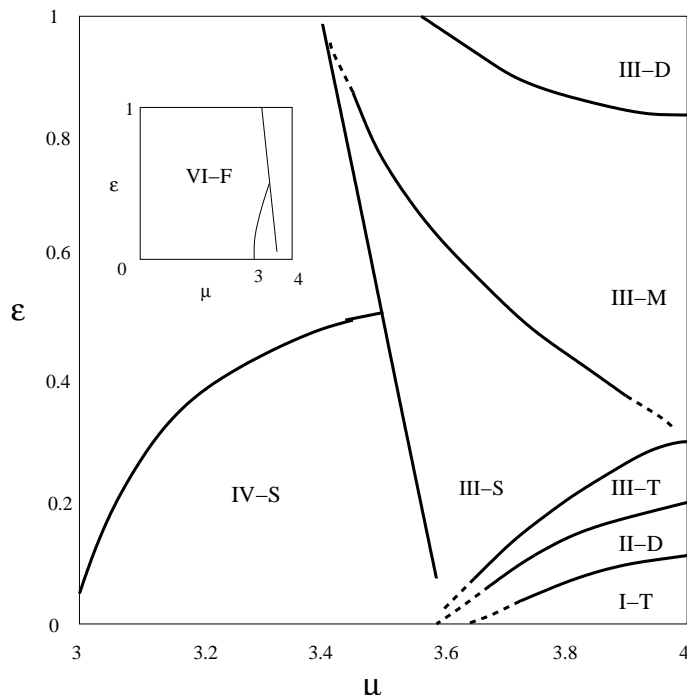


**Figure 3.8:** Phase diagram showing turbulent, phase synchronized and coherent regions in the two parameter space of  $\mu$  and  $\epsilon$  for scale free network for  $f(x) = \mu x(1 - x)$  and  $g(x) = f(x)$ . The determination of region boundaries and their classification and symbols are as explained in Fig. 3.1. Calculations are for  $N = 50, m = 1, T = 100$ . The inset shows the phase diagram for the entire range of parameter  $\mu$  i.e. from 0 to 4.

other networks (with  $f(x) = g(x)$ ) having same degree per node, phase synchronized clusters are observed for small coupling strengths only (region II-D) and not in region III (see e.g. one dimensional nearest neighbor coupled network with degree two per node). It is interesting to note that for the scale-free network and for the nonlinear coupling, largest Lyapunov exponent is always positive (Fig. 3.9) i.e. the whole system remains chaotic but we get phase-synchronized behavior.

### 3.2.3 Dependence on the Number of Connections

So far we have treated the scale free network with  $m = 1$  which gives a tree structure and the number of connections is of the order of the number of nodes ( $N_c = N - 1$ ). As  $m$  increases the number of connections increases. Now we present some results for networks with large number of connections.

For  $m > 1$  and  $g(x) = x$ , though perfect inter- and intra-cluster couplings between

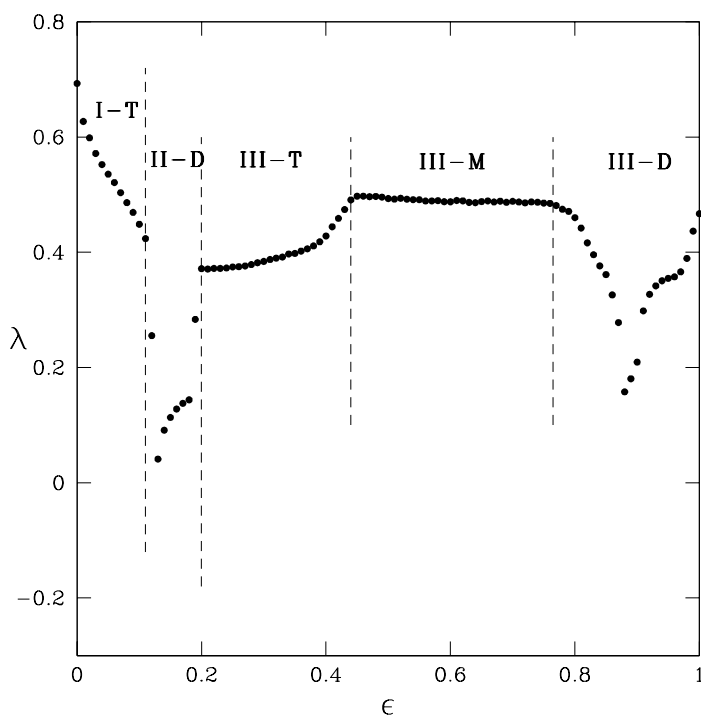


**Figure 3.9:** Largest Lyapunov exponent,  $\lambda$ , is plotted as a function of  $\epsilon$  for scale-free network and  $f(x) = 4x(1-x)$  and  $g(x) = f(x)$ . Different regions are labeled as in Fig. 3.8.

the nodes as displayed in Figs. 3.3(b) and 3.3(d) are no longer observed, the dynamics of Eq. (3.1) leads to a similar phase diagram as in Fig. 3.1 with region II-S dominated by the self-organized synchronization and regions IV-DQ and IV-DP dominated by the driven synchronization. As  $m$  increases the regions I and II are mostly unaffected, but region IV shrinks while region III grows in size. Fig. 3.12 shows different types of clusters in node-node diagram for different coupling strengths. Fig. 3.12(a) is plotted for  $m = 3$  in the variable region ( $\epsilon = 0.19$ ) with nodes forming two clusters. It is clear that synchronization of nodes is mainly because of intra-cluster connections but there are a few inter-cluster connections also. Fig. 3.12(b) is plotted for ordered periodic region at coupling strength  $\epsilon = 0.78$ , here clusters are mainly of driven type but they have intra-cluster connections also. In Figures 3.12(a) and (b) the average degree of a node is 6, and breaking the network into clusters with only inter-cluster or intra-cluster couplings is not possible. As average degree of a node increases further  $f_{intra}$  increases and for  $\epsilon > \epsilon_c$ , we observe dominance of the self-organized behaviour, and when number of connections becomes of the order of

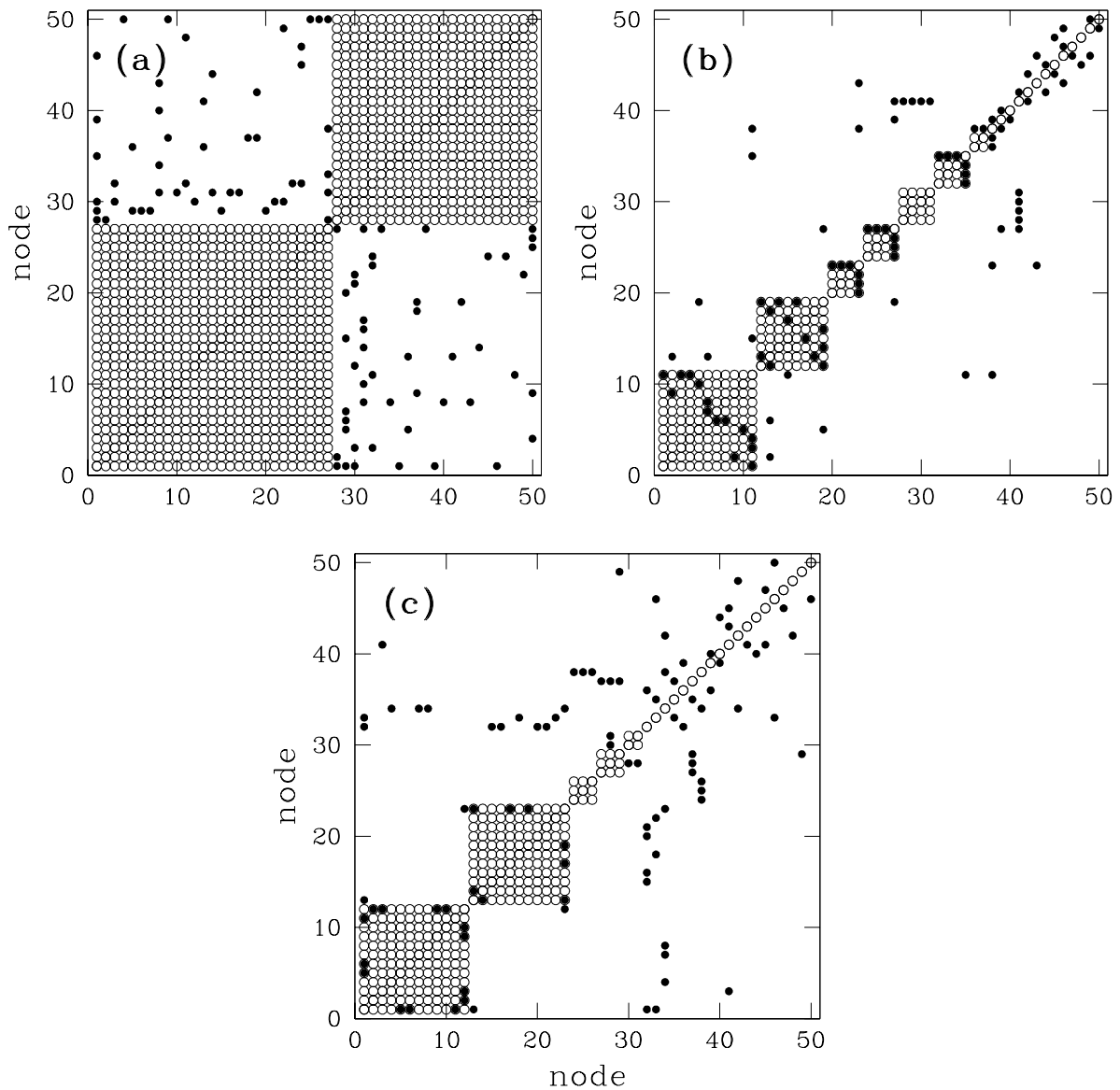


**Figure 3.10:** The figure shows several examples illustrating the phase synchronization for scale-free network with coupling form  $g(x) = f(x)$  using node versus node diagram for  $N = N_c = 50$ . After an initial transient (about 2000 iterates) phase synchronized clusters are studied for  $T = 100$ . The logistic map parameter  $\mu = 4$ . The solid circles show that the two corresponding nodes are coupled and the open circles show that the corresponding nodes are phase synchronized. In each case the node numbers are reorganized so that nodes belonging to the same cluster are numbered consecutively and the clusters get displayed in decreasing sizes. (a) Figure show an ideal driven phase synchronization for  $\epsilon = 0.13$ . (b) Mixed behavior for  $\epsilon = 0.61$ . (c) A dominant driven behavior for  $\epsilon = 0.87$ . The scale free networks were generated with  $N_0 = 1$  and  $m = 1$ .

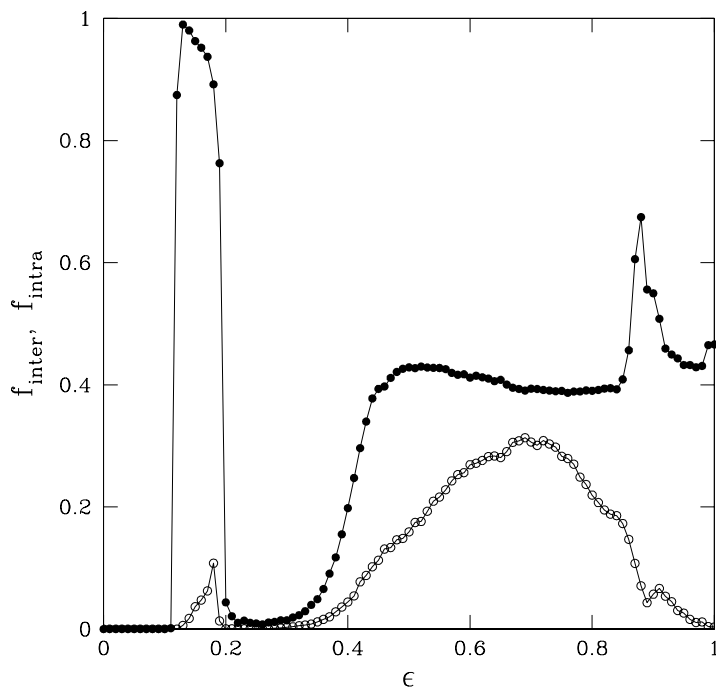


**Figure 3.11:** The fraction of intra-cluster and inter-cluster couplings,  $f_{inter}$  (solid circles) and  $f_{intra}$  (open circle) are shown as a function of the coupling strength  $\epsilon$  for the scale-free networks with  $g(x) = f(x)$ . The figure is obtained by averaging over 20 realizations of the network and 50 random initial conditions for each realization.

$N^2$ , for large values of  $\epsilon$  we get one big synchronized cluster.

For  $m > 1$  and  $g(x) = f(x)$  we get similar kind of behaviour as for  $m = 1$  with dominant driven clusters for most of the coupling strength region, but we do not get any ideal driven clusters. Fig. 3.12(c) is plotted for coupling strength  $\epsilon = 0.9$  and  $m = 3$ . As  $m$  increases, region I showing turbulent behaviour remains unaffected, but mixed region II grows in size while III region shrinks. As  $m$  increases, more and more nodes participate in cluster formation (it is discussed for the 1-d lattice in the section 3.3.1). Self-organized behaviour increases with increase in  $m$ . Fig. 3.12(d) is plotted for  $m = 10$ , all nodes form one cluster which is obviously of the self-organized type.

We have also studied the effect of size of the network on the synchronized cluster formation. The phenomena of self-organized and driven behavior persists for the largest size network that we have studied ( $N = 1000$ ). The region II showing self-organized or driven

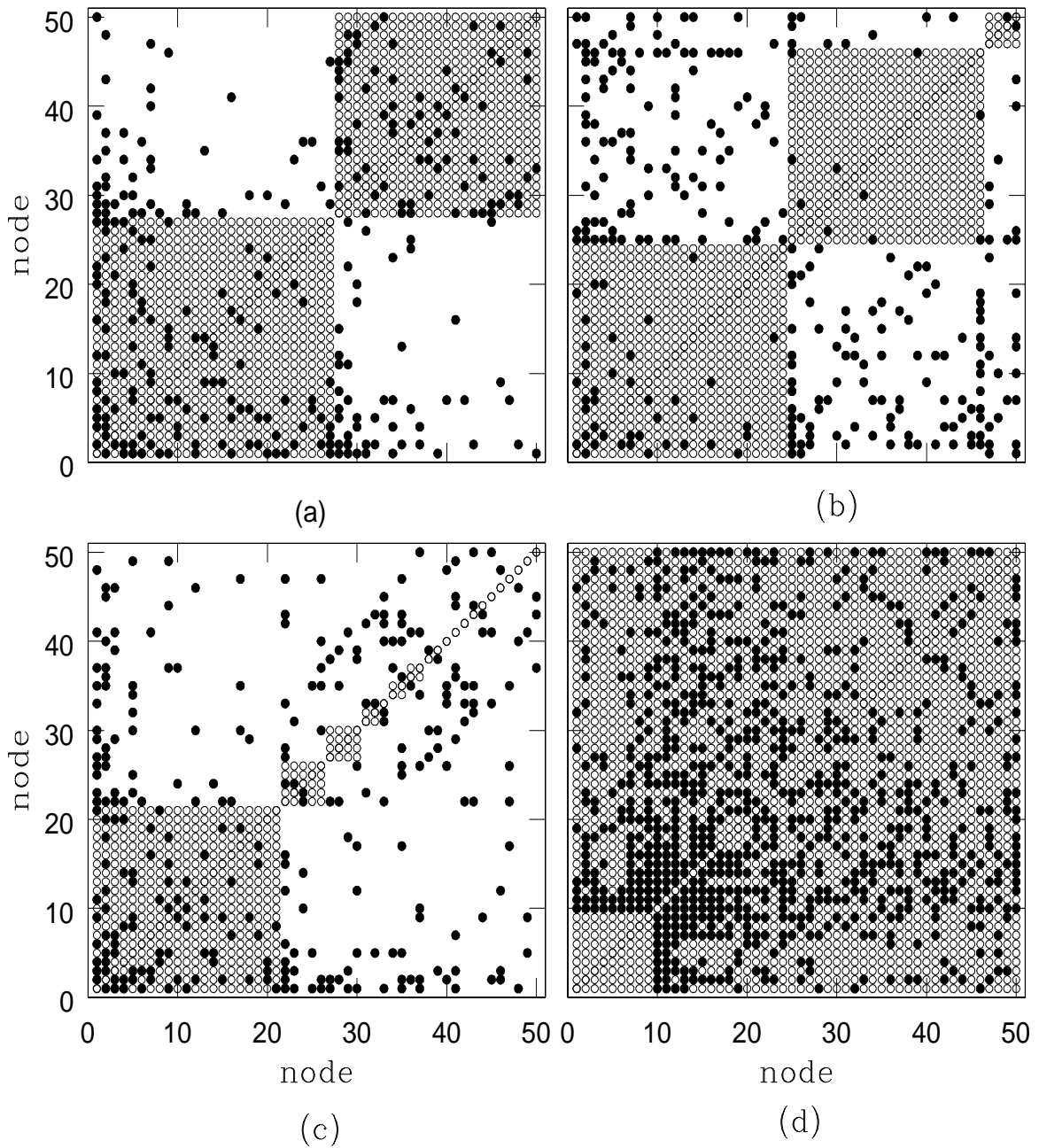


*Figure 3.12: Figure illustrates the cluster formation for the scale-free network as node vs node plot for  $N = 50$  as in Fig. 3.3 but with larger number of connections. (a) and (b) are plotted for  $g(x) = x$  and  $m = 3$  and respectively for  $\epsilon = 0.19$  and  $\epsilon = 0.78$ . (c) and (d) are plotted for  $g(x) = f(x)$ ,  $\epsilon = 0.90$  and respectively for  $m = 3$  and  $m = 10$ .*

behavior is mostly unaffected while the ordered regions showing driven behavior for large coupling strengths show a small shrinkage in size.

### 3.3 Coupled Maps on Other Different Networks

We now consider several other networks and investigate synchronization properties of these networks.

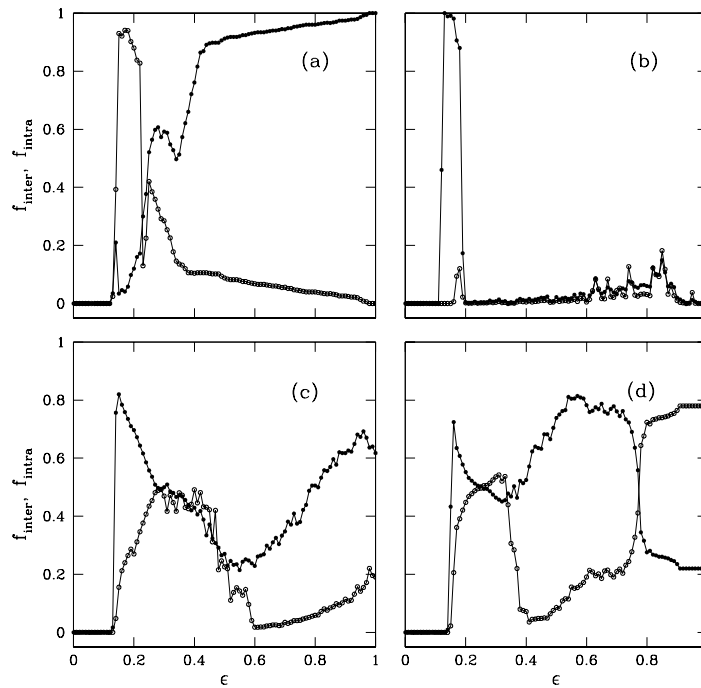


**Figure 3.13:** The fraction of intra-cluster and inter-cluster couplings,  $f_{inter}$  (solid circles) and  $f_{intra}$  (open circles) are shown as a function of the coupling strength  $\epsilon$ . Figures (a) and (b) are for the one-d coupled maps with nearest neighbor coupling ( $m = 1$ ) and for  $g(x) = x$  and  $g(x) = f(x)$  respectively. Figures (c) and (d) are for  $g(x) = f(x)$  and respectively  $m = 5$  and  $m = 10$ . The figures are for  $N = 50$  and are obtained by averaging over 50 random initial conditions.

#### 3.3.1 One-Dimensional Networks

For one dimensional coupled map network, each node is connected with  $m$  nearest neighbors (degree per node is  $2m$ ). First we consider  $m = 1$ , i.e each map is connected with just next neighbors on both sides. Fig. 3.13(a) and (b) show  $f_{intra}$  and  $f_{inter}$  verses  $\epsilon$  for  $g(x) = x$

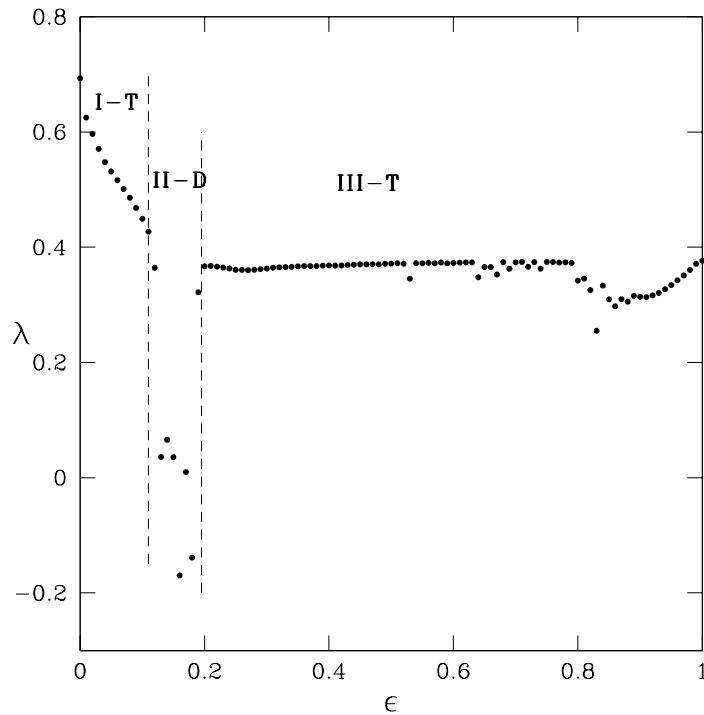


**Figure 3.14:** Largest Lyapunov exponent,  $\lambda$ , is plotted as a function of  $\epsilon$  for 1-d nearest neighbor coupled network for  $f(x) = 4x(1-x)$  and  $g(x) = f(x)$ . Different regions are labeled as for scale-free network (see Fig. 3.8 and Fig. 3.9.)

and  $g(x) = f(x)$  respectively and  $\mu = 4$ ,  $N = 50$ . For  $g(x) = x$ , after an initial turbulent region ( $\epsilon > \epsilon_c$ ), nodes form self-organized clusters (region II-S in Fig. 3.1) and as the coupling strength increases we observe a crossover to the driven clusters. The behaviour of clusters as well as Lyapunov exponent graphs are similar to the scale-free network with the coupling form  $f(x) = x$ . Note that the nearest neighbor coupled map network with  $m = 1$  is a tree and can be geometrically organized into both self-organized and driven type of clusters.

However, for  $g(x) = f(x)$  coupling and  $m = 1$  we observe a considerable deviation from the corresponding behavior for the scale free network. In region I-T of Fig. 3.8, we get turbulent behavior as for the scale-free network but we observe cluster formation only for small coupling strength region (corresponding to region II-D of Fig. 3.8) as seen from Fig. 3.13(b). Fig. 3.14 shows largest Lyapunov exponent as a function of  $\epsilon$  for  $g(x) = f(x)$  and  $\mu = 4.0$ . In region II-D the largest Lyapunov exponent is positive or negative, depending on the initial conditions and  $\epsilon$  values and for the rest of the coupling strength region

Lyapunov exponent is positive. For rest of the coupling strength region, i.e. region III in Fig. 3.8, there is almost no cluster formation and the behavior is close to turbulent and chaotic.

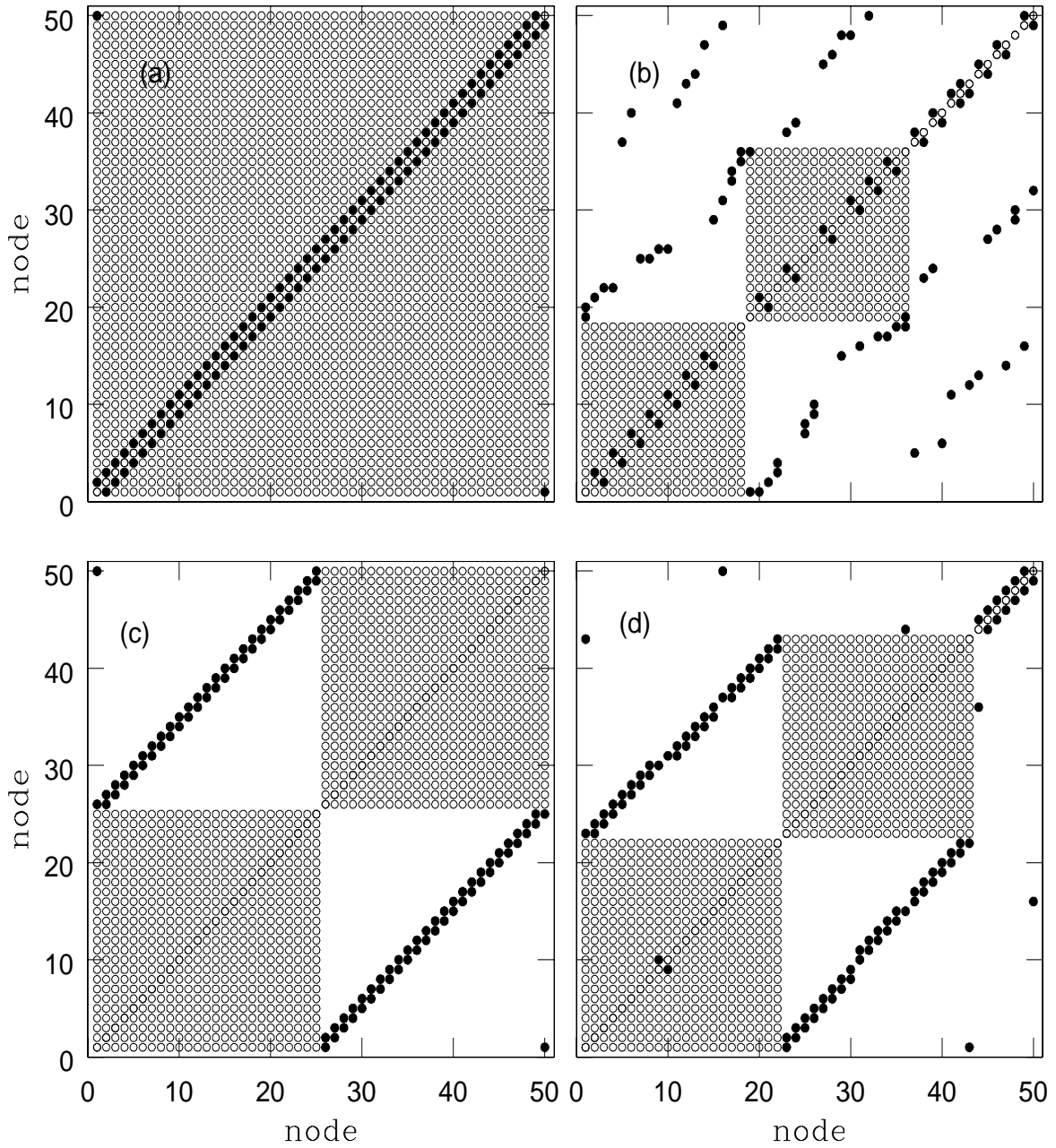
Fig. 3.15 shows node-node plot showing synchronized clusters. Fig. 3.15(a) shows one self-organized cluster in region II-S (see Fig. 3.1) for  $g(x) = x$ . In this region we also get two self-organized clusters depending on the initial values and  $\epsilon$ . Fig. 3.15(b) shows two clusters of mixed type as well as several isolated nodes for  $\epsilon$  in region III-M for  $g(x) = x$ . Figs. 3.15(c) and 3.15(d) show driven clusters for  $g(x) = f(x)$  for  $\epsilon$  values in regions II-D of Fig. 3.14.

We now consider the case  $m > 1$ . For  $g(x) = x$  we observe self-organized clusters with some inter-cluster connections for coupling strength region II-S and as coupling strength increases there is a crossover to driven clusters. As  $m$  increases  $f_{intra}$  increases and for  $\epsilon > \epsilon_c$  we observe dominance of self-organized behaviour and for  $\epsilon > 0.7$  instead of forming driven clusters (as is observed for  $m = 1$ ) nodes form one synchronized cluster. For  $m = 5$ , and for coupling strength  $\epsilon > \epsilon_c (\approx 0.13)$ , all nodes form one or two clusters. For one cluster  $f_{intra} = 1$  and for two clusters intra-cluster and inter-cluster couplings are almost equally distributed. As number of connections increases and typically becomes of the order  $N^2$  that is a globally coupled state, after coupling strength greater than some critical value, we get one cluster of self-organized type.

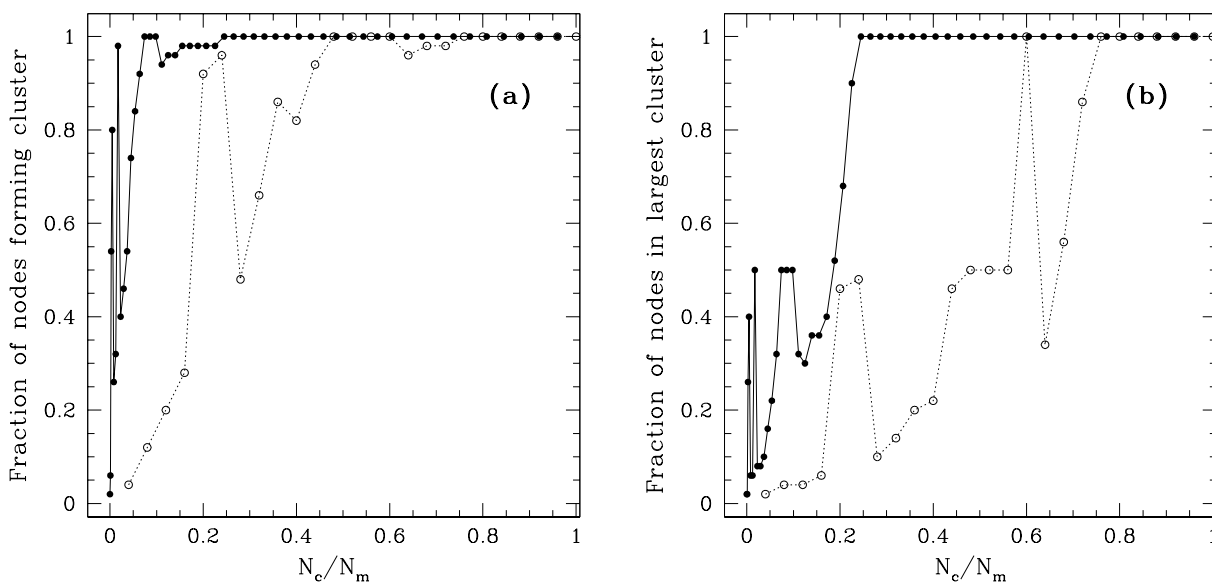
For  $g(x) = f(x)$  and  $m > 1$ , we find that as the number of connections increases for small coupling strength (region II-D) we get two dominant driven phase synchronized clusters. For large coupling strength number of nodes forming clusters and size of cluster both increase with the increase in number of connections in the network. This behaviour is seen in Figs. 3.13(c) and (d) which show  $f_{intra}$  and  $f_{inter}$  verses  $\epsilon$  for  $g(x) = f(x)$ ,  $\mu = 4$  and respectively for  $m = 5$  and  $m = 10$ .

Fig. 3.16(a) shows the fraction of nodes forming clusters as a function of the number of connections  $N_c$  normalized with respect to the maximum number of connections  $N_m = N(N - 1)/2$  for two values of  $\epsilon$ . The overall increase in the number of nodes forming clusters is clearly seen. Fig. 3.16(b) shows the fraction of nodes in the largest cluster as a function  $N_c$  for two values of  $\epsilon$ . The overall growth in the size of the clusters with  $N_c$  is evident.

Cluster formation with large number of connections (of the order of  $N^2$ ) and its depen-



*Figure 3.15: The figure illustrates the cluster formation for one-d nearest neighbor network using node-node plot as in Fig. 3.3. (a) and (b) are for  $g(x) = x$  and  $\epsilon = 0.16$ , and  $\epsilon = 0.30$  respectively. (c) and (d) are for  $g(x) = f(x)$  and  $\epsilon = 0.13$  and  $\epsilon = 0.15$  respectively.*



**Figure 3.16:** Figure (a) shows the fraction of nodes forming clusters as a function of the fraction of couplings  $N_c/N_m$  where  $N_m = N(N - 1)/2$ . The figures are plotted for 1-d coupled maps with  $g(x) = f(x)$  and for  $\epsilon = 0.49$  (closed circles) and  $\epsilon = 0.7$  (open circles). The results are for  $N = 50$  and are obtained by averaging over 100 random initial conditions. Figure (b) shows the fraction of nodes in the largest cluster as a function of  $N_c/N_m$  for  $\epsilon = 0.49$  (closed circles) and  $\epsilon = 0.7$  (open circles). Other parameters are same as above.

dence on coupling strength is discussed in Refs. [148, 149]. It is reported that for these networks it is the coupling strength which affects the synchronized clusters and not the number of connections. We find that when the number of connections is of the order of  $N$  there are significant deviations from this reported behaviour. We find that the size of the clusters and number of nodes forming clusters increases as the number of connections increase as discussed above. This behaviour approaches the reported behaviour as the number of connections increases and becomes of the order of  $N^2$ .

### 3.3.2 Small World Networks

The general construction and properties of small world networks are given in the chapter I. We construct small world networks using the algorithm given by Watts and Strogatz [5]. Here we present results for  $N = 50$  and  $m = 1$ . Figs. 3.17(a) and 3.17(b) plot  $f_{\text{intra}}$  and  $f_{\text{inter}}$  for  $g(x) = x$  and  $g(x) = f(x)$  respectively as a function of  $\epsilon$  for  $\mu = 4$ . We find that for  $g(x) = x$ , behaviour is very similar to that for the scale free networks and one-d lattice. We get self-organized clusters for  $\epsilon > \epsilon_c$  and there is a crossover to driven behavior as

epsilon increases (Fig. 3.17(a) ). But for  $g(x) = f(x)$ , nodes form clusters only for region II-D of coupling strength and there is almost no cluster formation for larger values of  $\epsilon$  ( Fig. 3.17(b) ). This behaviour changes as  $k$  increases and we observe some clusters for large  $\epsilon$  values also. This behavior is similar to that of one-d network. Fig. 3.18(a) shows node-node plot of clusters for  $\epsilon = 0.45$ ,  $m = 1$  and  $g(x) = x$  showing dominant driven clusters.

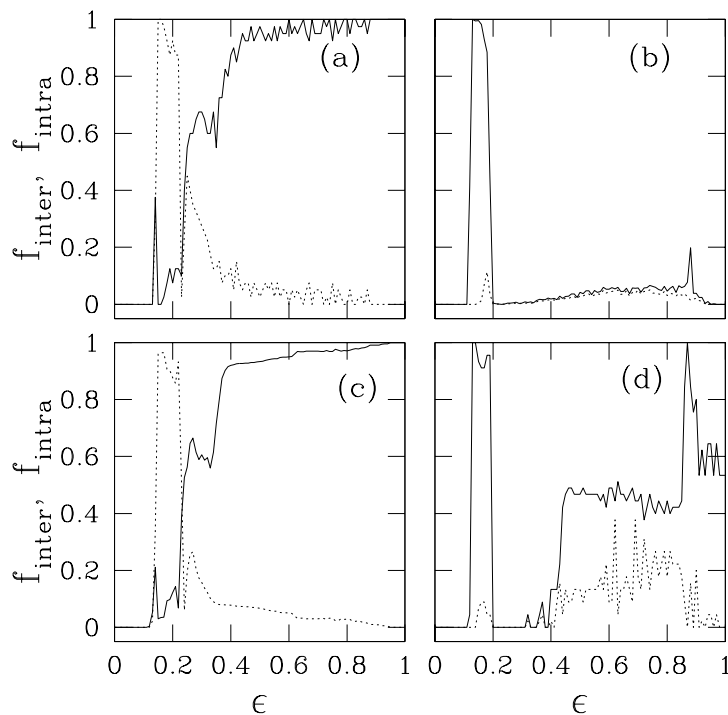


**Figure 3.17:** Fraction of intra-cluster and inter-cluster couplings,  $f_{inter}$  (solid line) and  $f_{intra}$  (dashed line) are shown as a function of the coupling strength  $\epsilon$ . Figures (a) and (b) are for the small world network for  $g(x) = x$  and  $g(x) = f(x)$  respectively and  $N = 50$ . Figures (c) and (d) are for the Cayley tree with  $g(x) = x$  and  $g(x) = f(x)$  respectively and  $N = 47$ . The figures are obtained by averaging over 50 random initial conditions. Small world networks are generated with  $m = 1$  and  $p = 0.06$  [3]. Cayley trees are generated with coordination number three [27].

### 3.3.3 Cayley Trees

Cayley tree is generated using algorithm given in Ref. [140]. Starting with three branches at first level, we split each branch into two at each level. For  $g(x) = x$ , the behaviour is similar to all other networks with same number of connections (Fig. 3.17(c)). Fig. 3.18(b)

shows node-node plot of two ideal driven phase synchronized clusters for  $\epsilon = 0.92$ ,  $\bar{k} = 2$ ,  $N = 47$  and  $g(x) = x$ . For  $g(x) = f(x)$  we get all nodes forming clusters for region II-D, and for larger coupling strengths about 40% of nodes form clusters of driven types (Fig. 3.17)(d)).

### 3.3.4 Higher Dimensional Lattices

Coupled maps on higher dimensional lattices also form synchronized clusters. First we give the result for two-d square lattices. Figs. 3.19(a) and 3.19 (b) plot  $f_{\text{intra}}$  and  $f_{\text{inter}}$  for  $g(x) = x$  and  $g(x) = f(x)$  respectively as a function of  $\epsilon$  for  $\mu = 4$ . For  $g(x) = x$  cluster formation is similar to other networks described earlier except for very large  $\epsilon$  close to one where we get a single self-organized cluster. For  $g(x) = f(x)$  cluster formation is similar to that in one-d networks with nearest and next nearest neighbor couplings. In small coupling strength region II-D (see Fig. 3.8), nodes form two clusters of driven type and for large coupling strength also driven clusters are observed with 25-30% nodes showing synchronized behaviour (Fig. 3.19(b)). Fig. 3.18(c) and (d) show node-node plot of self-organized behaviour for  $g(x) = x$  and dominant driven behaviour for  $g(x) = f(x)$ .

Coupled maps on three-d cubic lattice (degree per node is six) for  $g(x) = x$  show clusters similar to the other networks discussed earlier. For  $g(x) = f(x)$ , nodes form driven type of clusters at small coupling strength (region II-D) and mainly it gives three clusters. For large coupling strength also nodes form driven clusters and the nodes participating in cluster formation is now much larger than two-d case.

### 3.3.5 Random Networks

Random networks are constructed by connecting each pair of nodes with probability  $p$ . First consider the case where the average degree per node is two. For linear coupling  $g(x) = x$  cluster formation is same as for other networks with same average degree. For  $g(x) = f(x)$  driven type clusters are observed in region II-D and no significant cluster formation is observed for larger coupling strengths. This behaviour is similar to one-d network with  $k = 2$  but different from the corresponding scale free network. For coupled maps on random networks with average degree per node equal to four and  $g(x) = f(x)$ , clusters with dominant driven behaviour are observed for all  $\epsilon > \epsilon_c$ .

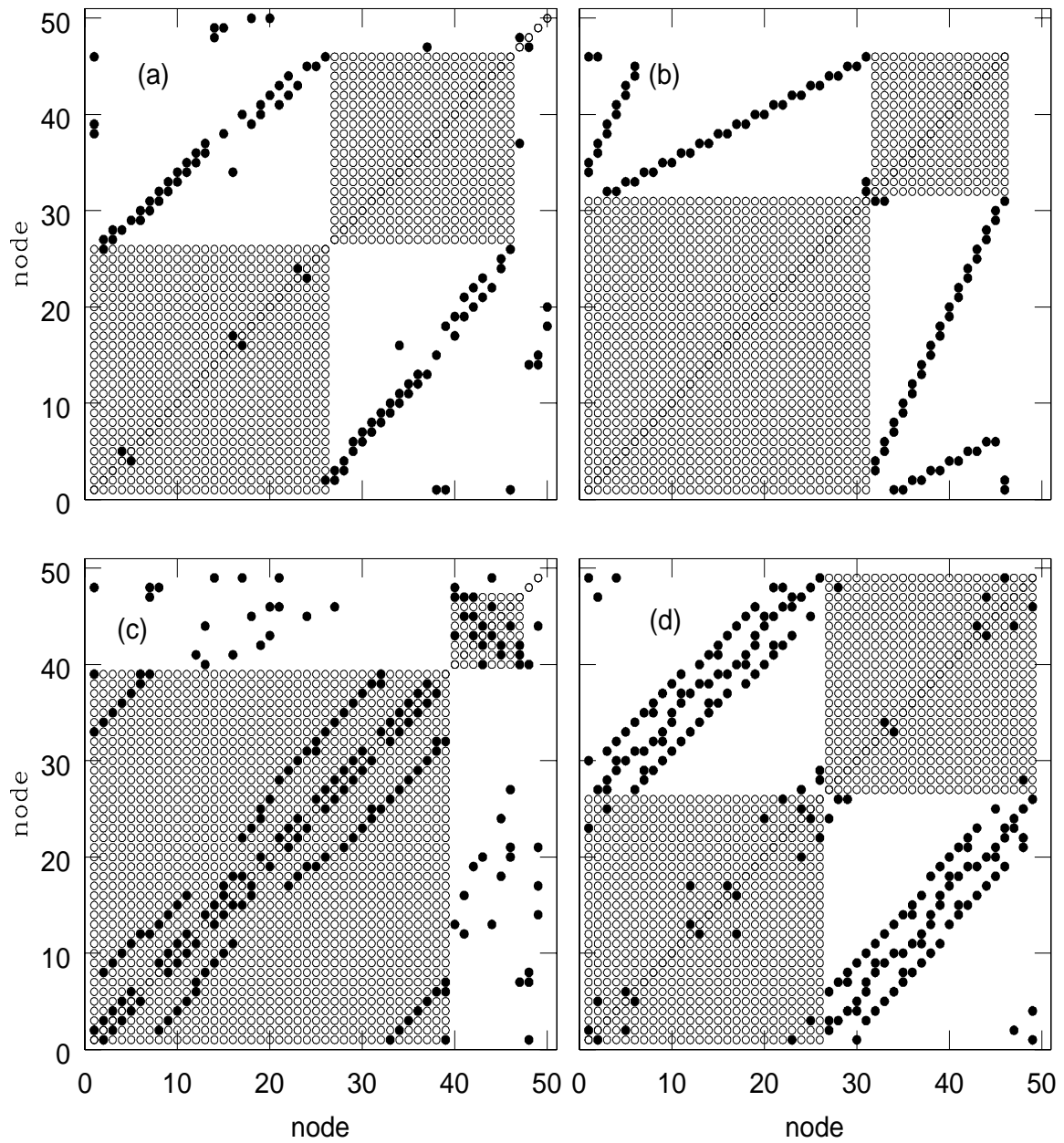


**Figure 3.18:** Figure illustrates the cluster formation for different networks as node vs node plot as in Fig. 3.3. (a) is plotted for small world network with  $\epsilon = 0.45$ ,  $N = 50$  and  $g(x) = x$ . (b) is plotted for Cayley tree with  $\epsilon = 0.92$ ,  $N = 47$  and  $g(x) = x$ . (c) and (d) are plotted for 2-d lattice ( $N = 49$ ) with  $\epsilon = 0.21$ ,  $g(x) = x$  and  $\epsilon = 0.19$ ,  $g(x) = f(x)$  respectively.

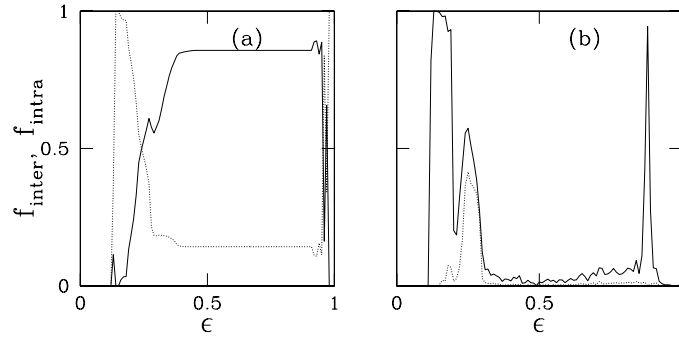


**Figure 3.19:** The fraction of intra-cluster and inter-cluster couplings,  $f_{inter}$  (solid line) and  $f_{intra}$  (dashed line) are shown as a function of the coupling strength  $\epsilon$  for two-d lattice. Figures (a) and (b) are for  $g(x) = x$  and  $g(x) = f(x)$  respectively. The figures are for  $N = 49$  and are obtained by averaging over 50 random initial conditions.

### 3.4 Examples of Self-organized and Driven Behavior

There are several examples of self-organized and driven behaviour in naturally occurring systems. An important example in physics that includes both self-organized and driven behavior, is the nearest neighbor Ising model treated as Kawasaki dynamics. As the strength of the Ising interaction between spins changes sign from positive to negative there is a change of phase from a ferromagnetic (self-organized) to an antiferromagnetic (driven) behavior. In the antiferromagnetic state, i.e. driven behavior, the lattice splits into two sub-lattices with only inter-cluster interactions and no intra-cluster interactions.

Self-organized behaviour is more common and is easily observed. Examples are social, ethnic and religious groups, political groups, cartel of industries and countries, herds of animals and flocks of birds, different dynamic transitions such as self-organized criticality etc. The driven behaviour is not so common. An interesting example is the behaviour of fans during a match between traditional rivals. Before the match the fans may act as individuals (turbulent behavior) or form self-organized clusters such as a single cluster of fans of the game or several clusters of fans of different star players. During the match there can be a crossover to a driven behaviour. When the match reaches a feverish pitch, i.e. the strength of the interaction increases, the fans are likely to form two phase synchronized groups. The response of the two groups will be anti-phase synchronized with each other.

### 3.5 Circle Map

We have studied cluster formation by considering circle map as defining the local dynamics, given by

$$f(x) = x + \omega + (k/2\pi)\sin(2\pi x), \quad (\text{mod } 1)$$

Due to the modulo condition, instead of using the variable  $x_t$ , we use a function of  $x_t$  such as  $\sin(\pi x_t)$  satisfying periodic boundary conditions to decide the location of maxima and minima which are used to determine the phase synchronization of minima which are used to determine the phase synchronization of two nodes (Eq. (2.4)). With circle map also we observe formation of clusters with the time evolution starting from initial random conditions. Here we discuss the results with the parameters of the circle map in the chaotic region ( $\omega = 0.44$  and  $k = 6$ ). For linear coupling  $g(x) = x$  and scale-free networks with  $m = 1$ , for small coupling strength nodes evolve chaotically with no cluster formation. As coupling strength increases nodes form clusters for  $0.21 < \epsilon < 0.25$ . In most of this region the nodes form two cluster and these clusters are mainly of the driven type except in the initial part,  $\epsilon \approx 0.21$ , where self-organized clusters can be observed. As the coupling strength increases nodes behave in a turbulent manner and after  $\epsilon > 0.60$  nodes form clusters of dominant driven type. Here the number of nodes forming clusters and the sizes of clusters, both are small. For the one dimensional linearly coupled networks, for linear coupling the nodes form phase synchronized clusters for coupling strength region  $0.21 < \epsilon < 0.25$ . The clusters are mainly of the driven type except in the initial part,  $\epsilon \approx 0.21$ , where they are of the self-organized type. For large coupling strength they do not show any cluster formation.

For  $g(x) = f(x)$  we found very negligible cluster formation for the entire range of the coupling strength for both scale free and one-d network. However, as  $m$  increases the nodes form phase synchronized clusters for  $\epsilon$  larger than some critical  $\epsilon_c$ .

For the circle map the normalization factor  $(1 - \epsilon)$  in the first term of Eq. (3.1) is not necessary and the following modified model can also be considered.

$$x_{t+1}^i = f(x_t^i) + \frac{\epsilon}{k_i} \sum_{j=1}^N C_{ij} g(x_t^j), \quad (\text{mod } 1). \quad (3.3)$$

We now discuss the synchronized cluster formation for the same parameter values as above ( $\omega = 0.44$  and  $k = 6$ ) for this modified model. For linear coupling, clusters are

formed only for  $0.02 < \epsilon < 0.17$  with dominant self-organized behaviour for most of the range except near  $\epsilon \approx 0.17$  where the behaviour is of dominant driven type. For the scale free networks ( $m = 1$ ) we have ordered states while for the one-d networks we have partially ordered states. For nonlinear coupling, the clusters are formed for  $0.0 < \epsilon < 0.09$ . The scale-free networks show mostly mixed type clusters while one-d networks show dominant self-organized clusters. There is no cluster formation for larger coupling strengths for both linear and nonlinear coupling. However, as for the logistic map, as the number of connections increases, synchronized clusters are observed for large  $\epsilon$  values.

### 3.6 Summary

We study the properties of coupled dynamical elements on different types of networks. We find that in the temporal evolution, dynamical elements show the formation of phase synchronized clusters. We have mainly studied networks with small number of connections ( $N_c \sim N$ ). With small number of connections, it is easy to identify the relation between the dynamical evolution, the cluster formation and the geometry of networks.

We identify two mechanisms of cluster formation, self-organized (s) and driven (d) phase synchronization. Apart from dominant s- and d- synchronization, we observe ideal behaviour of both types that is all the nodes forming driven clusters ( $f_{inter} = 1$ ) or all nodes forming self-organized clusters ( $f_{inter} = 1$ ). For the local dynamics in the chaotic regime, in most cases where ideal behaviour is observed, the largest Lyapunov exponent is negative or zero giving stable clusters giving periodic evolution. However, in some cases ideal behaviour is also observed in the chaotic region.

By defining different states of the dynamical system using the number and type of clusters, we consider the phase-diagram in the  $\mu - \epsilon$  plane for the local dynamics governed by the *logistic map*. When the local dynamics is in the chaotic region, for small coupling strengths we observe turbulent behaviour. There is a critical value  $\epsilon_c$  above which phase synchronized clusters are observed. For  $g(x) = x$  type of coupling, self-organized clusters are formed when the strength of the coupling is small. As the coupling strength increases there is a crossover from the self-organized to the driven behavior which also involves re-organization of nodes into different clusters. This behaviour is almost independent of the type of networks. For non linear coupling of type  $g(x) = f(x)$ , for small coupling strength

phase synchronized clusters of driven type are formed, but for large coupling strength number of nodes forming cluster as well as size of cluster both are very small and almost negligible for many network. Only for scale-free networks and Cayley tree show some cluster formation for large coupling strengths. In the partially ordered regions synchronized clusters are associated with isolated nodes which do not belong to any cluster. Some of these nodes are of *floating type*, the time spent by a floating node in the synchronized cluster shows an exponential distribution.

It is interesting to note that nodes can form two or more stationary clusters even though coupled dynamics is in the chaotic regime. Here a stationary cluster means that constituents of the cluster are unique and once nodes form a stationary cluster they belong to that cluster forever, that is the structure of the cluster does not depend on time. For  $\mu = 4$ , we get stationary clusters when the nodes form two clusters, but they are not stationary when they form three or more clusters. Note that three or more stationary clusters can be formed for  $\mu < 4$ . For  $\mu = 4$  if the largest Lyapunov exponent is negative, the variables show periodic behaviour with even period. For  $\mu < 4$  the periodic behaviour can have both odd and even periods.

As the number of connections increases, most of the clusters become of the mixed type where both the mechanisms contribute. We find that in general, the self-organized behaviour is strengthened and also the number of nodes forming clusters as well as the size of clusters increase. As the number of connections become of the order of  $N^2$ , self-organized behaviour with a single spanning cluster is observed for  $\epsilon$  larger than some value.

## Chapter 4

# Temporal Dynamics and Synchronization in CMNs: Stability Analysis

---

---

### 4.1 Introduction

In this chapter we study the dynamics of some simple networks analytically and numerically with a view to get a better understanding of the two mechanisms of the cluster formation discussed in the previous chapter. Mainly we study the asymptotic stability of self-organized and driven synchronization in networks with small number of nodes, i.e. two and three nodes, and extension of these small networks to networks with large number of nodes. As an example of large networks showing self-organized synchronized clusters we take globally coupled maps [112, 113, 114] and for driven synchronized clusters we take complete bipartite coupled maps [151] and multipartite coupled maps.

Here in this chapter we will mostly concentrate on exact synchronization. Though the numerical work in the previous chapter was carried out using phase synchronization, it is not easy to treat phase synchronization analytically and hence, for the analytical work we restrict ourselves to exact synchronization. Interestingly the phase diagrams for exact synchronization have considerable similarity with that of phase synchronization. Thus some general conclusions can be drawn from the analytical studies.

We use two types of analysis to determine the stability of synchronized state. First is the linear stability analysis [97, 135, 128, 122, 123, 124, 125, 126] and the second is Lyapunov functional [152, 153]. We briefly discuss these two methods.

### 4.1.1 Linear Stability Analysis

If Jacobian matrix  $\mathbf{J}_t$  (see ‘Measure of Chaos’ in Chapter I), corresponding to evolution of tangent vector is a diagonal matrix, or the similarity transformation which diagonalizes  $\mathbf{J}_t$  is independent of  $t$ , then the Lyapunov exponents can be written in terms of the eigenvalues of  $\mathbf{J}_t$  as follows,

$$\lambda_i = \lim_{\tau \rightarrow \infty} \frac{1}{\tau} \sum_{t=1}^{\tau} \ln |\Lambda_i(t)| \quad (4.1)$$

where  $\Lambda_i(t)$  is the  $i$ -th eigenvalue of Jacobian matrix at time  $t$ . If  $J_t$  does not satisfy the above mentioned conditions then it is necessary to consider product of Jacobian matrices to obtain Lyapunov exponents (see chapter I).

To study the stability of synchronized state it is sufficient to consider transverse Lyapunov exponents which characterize the behavior of infinitesimal vectors transversal to the synchronized manifold, and these determine the stability of a synchronized state [152]. If all the transverse Lyapunov exponents are negative then the synchronized state is stable.

### 4.1.2 Global Stability Analysis

Condition for global stability can be derived using the Lyapunov functional methods [152, 153]. Global stability in a neighborhood of an equilibrium (stable) point is confirmed if there exist a positive definite function defined in that neighborhood, whose total time derivative is negative semi-definite.

To get the conditions for the global stability of synchronization of two trajectories  $x_t^i$  and  $x_t^j$ , we define Lyapunov function as,

$$V_t^{ij} = (x_t^i - x_t^j)^2 \quad (4.2)$$

Clearly  $V_{ij}(t) \geq 0$  and the equality holds only when the nodes  $i$  and  $j$  are exactly synchronized. For the asymptotic global stability of the synchronized state, Lyapunov function should satisfy the following condition in the region of stability,

$$V_{t+1} < V_t$$

This condition can also be written as,

$$\frac{V_{t+1}}{V_t} < 1. \quad (4.3)$$

The chapter is organized as follows. After giving the introduction of linear stability analysis and Lyapunov function analysis in the first section, in section 4.2, we discuss two networks showing self-organized synchronization, i.e. two nodes network and globally connected network. Section 4.3 considers two networks showing driven synchronization, i.e. three nodes bipartite network and complete bipartite network. In these sections we study coupled maps dynamics using linear stability and Lyapunov function analysis. In section 4.4, we discuss the origin of self-organized and driven mechanisms based on analysis presented in the earlier sections. In section 4.5, we present our results for coupled dynamics on multipartite networks. It is just a extension of coupled dynamics on bipartite networks and both the analysis remain almost same except few changes because of extra dimensionality introduced by the multipartite structure of the multipartite networks. Section 4.6 discuss the origin of floating node. Section 4.7 summarizes the chapter.

## 4.2 Stability Analysis for Self-organized Synchronization

We first consider the simplest and smallest network showing self-organized clusters, i.e synchronization of two coupled nodes which is obviously of self-organized type. As a generalization of two nodes network to larger networks, we study the self-organized synchronization in globally coupled maps.

### 4.2.1 Coupled Network with $N = 2$

We begin by taking the simplest case where number of nodes is two and these two nodes are coupled with each other [151]. The dynamics of the two nodes can be rewritten as (Eq. (2.1)),

$$\begin{aligned}x_{t+1}^1 &= (1 - \epsilon)f(x_t^1) + \epsilon g(x_t^2) \\x_{t+1}^2 &= (1 - \epsilon)f(x_t^2) + \epsilon g(x_t^1)\end{aligned}\tag{4.4}$$

### Linear stability analysis

Following Ref. [19], we first define addition and difference variables as follows,

$$\begin{aligned} s_t &= \frac{x_t^1 + x_t^2}{2} \\ d_t &= \frac{x_t^1 - x_t^2}{2} \end{aligned} \quad (4.5)$$

Dynamical evolution for these newly defined variables is given by,

$$\begin{aligned} s_{t+1} &= \frac{1-\epsilon}{2}[f(s_t + d_t) + f(s_t - d_t)] \\ &\quad + \frac{\epsilon}{2}[g(s_t + d_t) + g(s_t - d_t)] \\ d_{t+1} &= \frac{1-\epsilon}{2}[f(s_t + d_t) - f(s_t - d_t)] \\ &\quad - \frac{\epsilon}{2}[g(s_t + d_t) - g(s_t - d_t)] \end{aligned} \quad (4.6a)$$

For synchronous orbits to be observed, the fully synchronized state  $d_t = 0$  i.e.  $x_t^1 = x_t^2 = x_t = s_t$ , should be a stable attractor. The Jacobian matrix for the synchronized state is,

$$J_t = \begin{pmatrix} (1-\epsilon)f'(x_t) + \epsilon g'(x_t) & 0 \\ 0 & (1-\epsilon)f'(x_t) - \epsilon g'(x_t) \end{pmatrix}$$

where the prime indicates the derivative of the function. The above Jacobian is a diagonal matrix and Lyapunov exponents can be easily written in terms of eigenvalues of product of such Jacobian matrices calculated at different time. The two Lyapunov exponents are

$$\lambda_{s,d} = \lim_{\tau \rightarrow \infty} \frac{1}{\tau} \sum_{t=1}^{\tau} \ln |(1-\epsilon)f'(x_t) \pm \epsilon g'(x_t)| \quad (4.7)$$

The synchronous orbits are stable if Lyapunov exponent corresponding to the difference variable  $d_t$ , i.e.  $\lambda_d$  or the transverse Lyapunov exponent, is negative. If the other Lyapunov exponent  $\lambda_s$  is positive then the synchronous orbits are chaotic while if it is negative then they are periodic.

Coupling function  $g(x) = f(x)$ : Two coupled maps with  $g(x) = f(x)$  type of coupling are studied extensively in the literature both analytically and numerically [19, 122]. For the synchronized state Lyapunov exponent  $\lambda_s$  is nothing but the Lyapunov exponent for uncoupled logistic map ( $\lambda_u$ ) and the other Lyapunov exponent can be written in terms of

the  $\lambda_u$  and from Eq. (4.7) we get,

$$\lambda_s = \lambda_u = \lim_{\tau \rightarrow \infty} \frac{1}{\tau} \sum_{t=1}^{\tau} \ln |f'(x_t)| \quad (4.8a)$$

$$\lambda_d = \ln |1 - 2\epsilon| + \lambda_u \quad (4.8b)$$

The synchronous orbits are stable if Lyapunov exponent corresponding to the difference variable  $d_t$  is negative, i.e.  $\lambda_d < 0$ . Thus the range of stability of the synchronized state is given by

$$\frac{1 - e^{-\lambda_u}}{2} < \epsilon < 0.5 \frac{1 + e^{-\lambda_u}}{2} \quad (4.9)$$

For logistic map with  $\mu = 4$ , above expression gives  $0.25 < \epsilon < 0.75$ , as the range for the stability of the synchronized state.

Coupling function  $g(x) = x$ : For  $g(x) = x$  type of coupling, numerical results show that as the coupled nodes evolve, dynamics shows different types of synchronized and periodic behaviors depending upon the coupling strength  $\epsilon$  and the parameter of the map  $f$ . First let us start with the general case where coupled dynamics lies on a synchronized attractor. Using Eq. (4.7), Lyapunov exponents can be easily written as

$$\lambda_{s,d} = \lim_{\tau \rightarrow \infty} \frac{1}{\tau} \sum_{t=1}^{\tau} \ln |(1 - \epsilon)f'(s_t) \pm \epsilon|$$

For stable synchronous orbits Lyapunov exponent corresponding to the difference variable, i.e.  $\lambda_d$ , should be negative. Now we consider some special cases, when coupled dynamics lies on periodic or fixed point attractor.

We will restrict ourselves to period two orbits. Higher periodic orbits exist but are difficult to treat analytically. Also major features of phase diagram are understood by using fixed point and period two orbits.

*Case I. Synchronization to period two orbit*: Consider the special case where the solution of Eq. (4.4) or Eq. (4.6a) is a periodic orbit of period two, with the difference variable given by  $d_{t+1} = d_t = 0$  and addition variable given by  $s_{t+2} = s_t = s_1$ ,  $s_{t+3} = s_{t+1} = s_2$ . Eigenvalues for the product matrix  $J_1 J_2$ , where  $J_1$  and  $J_2$  are Jacobian matrices for consecutive time steps, are given by

$$\Lambda_{1,2} = (1 - \epsilon)^2 f'_1 f'_2 + \epsilon^2 \pm (1 - \epsilon)\epsilon(f'_1 + f'_2) \quad (4.10)$$

where  $f'_1$  and  $f'_2$  are derivatives of  $f$  at the two periodic points  $(s_1, d = 0)$  and  $(s_2, d = 0)$  respectively. The  $\epsilon$  range for which the dynamical evolution gives a stable periodic orbit, is

obtained when the modulus of the eigenvalues for matrix  $J_1 J_2$  are less than one. For local dynamics given by logistic map  $f(x) = \mu x(1 - x)$ , the two periodic points are,

$$s_{1,2} = \frac{1 + \epsilon + \mu(1 - \epsilon) \pm \sqrt{\epsilon(\epsilon - 2)(\mu - 1)^2 - 3 - 2\mu + \mu^2}}{2\mu(1 - \epsilon)} \quad (4.11)$$

For  $\mu = 4$ ,

$$s_{1,2} = \frac{5 - 3e + \sqrt{5 - 18e + 9e^2}}{8(1 - e)} \quad (4.12)$$

which gives the coupling strength range  $0.18.. < \epsilon < 0.24..$  for which the periodic orbit,  $(s_1, d = 0)$  and  $(s_2, d = 0)$ , is stable.

*Case II. Attractor on period two orbit:* There is a range of  $\epsilon$  values that give the following stable period two behaviour,

$$\begin{aligned} x_t^1 &= x_{t+1}^2 = x_{t+2}^1 = X_1^p, \\ x_t^2 &= x_{t+1}^1 = x_{t+2}^2 = X_2^p \end{aligned}$$

Lyapunov exponents for this periodic state can be found from the eigenvalues of the product of Jacobians at the two periodic points. Jacobian matrix at  $(X_1^p, X_2^p)$  is given by,

$$J_1 = \begin{pmatrix} (1 - \epsilon)f_1' & \epsilon \\ \epsilon & (1 - \epsilon)f_2' \end{pmatrix} \quad (4.13)$$

where  $f_1'$  and  $f_2'$  are the derivative of  $f$  at  $X_1^p$  and  $X_2^p$  respectively. Eigenvalues of the product matrix  $J_1 J_2$  are,

$$\Lambda_{1,2} = \left( \epsilon \pm (1 - \epsilon) \sqrt{f_1' f_2'} \right)^2 \quad (4.14)$$

If  $f_1' f_2' < 0$  which is the interesting case, then the condition for the stability of the periodic orbit become

$$\frac{f_1' f_2' - 1}{f_1' f_2' + 1} < \epsilon < 1. \quad (4.15)$$

For  $f(x) = \mu x(1 - x)$ ,  $X_1^p$  and  $X_2^p$  which satisfy Eq. (4.13) are given by

$$X_{1,2}^p = \frac{(1 + \frac{1}{\mu}) \pm \sqrt{(1 + \frac{1}{\mu})^2 - \frac{4}{\mu}(1 + \frac{1}{\mu})}}{2} \quad (4.16)$$

For stable periodic orbits modulus of both eigenvalues  $\Lambda_1$  and  $\Lambda_2$  are less than one which gives the coupling strength range for stability as,

$$1 - \frac{2}{\mu^2 - 2\mu - 3} < \epsilon \leq 1 \quad (4.17)$$

For  $\mu = 4$ , we get coupling strength range ( $0.6 < \epsilon < 1$ ) for which periodic orbit as given in Eq. (4.13) is stable and coupled dynamics lies on a periodic attractor.

### Lyapunov function analysis

From Eqs. (4.2) and (4.4), Lyapunov function for two nodes is written as

$$\begin{aligned} V_{t+1}^{12} &= V_{t+1} \\ &= [(1 - \epsilon)(f(x_t^1) - f(x_t^2)) - \epsilon(g(x_t^1) - g(x_t^2))]^2 \end{aligned} \quad (4.18)$$

Using Taylor expansion of  $f(x_t^1)$  and  $g(x_t^1)$  about  $x_t^2$ , we get Lyapunov function at time  $t + 1$  as,

$$\begin{aligned} V_{t+1} &= V_t [(1 - \epsilon)f'(x_t^2) - \epsilon g'(x_t^2) \\ &\quad + \frac{x_t^1 - x_t^2}{2} ((1 - \epsilon)f''(x_t^2) - \epsilon g''(x_t^2)) + \mathcal{O}(x_t^1 - x_t^2)^2]^2 \end{aligned} \quad (4.19)$$

If the expression in the square bracket on the RHS is less than one then the synchronized state is stable.

For the nonlinear coupling function  $g(x) = f(x)$  the expression (4.19) for Lyapunov function simplifies and we get

$$\frac{V_{t+1}}{V_t} = (1 - 2\epsilon)^2 [f'(x_t^2) \frac{x_t^1 - x_t^2}{2} f''(x_t^2) + \mathcal{O}(x_t^1 - x_t^2)^2]^2 \quad (4.20)$$

If the expression in the square bracket on the RHS is bounded then there will always some range of  $\epsilon$  values around 0.5 for which the synchronized state will be stable. For logistic map  $f(x) = \mu x(1 - x)$ , we get,

$$V_{t+1} = V_t (1 - 2\epsilon)^2 \mu^2 [1 - (x_t^1 + x_t^2)]^2$$

Using  $0 \leq x_t^1 + x_t^2 \leq 2$ , we get the following range of  $\epsilon$  values for which the synchronization condition given by Eq. (4.3) is satisfied,

$$\frac{1}{2} \left(1 - \frac{1}{\mu}\right) < \epsilon < \frac{1}{2} \left(1 + \frac{1}{\mu}\right) \quad (4.21)$$

For  $\mu = 4$ , it gives the coupling strength range  $0.325 < \epsilon < 0.675$ . However, a better  $\epsilon$  range can be obtained by putting more realistic bounds for  $x_t^1 + x_t^2$  as

$$\frac{1}{2} \left(1 - \frac{1}{\mu X}\right) < \epsilon < \frac{1}{2} \left(1 + \frac{1}{\mu X}\right) \quad (4.22)$$

where  $X = \sup_t (|1 - x_t^1 - x_t^2|)$ .

### 4.2.2 Globally Coupled Networks

Globally coupled networks have all pairs of nodes connected to each other i.e. number of connections,  $N_c = N(N - 1)/2$  where  $N$  is the number of nodes. For such global coupling we write our dynamical model as

$$x_{t+1}^i = (1 - \epsilon)f(x_t^i) + \frac{\epsilon}{N-1} \sum_{j \neq i, j=1}^N g(x_t^j) \quad (4.23)$$

Let the state  $x_t^1 = x_t^2 = \dots = x_t^N = x_t$  be the fully synchronized state. We now consider the stability of this state.

#### Linear Stability Analysis

Jacobian matrix at time  $t$  for the fully synchronized state is

$$J_t = \begin{pmatrix} (1 - \epsilon)f'_t & \frac{\epsilon}{N-1}g'_t & \dots & \frac{\epsilon}{N-1}g'_t \\ \frac{\epsilon}{N-1}g'_t & (1 - \epsilon)f'_t & \dots & \frac{\epsilon}{N-1}g'_t \\ \vdots & \vdots & \ddots & \vdots \\ \frac{\epsilon}{N-1}g'_t & \frac{\epsilon}{N-1}g'_t & \dots & (1 - \epsilon)f'_t \end{pmatrix}$$

where  $f'_t$  and  $g'_t$  are the derivative at the synchronous value  $x_t$ . Eigenvectors of the above Jacobian matrix are,

$$E_n = \left( \exp(2\pi i \frac{m}{N}), \exp(4\pi i \frac{m}{N}), \dots, \exp(2N\pi i \frac{m}{N}) \right)^T$$

where  $m = 0, 1, \dots, N - 1$  and  $T$  denotes the transpose. From these eigenvectors we find that  $J_t$  has an eigenvalue  $(1 - \epsilon)f'_t + \epsilon g'_t$  and  $(N - 1)$ -fold degenerate eigenvalues  $(1 - \epsilon)f'_t - \frac{\epsilon}{N-1}g'_t$ . Lyapunov exponents can be written in terms of the eigenvalues of the Jacobian matrix as,

$$\lambda_1 = \lim_{\tau \rightarrow \infty} \frac{1}{\tau} \sum_{t=1}^{\tau} \ln |(1 - \epsilon)f'_t + \epsilon g'_t| \quad (4.24a)$$

$$\begin{aligned} \lambda_2 &= \lambda_3 \dots = \lambda_N \\ &= \lim_{\tau \rightarrow \infty} \frac{1}{\tau} \sum_{t=1}^{\tau} \ln \left| (1 - \epsilon)f'_t - \frac{\epsilon}{N-1}g'_t \right| \end{aligned} \quad (4.24b)$$

Lyapunov exponents  $\lambda_2, \lambda_3 \dots \lambda_n$  are transverse Lyapunov exponents since they characterize the behaviour of infinitesimal vectors transverse to the synchronization manifold.

For the stability of the synchronous orbits, all transverse Lyapunov exponents should be negative.

Coupling function  $g(x) = f(x)$ : Linear stability analysis of the globally coupled maps for the fully synchronous state, are studied extensively with  $g(x) = f(x)$  type of coupling [97, 123]. Following reference [123], Lyapunov exponents for globally coupled maps, with  $g(x) = f(x)$  type of coupling, can be written as,

$$\lambda_1 = \lambda_u = \lim_{\tau \rightarrow \infty} \sum_{t=1}^{\tau} \ln |f'(x_t)| \quad (4.25a)$$

$$\lambda_2 = \lambda_3 = \dots = \lambda_N = \lambda_u + \ln\left(1 - \frac{N}{N-1}\epsilon\right) \quad (4.25b)$$

Except  $\lambda_u$  other Lyapunov exponents are transverse to the synchronization manifold. The critical value of coupling strength  $\epsilon_c$  beyond which the synchronized state with all nodes synchronized with each other is stable, is given by,

$$\epsilon_c = \frac{N-1}{N}(1 - e^{-\lambda_u}) \quad (4.26)$$

For large  $N$  with  $f(x) = 4x(1-x)$ , we have  $\lambda_u = \ln 2$ . So from above expression we get  $\epsilon_c = 0.5$ .

Coupling function  $g(x) = x$ : From the expressions (4.24a) and (4.24b), it is difficult to determine when the synchronous orbits are stable. Rather it is easier to determine the stability of the synchronous orbits using Lyapunov function which we will consider in the next subsection. Here, we consider some special cases when coupled dynamics of the fully synchronized state lies on periodic or fixed point attractors.

*Case I. Synchronization to fixed point* : First we consider the fixed point  $X^* = x_t$  of the fully synchronized state. The fixed point is given by  $X^* = f(X^*)$ . The conditions for the stability of the synchronous fixed point are  $\ln |(1-\epsilon)f' + \epsilon| < 0$  and  $\ln |(1-\epsilon)f' - \frac{\epsilon}{N-1}| < 0$ . where  $f'$  is the derivative of  $f$  at  $X^*$ . For  $f' < 0$  which is the interesting case, the fixed point is easily found to be stable in the range

$$\frac{|f'| - 1}{|f'| - \frac{1}{N-1}} < \epsilon < 1. \quad (4.27)$$

For  $N = 2$  this solution is not stable and the range of stability increases with  $N$ . This is a surprising result since with increasing  $N$  the number of transverse eigenvectors along which the synchronized solution can become unstable also increases. This feature of increasing range of stability with  $N$  is more general and will be noticed for other solutions

also as will be discussed in subsequent analysis. For large  $N$  synchronous fixed point is stable for

$$\frac{|f'| - 1}{|f'|} < \epsilon < 1 \quad (4.28)$$

For  $f(x)$  given by logistic map,  $X^* = 1 - 1/\mu$ ,  $f'(X^*) = 2 - \mu$  and range of stability of the synchronous fixed point is given by

$$\frac{\mu - 3}{\mu - 2 - \frac{1}{N-1}} < \epsilon < 1. \quad (4.29)$$

*Case II. Synchronization to period two orbit* : We now consider synchronous period two solution. The Lyapunov exponents can be obtained using Eqs. (4.24a) and (4.24b). The conditions for the stability of the period two solution are

$$\ln \left| \left( (1 - \epsilon)f'_1 + \epsilon \right) \left( (1 - \epsilon)f'_2 + \epsilon \right) \right| < 0 \quad (4.30a)$$

$$\ln \left| \left( (1 - \epsilon)f'_1 - \frac{\epsilon}{N-1} \right) \left( (1 - \epsilon)f'_2 - \frac{\epsilon}{N-1} \right) \right| < 0 \quad (4.30b)$$

For  $f(x)$  given by logistic map, the period two synchronized solution is the same as given by Eqs. (4.11) and (4.12). For  $\mu = 4$ , the range of stability of this solution is

$$1 - \frac{\sqrt{54}}{9} < \epsilon < \frac{10 + \frac{1}{N-1} - \sqrt{60 + \frac{30}{N-1} + \frac{6}{(N-1)^2}}}{8 - \frac{2}{N-1} - \frac{1}{(N-1)^2}} \quad (4.31)$$

For  $N = 2$ , this gives the  $\epsilon$  range (0.18..,0.24..) for the stability of period two solution as noted in Case1 of two node case with  $g(x) = x$ . For large  $N$ , this range of stability for  $\epsilon$  values expands to (0.18..,0.28..). Here increase in the stability range is accompanied by the decrease in stability attractor range. So starting with any random initial conditions, this increase in the range is not observed numerically.

### 4.2.3 Lyapunov Function Analysis

From Eqs. (4.2) and (4.23), we write Lyapunov function for any two nodes of globally coupled network as,

$$V_{t+1}^{i,j} = \left[ (1 - \epsilon) \left( f(x_t^i) - f(x_t^j) \right) - \frac{\epsilon}{N-1} \left( g(x_t^i) - g(x_t^j) \right) \right]^2$$

Performing Taylor expansion around  $x_t^j$ , we get

$$\begin{aligned} \frac{V_{t+1}}{V_t} = & \left[ (1 - \epsilon)f'(x_t^j) - \frac{\epsilon}{N-1}g'(x_t^j) \right. \\ & \left. + \frac{x_t^i - x_t^j}{2} \left( (1 - \epsilon)f''(x_t^j) - \frac{\epsilon}{N-1}g''(x_t^j) \right) + \mathcal{O}[(x_t^1 - x_t^2)^2] \right]^2 \end{aligned} \quad (4.32)$$

Coupling function  $g(x) = f(x)$ : In this case the expression (4.32) simplifies to

$$\frac{V_{t+1}}{V_t} = \left( 1 - \frac{N}{N-1}\epsilon \right)^2 \left[ f'(x_t^j) + \frac{x_t^i - x_t^j}{2}f''(x_t^j) + \mathcal{O}[(x_t^1 - x_t^2)^2] \right]^2$$

If the expression in the square bracket on the RHS is bounded then for large  $N$  there will be a critical value of  $\epsilon$  beyond which the condition (4.3) will be satisfied and the globally synchronized state will be stable. For  $f(x) = \mu x(1 - x)$  and using  $(0 \leq x_t^i + x_t^j \leq 2)$ , we get the following range of coupling strength values for which the globally synchronized state is stable.

$$\frac{N-1}{N} \left( 1 - \frac{1}{\mu} \right) < \epsilon \leq 1 < \frac{N-1}{N} \left( 1 + \frac{1}{\mu} \right) \quad (4.33)$$

For  $\mu = 4$  and for very large  $N$ , coupling strength range is  $0.75 < \epsilon < 1$ . A better  $\epsilon$  range is obtained by putting more realistic bounds as  $X^- \leq x_t^i + x_t^j \leq X^+$ , which gives the range of stability as,

$$\frac{N-1}{N} \left( 1 - \frac{1}{\mu A} \right) < \epsilon \leq 1 \quad (4.34)$$

where  $A = \max(|1 - X^+|, |1 - X^-|)$ .

Coupling function  $g(x) = x$ : In this case, for logistic map, the expression (4.32) simplifies to

$$\frac{V_{t+1}^{ij}}{V_t} = \left[ (1 - \epsilon)(1 - (x_t^i + x_t^j)) - \frac{\epsilon}{N-1} \right]^2$$

Since  $0 \leq x_t^i + x_t^j \leq 2$  we get a range of  $\epsilon$  values for which the globally synchronized state is stable (Eq. (4.3))

$$\frac{\mu - 1}{\mu - \frac{1}{N-1}} < \epsilon < \frac{\mu + 1}{\mu - \frac{1}{N-1}} \quad (4.35)$$

which for large  $N$  reduces to

$$\frac{\mu - 1}{\mu} < \epsilon < \frac{\mu + 1}{\mu} \quad (4.36)$$

For  $\mu = 4$ , we get the coupling strength range  $0.75 < \epsilon \leq 1$  for which the globally synchronized state is stable. We also note that for  $N = 2$  the condition (4.35) for synchronization is not satisfied for any value of  $\epsilon \leq 1$ .

### 4.3 Stability Analysis for Driven Synchronization

Driven synchronization leads to clusters with dominant inter-cluster couplings. For the ideal driven clusters, there are only inter-cluster connections with no connections between the constituents of the same cluster. A complete bipartite network consists of two sets of nodes with each node of one set connected with all the nodes of the other set. Clearly this type of network is an ideal example for studying driven synchronization. We take a bipartite network consisting of two sets of nodes,  $N = N_1 + N_2$ , with each node of  $N_1$  connected to every node of  $N_2$  and there are no connections between the nodes of the same set [151]. We study dynamics of coupled maps on such type of bipartite network and determine the stability criteria for formation of driven synchronized clusters. Our model for coupled complete bipartite network can be written as,

$$\begin{aligned} x_{t+1}^i &= (1 - \epsilon)f(x_t^i) + \frac{\epsilon}{N_2} \sum_{j=N_1+1}^N g(x_t^j), \quad \text{for } i = 1, \dots, N_1 \\ &= (1 - \epsilon)f(x_t^i) + \frac{\epsilon}{N_1} \sum_{j=1}^{N_1} g(x_t^j), \quad \text{for } i = N_1 + 1, \dots, N. \end{aligned} \quad (4.37)$$

where all terms are having the same meaning as defined for Eq. (2.1).

#### 4.3.1 Coupled Networks with $N = 3$

First we take a simple network of three nodes with  $N_1 = 2, N_2 = 1$  which is the smallest possible network to show the behaviour displayed by Eq. (4.37). The evolution equations can be written as

$$\begin{aligned} x_{t+1}^1 &= (1 - \epsilon)f(x_t^1) + \epsilon g(x_t^3) \\ x_{t+1}^2 &= (1 - \epsilon)f(x_t^2) + \epsilon g(x_t^3) \\ x_{t+1}^3 &= (1 - \epsilon)f(x_t^3) + \frac{\epsilon}{2}(g(x_t^1) + g(x_t^2)) \end{aligned} \quad (4.38)$$

Here, the driven synchronized state corresponds to the nodes 1 and 2 being synchronized with each other but not with node 3.

#### Linear Stability Analysis

Here, we use addition and difference variables  $s_t$  and  $d_t$  as defined in Eq. (4.5) for the

first two nodes. Thus Eqs. (4.38) can be rewritten as,

$$s_{t+1} = \frac{1-\epsilon}{2}[f(s_t + d_t) + f(s_t - d_t)] + \epsilon g(x_t^3) \quad (4.39a)$$

$$d_{t+1} = \frac{1-\epsilon}{2}[f(s_t + d_t) - f(s_t - d_t)] \quad (4.39b)$$

$$x_{t+1}^3 = (1-\epsilon)f(x_t^3) + \frac{\epsilon}{2}[g(s_t + d_t) + g(s_t - d_t)] \quad (4.39c)$$

Jacobian matrix for the driven synchronized state ( $s_t, d_t = 0, x_t^3$ ) is given by,

$$J_t = \begin{pmatrix} (1-\epsilon)f'_1 & 0 & \epsilon g'_2 \\ 0 & (1-\epsilon)f'_1 & 0 \\ \epsilon g'_1 & 0 & (1-\epsilon)f'_2 \end{pmatrix} \quad (4.40)$$

$f'_1$  and  $g'_1$  are derivatives at  $s_t = x_t = x_t^1 = x_t^2$  and  $f'_2$  and  $g'_2$  are derivatives at  $(x_t^3)$ . Lyapunov exponent corresponding to the difference variable is found as,

$$\lambda_d = \ln(1-\epsilon) + \lambda_c \quad (4.41)$$

where  $\lambda_c$  is,

$$\lambda_c = \lim_{\tau \rightarrow \infty} \frac{1}{\tau} \sum_{t=1}^{\tau} \ln |f'(s_t)| \quad (4.42)$$

The coupling strength range for which the driven synchronized solution is stable, i.e.  $\lambda_d < 0$ , is given by,

$$1 - \frac{1}{\exp \lambda_c} < \epsilon \quad (4.43)$$

Coupling function  $g(x) = f(x)$ : We have investigated the network containing three nodes numerically with  $g(x) = f(x)$ . For logistic map with  $\mu = 4$ , we find that nodes get driven synchronized for coupling strength ranges  $0.15 < \epsilon < 0.2$  and  $0.5 < \epsilon \leq 1$ . When we investigate further these two  $\epsilon$  ranges we find that in the lower range the behaviour is mostly periodic while in the upper range it is periodic in the middle portion and is chaotic at both ends. For  $0.5 < \epsilon \leq 1$  it is easy to see why the synchronized dynamics gives a stable attractor. Since  $\ln(1-\epsilon) < -\ln 2$  for  $\epsilon > 0.5$ , from Eq. (4.41) we see that till  $\lambda_c$  is less than  $\ln 2$ , the value of Lyapunov exponent for an isolated logistic map at  $\mu = 4$ , the synchronized solution will be stable. The stability of the driven synchronized state for  $0.15 < \epsilon < 0.2$  appears to be because of either periodic attractor or chaotic attractor close the periodic attractor with very small value of  $\lambda_c$ .

Now we discuss the special cases where nodes are synchronized with variables showing periodic or fixed point behaviour. For this study we use the original variables.

*Case I. Synchronization to Fixed point :* Nodes get synchronized to a fixed point with one set of nodes having one value and the other set of nodes having a different value such as  $(x_t^1 = x_t^2 = X_1^*)$  and  $(x_t^3 = X_2^*)$ . Eigenvalues of Jacobian matrix (4.40) with  $g(x) = f(x)$  are,

$$\Lambda_1 = (1 - \epsilon)f_1' \quad (4.44a)$$

$$\begin{aligned} \Lambda_{2,3} &= \frac{1 - \epsilon}{2}(f_1' + f_2') \\ &\pm \frac{1}{2}\sqrt{(1 - \epsilon)^2(f_1' + f_2')^2 - 4(1 - 2\epsilon)f_1'f_2'} \end{aligned} \quad (4.44b)$$

where  $f_1'$  and  $f_2'$  are the derivatives at  $X_1$  and  $X_2$  respectively. By putting the condition that the magnitude of the above eigenvalues should be less than one, we get the  $\epsilon$  range for which the fixed point state is stable. When the first two nodes synchronize with each other, the three coupled maps system behaves like just two coupled maps and within this  $\epsilon$  range all the solutions are those of the two coupled maps. The expressions for  $X_1^*$  and  $X_2^*$  are

$$X_{1,2}^* = \frac{(1 - \mu + 2\mu\epsilon) \pm \sqrt{(1 - \mu + 2\mu\epsilon)^2 - 4\epsilon(1 - \mu + 2\mu\epsilon)}}{2\mu(2\epsilon - 1)} \quad (4.45)$$

From Eqs. (4.44a) and (4.44b) the coupling strength values for which the fixed point solution is stable must satisfy

$$|(1 - \epsilon)f_1'| < 1$$

and the following condition

$$\frac{1}{2} \left( 1 + \sqrt{\frac{3}{\mu(\mu - 2)}} \right) < \epsilon < \frac{3 + 2\mu(\mu - 2) + \sqrt{(3 + 2\mu(\mu - 2))^2 - 4\mu(\mu - 2)(\mu - 1)^2}}{4\mu(\mu - 2)} \quad (4.46)$$

*Case II. Synchronization to period two orbit :* Consider a periodic orbit of period two where the first two nodes are driven synchronized and have the value  $X_1^p$ , and the third node has the value  $X_2^p$ . The period two orbit is obtained by interchanging these two values at successive time steps. The Jacobian matrix for this periodic orbit can be written as  $J = J_1 J_2$  where

$$J_1 = \begin{pmatrix} (1 - \epsilon)f_1' & 0 & \epsilon f_2' \\ 0 & (1 - \epsilon)f_1' & \epsilon f_2' \\ \frac{\epsilon}{2}f_1' & \frac{\epsilon}{2}f_1' & (1 - \epsilon)f_2' \end{pmatrix} \quad (4.47)$$

where  $f'_1$  and  $f'_2$  are derivatives at  $X_1^p$  and  $X_2^p$  respectively and  $J_2$  is obtained by interchanging suffixes 1 and 2 in the expression for  $J_1$ . Eigenvalues of  $J$  are given by

$$\Lambda_1 = (1 - \epsilon)^2 f'_1 f'_2 \quad (4.48a)$$

$$\Lambda_{2,3} = \left( \frac{\epsilon}{2} (f'_1 + f'_2) \pm \sqrt{\frac{\epsilon^2}{4} (f'_1 + f'_2)^2 + (1 - 2\epsilon) f'_1 f'_2} \right)^2 \quad (4.48b)$$

For  $f(x)$  given by logistic map, the periodic points are

$$X_{1,2}^p = s \pm \sqrt{s(1 - s - \frac{1}{\mu})}, \quad (4.49)$$

where

$$s = \frac{1}{2} \left( 1 + \frac{1}{\mu(1 - 2\epsilon)} \right).$$

After imposing the condition  $|\Lambda_{1,2,3}| < 1$  we can get the  $\epsilon$  range for which the period two orbit is stable. The first eigenvalue gives us the condition that

$$1 - \epsilon < \frac{|1 - 2\epsilon|}{\sqrt{(1 + \mu - 2\epsilon\mu)(4\epsilon - 1 + \mu - 2\epsilon\mu)}}. \quad (4.50)$$

The other two eigenvalues give us the same condition as in Eq. (4.46) except that  $\epsilon$  in this inequality is substituted by  $1 - \epsilon$  similar to the case of two coupled maps [122]. For logistic map with  $\mu = 4$ , this range is given by  $0.16.. < \epsilon < 0.20...$

*Case III. Synchronization of all three nodes :* It is also possible that all the three nodes get synchronized (self-organized synchronization). The eigenvalues of Jacobian matrix for this synchronized state ( $x_t^1 = x_t^2 = x_t^3 = x_t$ ) can simply be written from Eqs. (4.44a) and (4.44b), by putting  $f'_1 = f'_2 = f'(x_t)$ , which gives Lyapunov exponents as,

$$\lambda_1 = \lambda_u = \frac{1}{\tau} \lim_{\tau \rightarrow \infty} \sum_{t=1}^{\tau} \ln |f'(x_t)| \quad (4.51a)$$

$$\lambda_2 = \ln(1 - \epsilon) + \lambda_u \quad (4.51b)$$

$$\lambda_3 = \ln(1 - 2\epsilon) + \lambda_u \quad (4.51c)$$

where  $\lambda_u$  is the Lyapunov exponent for an uncoupled map  $f(x)$ . For synchronous orbits to be stable, the two Lyapunov exponents ( $\lambda_2$  and  $\lambda_3$ ) corresponding to the transverse eigenvectors should be negative. We get the following  $\epsilon$  range for which both the transverse eigenvalues are negative,

$$1 - e^{-\lambda_u} < \epsilon < \frac{1}{2}(1 + e^{-\lambda_u}) \quad (4.52)$$

In this region coupled dynamics may lie on a chaotic or a periodic attractor depending upon the value of  $\lambda_u$ . For  $f(x) = \mu x(1 - x)$  with  $\mu = 4$ ,  $\lambda_u = \ln 2$  and thus the range of stability of the self-organized synchronization of all three nodes is  $(0.5, 0.75)$  and the dynamics is chaotic.

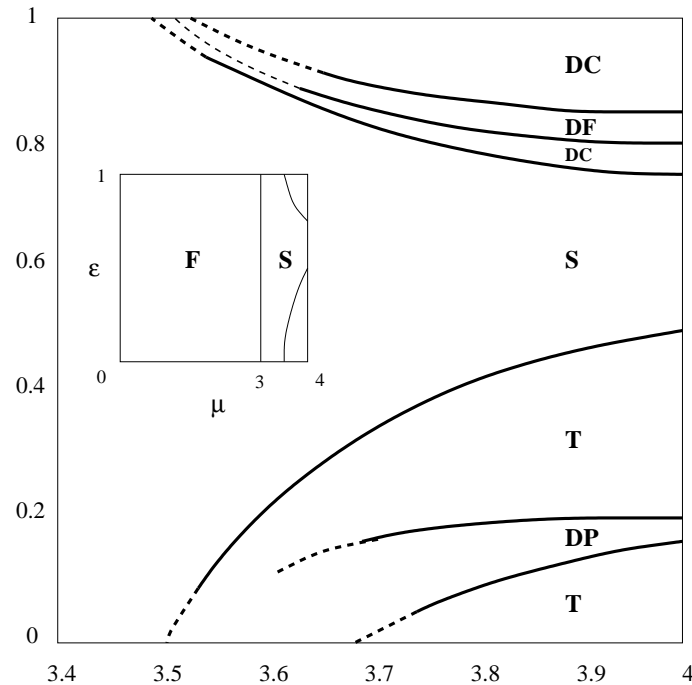


**Figure 4.1:** Phase space diagram showing different features of coupled dynamics in the two parameter space of  $\mu$  and  $\epsilon$  for three nodes bipartite network with logistic map as local map and coupling function  $g(x) = f(x)$ . Different regions are T. Turbulent region, DP. Driven periodic, DF. Driven fixed point, DC. Driven Chaotic, S. Self organized region and F. Fixed point. Region boundaries are determined based on the asymptotic behaviour using several initial conditions, synchronization behaviour and the largest Lyapunov exponent. The dashed lines indicate uncertainties in determining the boundaries. The inset shows the phase diagram for the entire range of parameter  $\mu$  from 0 to 4.

*Phase diagram in  $\mu - \epsilon$  plane :* Fig. 4.1 shows phase diagram in the  $\mu - \epsilon$  plane for three nodes bipartite network with  $g(x) = f(x)$ . For  $\mu < 3$  we get a fixed point solution. To understand the remaining phase diagram consider the line  $\mu = 4$ . Fig. 4.2 shows two sets of differences between the values of variables,  $|x^1 - x^2|$  (open circles) and  $|x^1 - x^3|$  (crosses) as a function of the coupling strength  $\epsilon$ . Bipartite driven synchronized state and global self-organized synchronized state are clearly seen.

Fig. 4.3(a) shows largest Lyapunov exponent and Fig. 4.4(a) shows the fractions of inter- and intra- couplings,  $f_{inter}$  and  $f_{intra}$ , as a function of  $\epsilon$  for  $m\mu = 4$  (for the definition of

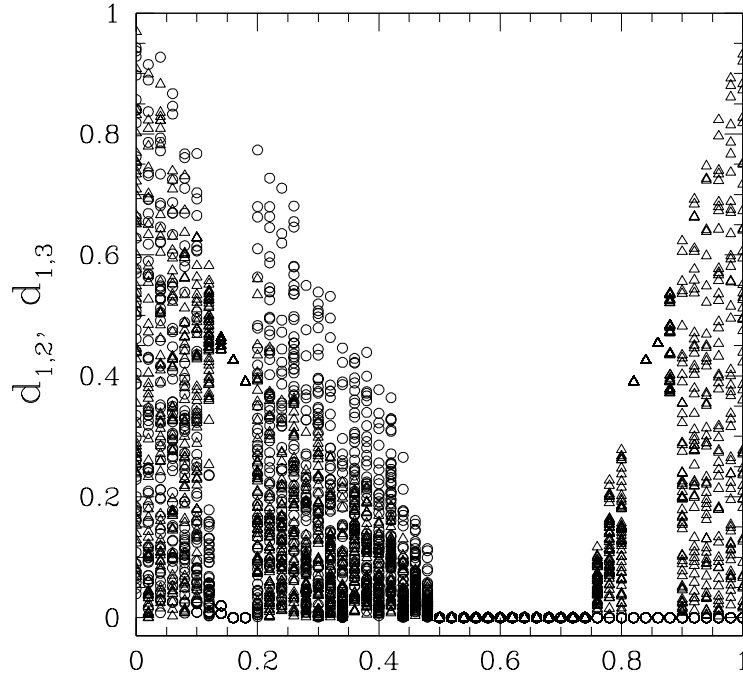


**Figure 4.2:** The figure shows the variation of two sets of difference,  $|x_t^1 - x_t^2|$  (open circles) and  $|x_t^1 - x_t^3|$  (crosses) for a three nodes network as a function of the coupling strength  $\epsilon$  for  $f(x) = \mu x(1-x)$  with  $\mu = 4$  and  $g(x) = f(x)$ . For each  $\epsilon$ , 100 values of the differences are plotted after an initial transient.

$f_{\text{intra}}$  and  $f_{\text{inter}}$ , see section 2.5, chapter 2).

Initially for small coupling strength values nodes are in the turbulent region (region T). As the coupling strength increases beyond a critical  $\epsilon_c$  we get bipartite driven synchronized state (region DP). This region corresponds to the Case II of period two orbits discussed above in this subsection. When the coupling strength increases further we get a reappearance of turbulent region. As the coupling strength is increased further all the nodes are synchronized giving one cluster with global self-organized synchronization (region S). This region corresponds to the case III discussed above and the range of  $\epsilon$  for this region is given by Eq. (4.52). In this region the coupled dynamics lies on a chaotic attractor. In the last three regions (DC, DP and DC), we get driven bipartite synchronization. The middle region (DP) displays driven fixed point solution (case I) while the other regions show chaotic behaviour.

For  $\mu < 4$ , the coupling strength range where all the nodes are synchronized (region S) increases in size and the coupling strength ranges where nodes show driven synchronization shift towards the nearest boundaries  $\epsilon = 0$  and  $\epsilon = 1$ .

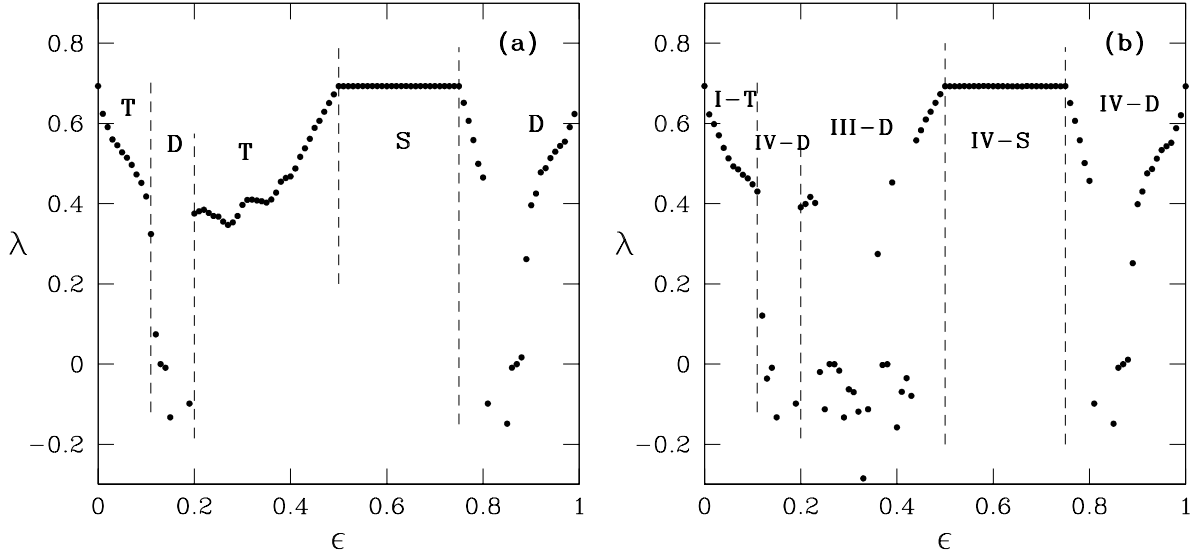


**Figure 4.3:** (a) The figure shows the largest Lyapunov exponent  $\lambda$  as a function of the coupling strength  $\epsilon$  for the three nodes bipartite network with logistic map as local map with  $\mu = 4$  and  $g(x) = f(x)$ . (b) Same as for (a) but for a bipartite network of 50 nodes with  $N_1 = N_2 = 25$ .

Coupling function  $g(x) = x$  : Numerical analysis shows periodic solutions which we now consider in detail. When the first two nodes are driven synchronized the solutions of the dynamical equations are similar to the two nodes case. This simplifies the analysis considerably.

*Case I. Driven synchronization to period two orbit* : First we consider the case where the coupled dynamics shows periodic attractor with period two behaviour and the variables take the values

$$\begin{aligned} x_t^1 &= x_t^2 = x_{t+1}^3 = X_1^p \\ x_t^3 &= x_{t+1}^1 = x_{t+1}^2 = X_2^p \end{aligned} \quad (4.53)$$

Using the product of Jacobians of Eq. (4.40) for two consecutive time steps the eigenvalues for this periodic orbit can be easily obtained. The eigenvalue  $\Lambda_d$  associated with the difference variable  $d_t$  is given by

$$\Lambda_d = (1 - \epsilon)^2 f_1' f_2', \quad (4.54)$$

The other two eigenvalues are the eigenvalues of product matrix  $J_1 J_2$ , where  $J_1$  is given by Eq. (4.13) and hence the eigenvalues are given by Eq. (4.14). The solution of the periodic

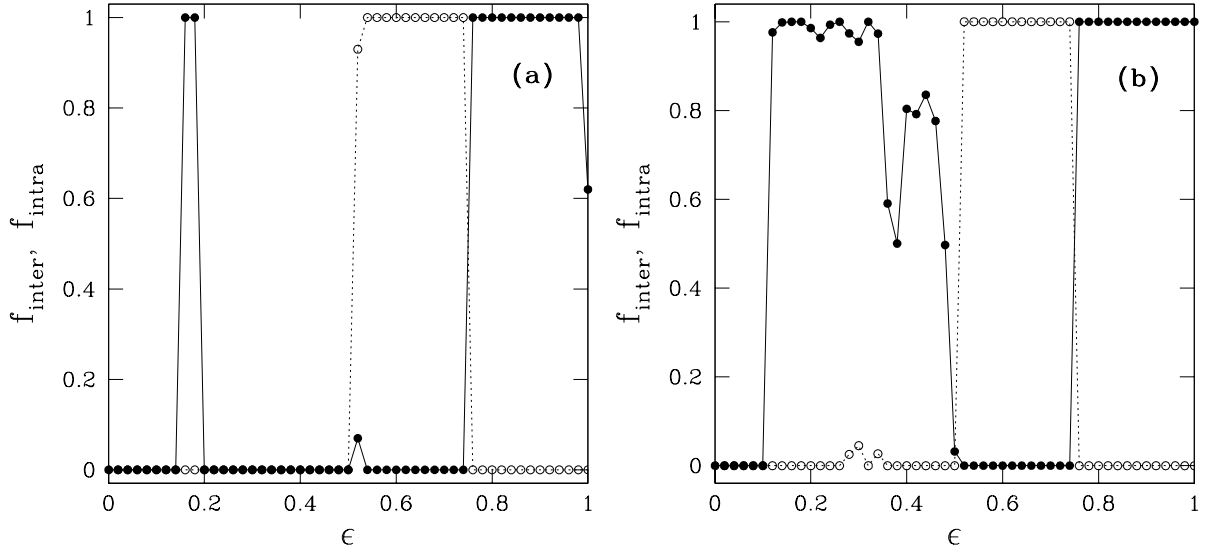


**Figure 4.4:** (a) The figure shows the fractions of inter- and intra-cluster couplings,  $f_{inter}$  and  $f_{intra}$ , as a function of the coupling strength  $\epsilon$  for the three nodes bipartite network, logistic map as local map with  $\mu = 4$  and  $g(x) = f(x)$ . The values are obtained by averaging over 50 random initial conditions. (b) Same as for (a) but for a bipartite network of 50 nodes with  $N_1 = N_2 = 25$ .

orbit is the same as for two coupled maps (Eq. (4.16)). Using all the three eigenvalues of Jacobian matrix, the coupling strength range, for which the periodic orbit given by Eq. (4.53) is stable, is given by

$$\max \left( 1 - \frac{1}{\sqrt{f'_1 f'_2}}, \frac{|f'_1 f'_2| - 1}{|f'_1 f'_2| + 1} \right) < \epsilon < 1 \quad (4.55)$$

The periodic points  $X_1$  and  $X_2$  are also the periodic points of uncoupled map  $f$  (Eq. (4.11)). For logistic map, we get the following range of coupling strength in terms of logistic map parameter  $\mu$ ,

$$1 - \frac{2}{\mu^2 - 2\mu - 3} < \epsilon < 1 \quad (4.56)$$

which is the same as Eq. (4.17). The lower bound of  $\epsilon$  matches exactly with the boundary between the regions IV-DP and IV-DQ of Fig. 1 of Chapter 3 and regions DP and DQ of Fig. 4.5.

*Case II. Synchronization of all three nodes :* All three nodes get synchronized for a small coupling strength region with dynamics lying on periodic orbits of period two such that

$$\begin{aligned} x_t^1 &= x_t^2 = x_t^3 = X_1^p \\ x_{t+1}^1 &= x_{t+1}^2 = x_{t+1}^3 = X_2^p \end{aligned} \quad (4.57)$$

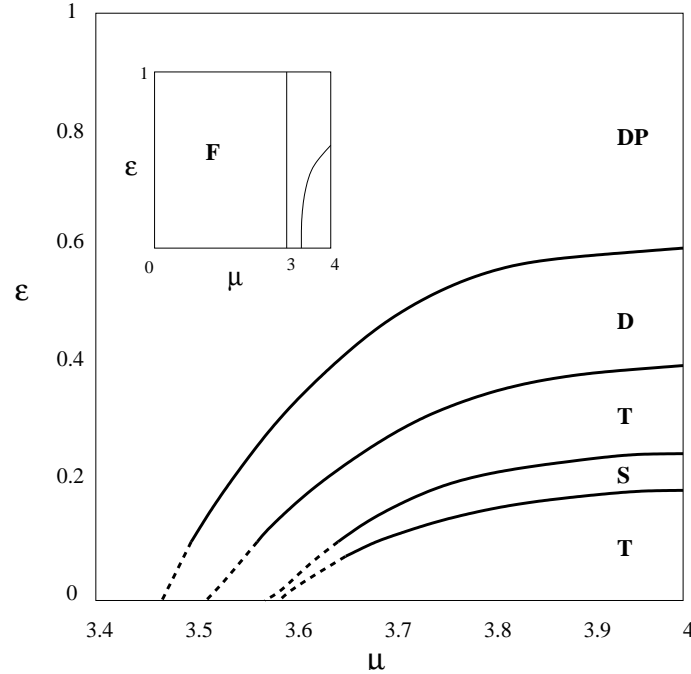


**Figure 4.5:** Phase space diagram showing different features of coupled dynamics in the two parameter space of  $\mu$  and  $\epsilon$  for three nodes bipartite network with logistic map as local map and coupling function  $g(x) = x$ . Different regions are T. Turbulent region, DP. Driven periodic, DF. Driven fixed point, DQ. Driven Quasiperiodic, DC. Driven Chaotic, S. Self organized region and F. Fixed point. Region boundaries are determined based on the asymptotic behaviour using several initial conditions, synchronization behaviour and the largest Lyapunov exponent. The dashed lines indicate uncertainties in determining the boundaries. The inset shows the phase diagram for the entire range of parameter  $\mu$  from 0 to 4.

The eigenvalue of the Jacobian for this periodic orbit for the difference variable is simply  $(1 - \epsilon)^2 f'_1 f'_2$  and the other two eigenvalues are the same as for two coupled maps and are given by Eq. (4.10). The periodic points are given by Eq. (4.12). The coupling strength range for which all three nodes are synchronized for logistic map with  $\mu = 4$ , is  $0.18... < \epsilon < 0.24...$  which is same as Case I for two coupled maps with  $g(x) = x$ .

*Phase diagram in  $\mu - \epsilon$  space :* Fig. 4.5 shows different phases in the  $\mu - \epsilon$  plane for three nodes bipartite network with  $g(x) = x$ . For  $\mu < 3$  we get a fixed point solution. To understand the remaining phase diagram consider the line  $\mu = 4$ . Fig. 4.6 shows two sets of differences between the values of variables,  $|x^1 - x^2|$  (open circles) and  $|x^1 - x^3|$  (crosses) as a function of the coupling strength  $\epsilon$ . Bipartite driven synchronized state and global self-organized synchronized state are clearly seen.

Fig. 4.7(a) shows largest Lyapunov exponent and Fig. 4.8(a) shows the fractions of inter- and intra- couplings,  $f_{inter}$  and  $f_{intra}$ , as a function of  $\epsilon$  for  $mu = 4$ . Initially for small cou-

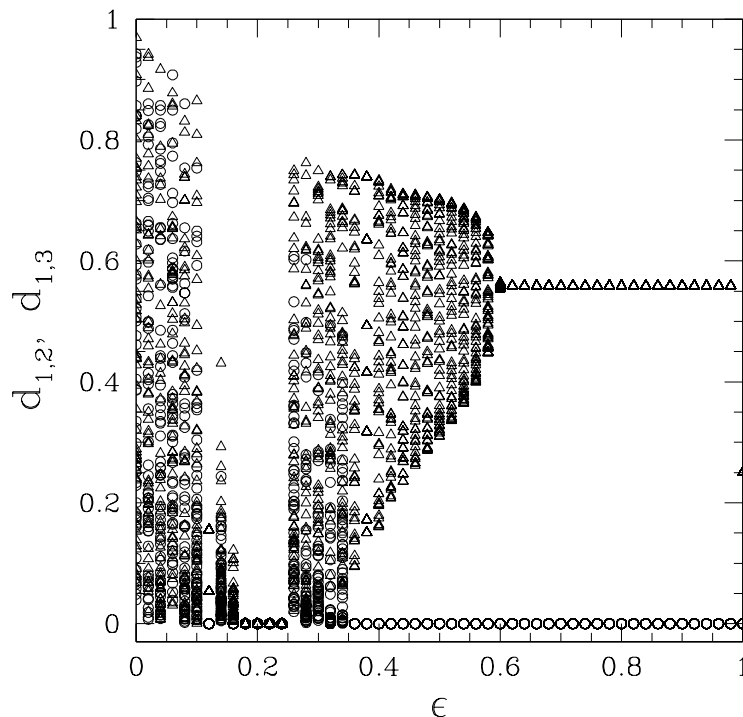


**Figure 4.6:** The figure shows the variation of two sets of difference,  $|x_t^1 - x_t^2|$  (open circles) and  $|x_t^1 - x_t^3|$  (crosses) for a three nodes network as a function of the coupling strength  $\epsilon$  for  $f(x) = \mu x(1-x)$  with  $\mu = 4$  and  $g(x) = x$ . For each  $\epsilon$ , 100 values of the differences are plotted after an initial transient.

pling strength values nodes are in turbulent region with no cluster formation at all (region T). As the coupling strength increases beyond a critical  $\epsilon_c$ , we get global self-organized state (region S). This region is the case II considered above. When the coupling strength increases further we get a reappearance of turbulent region. In the last two regions we get driven bipartite synchronization (regions DQ and DP). The last region corresponds to case I of period two discussed above in this subsection and the critical coupling strength for it is given by Eq. (4.55). For  $\mu < 4$ , the coupling strength region for driven synchronization gets wider and that for self-organized synchronization gets thinner with a shift towards  $\epsilon = 0$ .

### 4.3.2 Complete Bipartite Coupled Networks

Let us now consider a complete bipartite network of  $N = N_1 + N_2$  nodes and dynamics defined by Eq. (4.37). We define a bipartite synchronized state of the bipartite network as the one that has that all  $N_1$  elements of the first set synchronized to some value, say  $X_1(t)$ , and all  $N_2$  elements of the second set synchronized to some other value, say  $X_2(t)$ . Linear

stability analysis of the bipartite synchronized state can be done using the Jacobian matrix,

$$J_t = \begin{pmatrix} (1 - \epsilon)f'_1 & 0 & \dots & 0 & \frac{\epsilon}{N_2}g'_2 & \frac{\epsilon}{N_2}g'_2 & \dots & \frac{\epsilon}{N_2}g'_2 \\ \vdots & \vdots \\ 0 & 0 & \dots & (1 - \epsilon)f'_1 & \frac{\epsilon}{N_2}g'_2 & \frac{\epsilon}{N_2}g'_2 & \dots & \frac{\epsilon}{N_2}g'_2 \\ \frac{\epsilon}{N_1}g'_1 & \frac{\epsilon}{N_1}g'_1 & \dots & \frac{\epsilon}{N_1}g'_1 & (1 - \epsilon)f'_2 & 0 & \dots & 0 \\ \vdots & \vdots \\ \frac{\epsilon}{N_1}g'_1 & \frac{\epsilon}{N_1}g'_1 & \dots & \frac{\epsilon}{N_1}g'_1 & 0 & 0 & \dots & (1 - \epsilon)f'_2 \end{pmatrix} \quad (4.58)$$

where  $g'_1$  and  $g'_2$  are the derivative of  $g(x)$  at  $X_1$  and  $X_2$  respectively. It is easy to see that the eigenvectors and eigenvalues of the above Jacobian matrix can be divided into three sets,  $A, B, C$ , as,

set	Eigenvectors	Eigenvalue	No of eigenvalues	condition
$A$	$(\alpha_1 \dots \alpha_{N_1}, 0 \dots 0)$	$(1 - \epsilon)f'_1$	$N_1 - 1$	$\Sigma\alpha = 0$
$B$	$(0 \dots 0, \beta_1 \dots \beta_{N_2})$	$(1 - \epsilon)f'_2$	$N_2 - 1$	$\Sigma\beta = 0$
$C$	$(\alpha, \dots \alpha, \beta, \dots \beta)$	-	2	-

Here,  $(\alpha_1, \dots \alpha_{N_1}), (\beta_1, \dots \beta_{N_2})$  and  $\alpha, \beta$  are complex numbers satisfying the conditions specified in the last column. The two eigenvalues corresponding to the set  $C$  are the eigenvalues of the matrix

$$\begin{pmatrix} (1 - \epsilon)f'_1 & \epsilon g'_2 \\ \epsilon g'_1 & (1 - \epsilon)f'_2 \end{pmatrix} \quad (4.59)$$

We make the following observations. (a) The three sets of eigenvectors,  $A, B, C$ , are orthogonal to each other and the total space of eigenvectors may be written as a direct sum of these three sets. (b) The three sets of eigenvectors do not mix with each other under time evolution. (c) The eigenvectors belonging to the first two sets ( $A$  and  $B$ ) are also the eigenvectors of the product of any number of Jacobian matrices under time evolution. (d) The two sets of eigenvectors  $A$  and  $B$  are transverse to the synchronization manifold which is defined by the last set of eigenvectors  $C$ .

Lyapunov exponents corresponding to the transverse eigenvectors can be easily written as

$$\lambda_i = \ln |(1 - \epsilon)| + \frac{1}{\tau} \lim_{\tau \rightarrow \infty} \sum_{t=1}^{\tau} \ln |f'(X_1)|, \quad \text{for } i = 1, \dots, N_1 - 1 \quad (4.60a)$$

$$\lambda_i = \ln |(1 - \epsilon)| + \frac{1}{\tau} \lim_{\tau \rightarrow \infty} \sum_{t=1}^{\tau} \ln |f'(X_2)|, \quad \text{for } i = N_1, \dots, N - 2. \quad (4.60b)$$

The synchronized state is stable provided the transverse Lyapunov exponents are negative. If  $f'$  is bounded as is the case for the logistic map then from Eqs. (4.60) we see that for  $\epsilon$  larger than some critical value,  $\epsilon_c (< 1)$ , bipartite synchronized state will be stable. Note that this bipartite synchronized state will be stable even if one or both the remaining Lyapunov exponents corresponding to the set  $C$  are positive, i.e. the trajectories are chaotic.

Now we study the periodic behaviour of coupled dynamics of Eq. (4.37). Here we consider two cases, fixed point attractor and periodic attractor with period two, as we studied for three nodes.

Coupling function  $g(x) = f(x)$ : The fixed point bipartite synchronized solution with one set of nodes taking value  $X_1^*$  and the other set  $X_2^*$ , is given by Eq. (4.45). Jacobian matrix for this solution gives three sets of eigenvalues, first set of  $N_1 - 1$  degenerate eigenvalues  $(1 - \epsilon)f_1'$ , second set of  $N_2 - 1$  degenerate eigenvalues  $(1 - \epsilon)f_2'$  and third set of two eigenvalues given by Eq. (4.44b). The conditions for the stability of this solution is given by Eq. (4.46) and  $|(1 - \epsilon)f_{1,2}'| < 1$ .

The bipartite synchronous period two solution is obtained when one set of nodes take the value  $X_1^p$  and the other set of nodes take the value  $X_2^p$  and the two values alternate in time. This solution is the same as given by Eq. (4.49). The eigenvalues ( Eqs. (4.48a) and (4.48b), with the  $N - 2$  fold degeneracy of  $\Lambda_1$  ) and the conditions for stability of the solution are the same as for Case II of three nodes with  $g(x) = f(x)$ .

The global synchronized solution where all nodes of the bipartite network are synchronized, has the same Lyapunov exponents (except the degeneracy) as in Eqs. (4.51c) and the stability criterion is again given by Eq. (4.52).

Coupling function  $g(x) = x$ : Consider a periodic orbit of period two with bipartite synchronized state where all nodes of one set take value  $X_1$  and the other set take value  $X_2$ ,

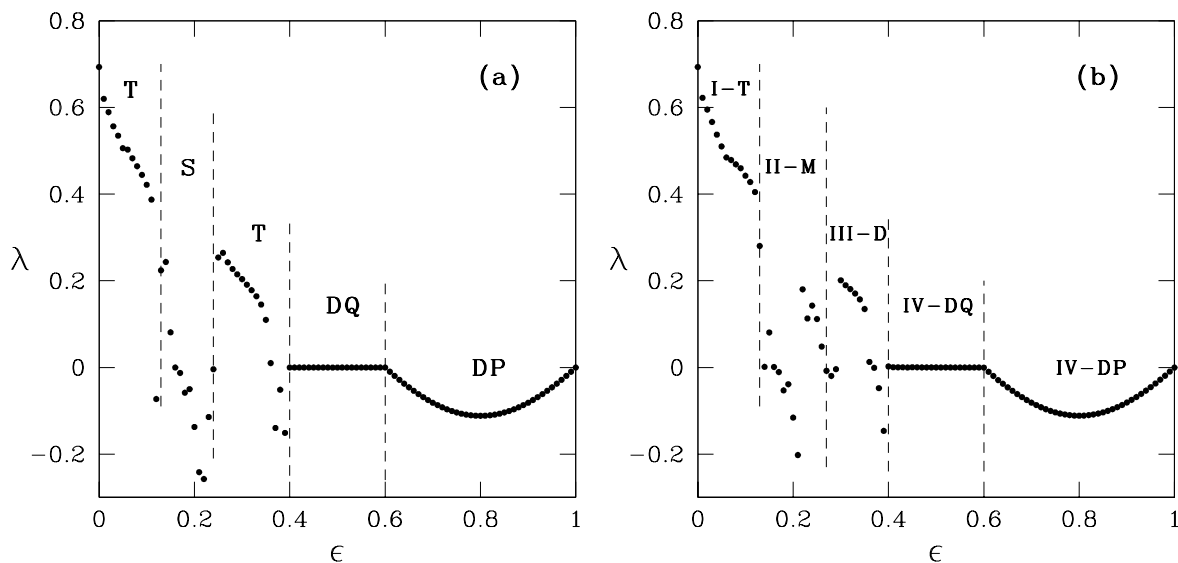


**Figure 4.7:** (a) The figure shows the largest Lyapunov exponent  $\lambda$  as a function of the coupling strength  $\epsilon$  for the three nodes bipartite network with logistic map as local map with  $\mu = 4$  and  $g(x) = x$ . (b) Same as for (a) but for a bipartite network of 50 nodes with  $N1 = N2 = 25$ .

and the two values alternate in time. The solutions is same as for case I of three nodes bipartite network. The stability ranges are given by Eqs. (4.55) and (4.56).

Fig. 4.3(b) plots the largest Lyapunov exponent as function of  $\epsilon$  and Fig. 4.4(b) plots  $f_{inter}$ ,  $f_{intra}$  as a function of  $\epsilon$  for the bipartite networks with  $g(x) = f(x)$  and  $\mu = 4$ . Comparing with the three nodes networks (Figs. 4.3(a) and 4.4(a) ) we find that the major difference is in the range  $0.20.. < \epsilon < 0.5$  where the turbulent region reappears for the three nodes network while mixed region having both driven and self-organized clusters is observed for the larger bipartite networks. The region boundaries for the period two, globally self-organized state and fixed point are the same as given for cases II, III and I respectively for three nodes bipartite network.

As in the case  $g(x) = f(x)$ , there is a similarity between the three nodes bipartite networks and the larger bipartite networks for  $g(x) = x$ . Fig. 4.7(b) and Fig. 4.8(b) plot respectively the largest Lyapunov exponent and  $f_{inter}$ ,  $f_{intra}$  as a function of  $\epsilon$  for the bipartite network with  $g(x) = x$  and  $\mu = 4$ . Comparing with the three nodes network (Fig. 4.7(a) and Fig. 4.8(a) ), we find that the main difference is in the range  $0.24.. < \epsilon < 0.35...$

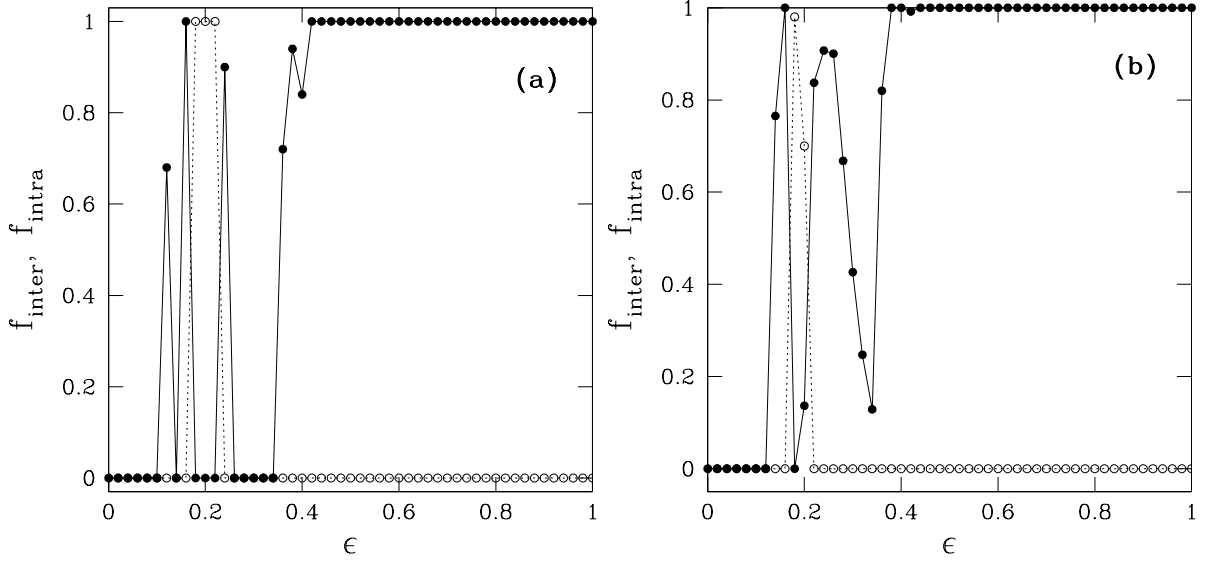


**Figure 4.8:** (a) The figure shows the fractions of inter- and intra-cluster couplings,  $f_{inter}$  and  $f_{intra}$ , as a function of the coupling strength  $\epsilon$  for the three nodes bipartite network, logistic map as local map with  $\mu = 4$  and  $g(x) = f(x)$ . The values are obtained by averaging over 50 random initial conditions. (b) Same as for (a) but for a bipartite network of 50 nodes with  $N_1 = N_2 = 25$ .

### 4.3.3 Lyapunov Function Analysis

For the complete bipartite networks, Lyapunov function as defined by Eq. (4.2), for any two nodes belonging to the same set is given by

$$V_{t+1}^{ij} = [(1 - \epsilon)(f(x_t^i) - f(x_t^j))]^2 \quad (4.61)$$

Expanding around  $x_t^j$  gives the ratio of Lyapunov functions at two successive times,

$$\frac{V_{t+1}^{ij}}{V_t^{ij}} = (1 - \epsilon)^2 \left[ f'(x_t^j) + \frac{x_t^i - x_t^j}{2} f''(x_t^j) + \mathcal{O}((x_t^i - x_t^j)^2) \right]^2$$

If the term in the square bracket on the RHS is bounded then there will be a critical value of  $\epsilon$  beyond which  $\frac{V_{t+1}^{ij}}{V_t^{ij}} < 1$  and thus the bipartite synchronized state will be stable.

We see that for driven synchronization, Lyapunov function for any pair of nodes does not depend on the size of the complete bipartite network and type of the coupling because in the expression for Lyapunov function, contribution of such couplings cancel out. This is not the case for globally coupled networks where contribution of the coupling terms for the two nodes under consideration do not exactly cancel and the size of the network has an effect on the asymptotic behaviour.

For the logistic map and using  $0 \leq x_t^i + x_t^j \leq 2$  and Eq. (4.3), we get the following range for  $\epsilon$  values for synchronization of nodes  $i$  and  $j$ ,

$$\frac{\mu - 1}{\mu} \leq \epsilon \leq 1 \quad (4.62)$$

A better  $\epsilon$  range can be obtained by taking a more appropriate boundary as  $X^- < x_t^i + x_t^j < X^+$ , which gives

$$1 - \frac{1}{\mu A} < \epsilon \leq 1$$

where  $A$  is defined after Eq. (4.34).

#### 4.4 Self-organized and Driven Synchronization

The analysis presented so far shades some light on the dynamical origin of the two types of synchronization namely self-organized and driven, that we have studied. From Eq. (4.6a)(b) we see that in the dynamics of the difference variable  $d_t$  for the two nodes network the coupling term adds an extra decay term. This is also seen from the expression (4.19) for Lyapunov function. On the other hand, from Eq. (4.39b) we see that in the dynamics of the difference variable for the three nodes network the coupling terms with the third variable cancel out (see also Eq. (4.61) for Lyapunov function). The situation is more complicated when we consider larger networks. The driven synchronization shows the same trend i.e. cancellation of the coupling terms in the dynamics of the difference variables and as well as in the expression for Lyapunov function (Eq. (4.61)). On the other hand, Eq. (4.32) for Lyapunov function for the globally coupled maps shows that the direct coupling term, between the two nodes under consideration, adds an extra term in the difference variable while the coupling terms to other variables cancel out.

#### 4.5 Coupled Maps on Multipartite Networks

In this section we study the coupled maps on the multipartite networks. It is just an extension of the study of the coupled maps on bipartite networks.



set	Eigenvectors	Eigenvalue	No of Eigenvalues	Condition
$A_1$	$(\alpha_1 \dots \alpha_{N_1}, 0 \dots 0, \dots, 0 \dots 0)$	$(1 - \epsilon)f'_1$	$N_1 - 1$	$\Sigma\alpha = 0$
$A_2$	$(0 \dots 0, \beta_1 \dots \beta_{N_2}, \dots, 0 \dots 0)$	$(1 - \epsilon)f'_2$	$N_2 - 1$	$\Sigma\beta = 0$
$\vdots$	$\vdots \dots \vdots$	$\vdots$	$\vdots$	$\vdots$
$A_n$	$(0 \dots 0 \dots 0 \dots 0, \eta_1 \dots \eta_{N_n})$	$(1 - \epsilon)f'_n$	$N_n - 1$	$\Sigma\eta = 0$
$A_{n+1}$	$(\alpha, \dots \alpha, \beta, \dots \beta, \dots \eta \dots \eta)$	-	n	-

Here,  $(\alpha_1, \dots, \alpha_{N_1}), (\beta_1, \dots, \beta_{N_2}), \dots, (\eta_1, \dots, \eta_{N_n})$  and  $\alpha, \beta, \dots, \eta$  are complex numbers satisfying the conditions specified in the last column. The  $n$  eigenvalues corresponding to the set  $A_{m+1}$  are the eigenvalues of the matrix

$$\begin{pmatrix} (1 - \epsilon)f'_1 & \frac{N_2\epsilon}{N-N_1}g'_2 & \dots & \frac{N_n\epsilon}{N-N_1}g'_n \\ \frac{N_1\epsilon}{N-N_2}g'_1 & (1 - \epsilon)f'_2 & \dots & \frac{N_n\epsilon}{N-N_2}g'_n \\ \vdots & \vdots & \vdots & \vdots \\ \frac{N_1\epsilon}{N-N_n}g'_1 & \dots & \dots & (1 - \epsilon)f'_n \end{pmatrix} \quad (4.64)$$

where  $g'_1, g'_2, \dots, g'_n$  are the derivatives of  $f$  at  $X_1, X_2, \dots, X_n$  respectively.

The  $(n + 1)$  sets of eigenvectors follow the properties of eigenvectors for bipartite synchronized state given in section 4.3. Set  $A_{n+1}$  defines the synchronized manifold and other  $n$  sets of eigen vectors  $A_1 \dots A_n$  are transverse to the synchronized manifold. Lyapunov exponents corresponding to the transverse eigenvectors are,

$$\begin{aligned} \lambda_1 = \lambda_i &= \ln|(1 - \epsilon)| + \frac{1}{\tau} \lim_{\tau \rightarrow \infty} \sum_{t=1}^{\tau} \ln|f'(X_1)|, \text{ for } i = 1, N - 1 \\ \lambda_2 = \lambda_i &= \ln|(1 - \epsilon)| + \frac{1}{\tau} \lim_{\tau \rightarrow \infty} \sum_{t=1}^{\tau} \ln|f'(X_2)|, \text{ for } i = N_1, N_1 + N_2 - 2 \\ &\vdots \\ \lambda_n = \lambda_i &= \ln|(1 - \epsilon)| + \frac{1}{\tau} \lim_{\tau \rightarrow \infty} \sum_{t=1}^{\tau} \ln|f'(X_n)|, \text{ for } i = N - N_n - n, N - n \end{aligned} \quad (4.65)$$

where  $\lambda_1, \lambda_2, \dots, \lambda_n$  are respectively  $N_1 - 1, N_2 - 1, \dots, N_n - 1$  fold degenerate. The synchronized state is stable provided the transverse Lyapunov exponents are negative. If  $f'$  is bounded as is the case for the logistic map then from Eqs. (4.65) we see that for  $\epsilon$  larger

than some critical value,  $\epsilon_b (< 1)$ , multipartite synchronized state will be stable. This bipartite synchronized state will be stable even if one or all  $n$  remaining Lyapunov exponents corresponding to the set  $A_{m+1}$  are positive, i.e. the trajectories are chaotic.

We study different cases of synchronization, and for this we make one simplification in the structure of the multipartite network. We consider equal number of nodes in all the sets of the multipartite network, i.e.  $N_1 = N_2 = \dots = N_n$ . With this simplification we can write rest  $n$  Lyapunov exponents corresponding to the Jacobian ( Eq. (4.64) ) as,

$$\lambda_{N-n+1} = \lim_{\tau \rightarrow \infty} \frac{1}{\tau} \sum_{t=1}^{\tau} \ln |(1 - \epsilon)f'_t + \epsilon g'_t| \quad (4.66a)$$

$$\lambda_{N-n+2} = \lambda_{N-n+3} \dots = \lambda_N = \lim_{\tau \rightarrow \infty} \frac{1}{\tau} \sum_{t=1}^{\tau} \ln \left| (1 - \epsilon)f'_t - \frac{\epsilon}{n-1}g'_t \right| \quad (4.66b)$$

Coupling function  $g(x) = f(x)$ : The global synchronized state, where all the nodes are synchronized, has the following Lyapunov exponents,

$$\begin{aligned} \lambda_1 &= \lambda_\mu = \frac{1}{\tau} \lim_{\tau \rightarrow \infty} \sum_{t=1}^{\tau} \ln |f'(x_t)| \\ \lambda_2 &= \ln\left(1 - \frac{n}{n-1}\epsilon\right) + \lambda_\mu \\ \lambda_3 &= \dots = \lambda_N = \ln(1 - \epsilon) + \lambda_\mu \end{aligned}$$

where  $\lambda_2$  and  $\lambda_3$  are respectively  $n - 1$  fold degenerate and  $N - n$  fold degenerate. Both  $\lambda_2$  and  $\lambda_3$  are transverse Lyapunov exponents. Condition for stability can easily be calculated as,

$$1 - e^{-\lambda_\mu} < \epsilon < \frac{n-1}{n}(1 + e^{-\lambda_\mu}) \quad (4.68)$$

We see that this range depends on the number of sets in the multipartite networks, not on the total number of nodes in each set.

Coupling function  $g(x) = x$ : From the expressions in Eqs. (4.66), it is difficult to determine the stability of the global synchronous state or periodic driven state. We consider a special case when coupled dynamics of the fully synchronized state lies on the fixed point attractors. Using set of Eqs. (4.66) and (4.65) and for  $f' < 0$ , the stable range for fixed point attractor is easily found as,

$$\frac{|f'| - 1}{|f'| - \frac{1}{n-1}} < \epsilon < 1 \quad (4.69)$$

It is clear from above expression that the fully synchronous fixed point solution is stable only for  $n > 2$ . For bipartite network we did not observe this global fixed point state, instead coupled dynamics got settled on periodic driven state for large coupling strength region.

## 4.6 Floating nodes

As discussed in the Chapter II, the nodes of a network can be divided into three types based on their asymptotic dynamical behavior, namely (a) cluster nodes: These nodes remain in a synchronized cluster for all the time, (b) isolated nodes: these nodes do not belong to a synchronized cluster at any time and (c) floating nodes: these nodes show an intermittent behavior between evolution synchronized with some cluster and isolated evolution. Here we try to analyze the reasons for the occurrence of floating nodes. Consider a floating node of degree  $k$  such that there are  $k_1$  connections to nodes belonging to the cluster and  $k_2 = k - k_1$  connections to nodes outside the cluster. Consider an evolution when the floating node is synchronized with the cluster. The dynamics of the floating node is given by

$$x_{t+1} = (1 - \epsilon)f(x_t) + \frac{\epsilon}{k} \left( k_1 g(x_t) + \sum_{i=1}^{k_2} g(x_t^i) \right). \quad (4.70)$$

Assume that the other nodes of the cluster remain in the synchronized state. Hence small deviation  $\delta x_t$  of the floating node evolves as

$$\delta x_{t+1} = (1 - \epsilon)f'(x_t)\delta x_t + \frac{\epsilon}{k} \sum_{i=1}^{k_2} g'(x_t^i)\delta x_t^i. \quad (4.71)$$

Since other nodes in the cluster remain in the synchronized state, we expect that on the average  $|(1 - \epsilon)f'(x_t)| < 1$  (see the expressions for the transverse Lyapunov exponents in Eq. (4.24b) for large  $N$  and Eq. (4.60)). Hence, the floating node can leave the cluster only if the magnitude of the second term in Eq. (4.71) is sufficiently large to overcome the first term. For this to happen, one or more of the following possibilities exist.

- (1)  $k_2$  is large.
- (2) These  $k_2$  nodes do not belong to a single synchronized cluster.
- (3) The  $k_2$  nodes evolve chaotically.

The numerical observation of the floating nodes supports these observations. We note

that the floating nodes are observed in the partially ordered region (region III in Figs. 3.8 and 3.9 of the previous chapter) where the evolution is chaotic. There are several clusters and isolated nodes. The floating nodes in general have some connections to other isolated or floating nodes. Though this simple argument is not sufficient for identifying the exact nodes which show floating behavior, it does give us some understanding of why and when a node can be a floating node.

## 4.7 Summary

We study self-organized and driven synchronization in coupled map networks using some simple networks, namely two and three nodes networks and their natural generalization to globally coupled and bipartite networks respectively. For this study we use both linear stability analysis and Lyapunov function approach and find out the different region for which synchronized states are stable.

For the globally coupled network we analyze the global synchronized state while for the complete bipartite network we analyze the bipartite synchronized state. We also consider fixed point and period two synchronized states. The linear stability analysis for different states gives different regions in the phase diagram, plotted in the  $\mu - \epsilon$  space. Synchronized states lie on different periodic or chaotic attractor depending on the coupling functions, coupling strength and underlying topology of the network. We see that most of the features of coupled dynamics of small networks with two or three nodes, are carried over to the larger networks of the same type. We also find that the phase diagrams for simple networks studied here in this chapter have features very similar to the different kinds of networks studied in the previous chapter.

From the Lyapunov function approach we see that for the difference variable for any two nodes, that are in driven synchronization, all the coupling terms cancel out whereas when they are in self-organized synchronization though coupling terms for couplings to other nodes may cancel, the coupling terms corresponding to the direct coupling, between the two nodes under consideration, do not cancel. We also make a simple analysis of the dynamics of a floating node and it gives us an understanding of the conditions for the occurrence of the floating nodes.

We also study the coupled dynamics on multipartite networks. It is an extension of work

done for the coupled dynamics on bipartite networks. We perform linear stability analysis for the stability of different synchronized states. Though it is difficult to get the exact analytical range for  $n$ -partite driven synchronized state but we see in section 4.4.2 that  $n$  ideal driven synchronized state exists. Lyapunov function analysis for two nodes, in the driven synchronization, remains same for complete bipartite and complete multipartite networks.

The analysis presented in this chapter is for exact synchronization while previous chapter (Chapter III) considers phase synchronized clusters. However, we feel that the dynamical origin for the two mechanisms of cluster formation should be similar in both cases. This is supported by the very similar features of plots of phase space, largest Lyapunov exponent,  $f_{inter}$  and  $f_{intra}$  for the three nodes and complete bipartite networks and the corresponding plots for several networks considered in the previous chapter.

## Chapter 5

# Conclusions and Future Outlook

---

---

In conclusion, this thesis reports the different mechanisms of synchronization and cluster formation in coupled dynamics on the networks. We find that as dynamics evolves with time, after some critical coupling strength dynamical elements coupled via the links of the network, form synchronized clusters. Arrangement of the nodes in the synchronized clusters are of the two different types, based on the connections among them in the network. We study the mechanism of cluster formation as well as the behaviour of the individual nodes, both forming clusters and evolving independently. Our new findings are presented with extensive numerical results which are further supported by the physical explanations and analytical solutions. Following I present the brief summary of all the chapters and the future outlook.

In the temporal evolution of coupled maps on networks, we identify two different ways of cluster formation, self-organized synchronization which leads to the clusters with dominant intra-cluster couplings and driven synchronization which leads to the clusters with dominant inter-cluster couplings. We define different states of coupled dynamics as, turbulent state, partially ordered, ordered and coherent states depending on the number of clusters and the number of nodes forming clusters. We make extensive studies for the phase-diagram in the  $\mu - \epsilon$  plane, for the local dynamics governed by the *logistic map*.

We study the stability of self-organized and driven synchronization in some simple networks using both linear stability analysis and Lyapunov function approach. Linear stability analysis shows that self-organized and driven synchronization is stable with periodic, quasiperiodic and chaotic solution depending on the local dynamics, coupling function, coupling strengths and topology of the networks. Lyapunov function analysis shows the origin for self-organized and driven synchronization in the globally coupled and com-

plete bipartite networks and we feel that similar mechanisms are valid for other random networks studied in the chapter 3.

Now I restate the main theme of my thesis and provide the outlook for the future problems. The main theme of my thesis lies in the fact that different chaotic dynamical elements, when connected with each other via the links of a network, form synchronized clusters, and there exists two different ways (mechanisms) of cluster formation depending on the nodes, which are directly connected and nodes which are not directly connected. The study of coupled maps in the light of our newly found mechanisms of synchronization raises many questions. Few questions are; How does the dynamics of coupled maps select a particular configuration of synchronized clusters? In the partially ordered region we find floating nodes, what role these floating nodes play in synchronizing and desynchronizing the other nodes connected with them? What role do the highly connected nodes play in cluster formation? How does the synchronization gets affected with coupling strength? By looking at the dynamics of one single nodes or few nodes of the network whether one can know the topology of the entire network? Apart from above queries to be investigated in future, there are several other extensions of this thesis work, a simple and important extension is, to study the synchronization properties of coupled oscillators on the various networks.

## Appendix

Here we show that the definition of phase distance  $d_{ij}$  between two nodes  $i$  and  $j$  satisfies metric properties. Let  $\mathcal{N}_i$  denote the set of minima of the variable  $x_t^i$  in a time interval  $T$ . The phase distance satisfies the following metric properties.

(A)  $d_{ij} = d_{ji}$ .

(B)  $d_{ij} \geq 0$  and the equality hold only if  $\mathcal{N}_i = \mathcal{N}_j$ .

(C) Triangle inequality: Consider three nodes  $i, j$  and  $k$ . Denoting the number of elements of a set by  $|\cdot|$ , let,

(1)  $a = |\mathcal{N}_i \cap \mathcal{N}_j \cap \mathcal{N}_k|$ .

(2)  $b = |\mathcal{N}_i \cap \mathcal{N}_k| - a$ .

(3)  $c = |\mathcal{N}_j \cap \mathcal{N}_k| - a$ .

(4)  $d = |\mathcal{N}_i \cap \mathcal{N}_j| - a$ .

(5)  $e = |\mathcal{N}_i| - b - d - a$ .

(6)  $f = |\mathcal{N}_j| - c - d - a$ .

(7)  $g = |\mathcal{N}_k| - b - c - a$ .

We have

$$n_{ik} = a + b$$

$$n_{jk} = a + c$$

$$n_{ij} = a + d$$

$$n_i = a + b + d + e$$

$$n_j = a + c + d + f$$

$$n_k = a + b + c + g$$

Consider the combination

$$d_{ik} + d_{jk} - d_{ij} = 1 - X \tag{1.1}$$

where

$$X = \frac{n_{ik}}{\max(n_i, n_k)} + \frac{n_{jk}}{\max(n_j, n_k)} - \frac{n_{ij}}{\max(n_i, n_j)}$$

The triangle inequality is proved if  $X \leq 1$ . Consider the following three general cases.

Case a.  $n_i \leq n_j \leq n_k$ :

$$\begin{aligned} X &= \frac{a+b}{n_k} + \frac{a+c}{n_k} - \frac{a+d}{n_j} \\ &\leq \frac{a+b+c-d}{n_k} \\ &\leq 1 \end{aligned} \tag{1.2}$$

Case b.  $n_i \leq n_k \leq n_j$ :

$$\begin{aligned} X &= \frac{a+b}{n_k} + \frac{a+c}{n_j} - \frac{a+d}{n_j} \\ &\leq \frac{a+b+c}{n_k} \\ &\leq 1 \end{aligned} \tag{1.3}$$

Case c.  $n_k \leq n_i \leq n_j$ :

$$\begin{aligned} X &= \frac{a+b}{n_i} + \frac{a+c}{n_j} - \frac{a+d}{n_j} \\ &\leq \frac{a+b+c}{n_i} \\ &\leq \frac{a+b+c}{n_k} \\ &\leq 1 \end{aligned} \tag{1.4}$$

This proves the triangle inequality.

## References

- [1] S. H. Strogatz, 'Exploring Complex Networks,' *Nature* **410**, 268 (2001) and references therein.
- [2] R. Albert and A. L. Barabási, 'Statistical Mechanics of Complex Networks,' *Rev. Mod. Phys.* **74**, 47 (2002) and references therein.
- [3] Special issue on Networks, 26 September, *Science* **301**, (2003).
- [4] A. -L. Barabási, R. Albert, 'Emergence of Scaling in Random Networks,' *Science* **286**, 509 (1999).
- [5] D. J. Watts and S. H. Strogatz, 'Collective Dynamics of Small World Networks,' *Nature (London)* **393**, 440 (1998).
- [6] S. A. Pandit and R. E. Amritkar, 'Characterization and Control of Small-World Networks,' *Phys. Rev. E* **60**, R1119 (1999).
- [7] N. Mathias and V. Gopal, 'Small Worlds: How and Why,' *Phys. Rev. E* **63**, 021117 (2001).
- [8] N. Zekri and J. P. Clerc, 'Statistical and Dynamical Study of Disease Propagation in Small Worlds Network,' *Phys. Rev. E* **64**, 05611 (2001).
- [9] H. Hong, M. Y. Choi and B. J. Kim, 'Synchronization on Small-world Networks,' *Phys. Rev. E* **65** 026139 (2002)
- [10] Jonathan Ozik, Brian R. Hunt, and Edward Ott, 'Growing Networks with Geographical Attachment Preference: Emergence of Small Worlds,' *Phys. Rev. Lett.* **69**, 026108 (2004).
- [11] D. J. Watts, *Small worlds* (Princeton Univ. Press, Princeton, New Jersey, 1999).

- [12] R. Albert, H. Jeong, A. -L. Barabási, 'Internet: Diameter of the World-Wide-Web,' *Nature* **401**, 130 (1999).
- [13] R. Albert, H. Jeong, A. -L. Barabási, 'Error and Attack Tolerance of Complex Networks,' *Nature* **406**, 378 (2000).
- [14] A. -L. Barabasi, R. Albert, H. Jeong, 'A Mean Field Theorey for Scale-free Random Network,' *Physica A* **281**, 69 (2000).
- [15] M. Newman, 'The Power of Design,' *Nature* **405** 412 (2000).
- [16] R. M. May and A. L. Lloyd, 'Infection Dynamics on Scale-Free Networks' *Phys. Rev. E* **64**, 066112 (2001).
- [17] B. Bollobás and O. Riordan, 'Shortest Paths and Load Scaling in Scale-free Trees,' *Phys. Rev. E* **69**, 036114 (2004).
- [18] Y. Kuramoto, *Chemical Oscillations, Waves, and Turbulence* (Springer-Verlag, Berlin, 1984).
- [19] A. Pikovsky, M. Rosenblum and J. Kurth, *Synchronization : A Universal Concept in Nonlinear Dynamics* (Cambridge University Press, 2001).
- [20] S. Boccaletti, J. Kurths, G. Osipov, D.L. Valladares and C. S. Zhou, 'The Synchronization of Chaotic Systems,' *Physics Report* **366**, 1 (2002).
- [21] M. C. Cross and P. C. Hohenberg, 'Pattern Formation Outside of Equilibrium,' *Rev. Mod. Phys.* **65**, 851 (1993).
- [22] K. Kaneko, 'Overview of Coupled Map Lattices,' *Chaos* **2**, 279 (1992).
- [23] S. H. Strogatz, 'From Kuramota to Crawford: Exploring the Onset of Synchronization in Populations of Coupled Oscillators,' *Physica D* **143**, 1 (2000); and references therein.
- [24] B. Bollobás, *Random graphs*, (Cambridge University Press, Cambridge, 2001).
- [25] B. E. Warren, 'The Diffraction of X-Rays in Glass,' *Phys. Rev.* **45**, 657 (1934); M. Tarek and D. J. Tobias, 'Role of Protein-Water Hydrogen Bond Dynamics in the Protein Dynamical Transition,' *Phys. Rev. Lett.* **88**, 138101 (2002).

- [26] R. Ferrer i Cancho, C. Janssen and R. V. Solé, 'Topology of Technology Graphs: Small World Patterns in Electronic Circuit,' *Phys. Rev. E* **64**, 046119 (2001).
- [27] T.A. Vilgis, G. Heinrich, 'Dynamics of Heterogeneous Polymer Networks,' *Phys. Rev. E* **49**, 2167 (1994).
- [28] M.E.J. Newman, 'Percolation and Epidemics in a 2-Dimensional Small World,' *Phys. Rev. E* **65**, 021904 (2002).
- [29] C. Koch and G. Laurent, 'Complexity and the Nervous System,' *Science* **284**, 96 (1999).
- [30] H. Jeong, B. Tomber, R. Albert, Z. N. Oltvai, A. -L. Barabási, 'The Large-scale Organization of Metabolic Networks,' *Nature* **407**, 651 (2000).
- [31] A. Scala, L. A. N. Amaral and M. Barthélémy, 'Small-world Networks and the Conformation Space of a Short Lattice Polymer chain,' *Europhys. Lett.* **55**, 594 (2000).
- [32] Richard J. Williams, Nea D. Martinez, 'Simple Rules Yield Complex Food Webs,' *Nature* **404**, 180 (2000).
- [33] A. E. Motter and Y.-C. Lai, 'Cascade-based Attacks on Complex Networks,' *Phys. Rev. E* **66** 065102 (2002); R. Albert, I. Albert, and G. L. Nakarado, 'Structural Vulnerability of the North American Power Grid,' *Phys. Rev. E*, **69**, 025103 (2004).
- [34] S. Render, 'How Popular is your Paper ? An Empirical Study of Citation Distribution,' *Euro. Phys. J. B.* **4**, 131 (1998).
- [35] M. E. J. Newman, 'Scientific Collaboration Networks. I. Network Construction and Fundamental Results,' *Phys. Rev. E* **64** 016131 (2001).
- [36] S. Lawrence and C. Lee Giles, 'Searching the World Wide Web,' *Science* **280**, 98 (1998).
- [37] S. Wasserman and K. Faust, *Social Network Analysis*, (Cambridge Univ. Press, Cambridge 1994).
- [38] M. C. Conzález, A. O. Sousa and H. J. Hermann, 'Opinion Formation on a Deterministic Pseudo-fractal Network,' *arXiv: cond-mat/030753* (2003).

- [39] Anonymous, 'Media: Six Degrees from Hollywood,' *Newsweek* 11 October 1999, 6 (1999); B. Tjaden and G. Wasson (1997). Available on the internet at <http://www.cs.virginia.edu/oracle/>
- [40] R. P. Satorras and A. Vespignani, 'Epidemic Spreading in Scale-Free Networks,' *Phys. Rev. Lett.* **86**, 3200 (2001).
- [41] J. Abello, A. Buchsbaum and J. Westbrook, 'A Functional Approach to External Graph Algorithms,' *Lect. Notes Comput. Sci.* **1461**, 332 (1998).
- [42] A. E. Motter, A. P. S. de Moura, Y.-C. Lai, and P. Dasgupta, 'Topology of the Conceptual Network of Language,' *Phys. Rev. E* **65**, 065102 (2002).
- [43] P. Sen, S. Dasgupta, A. Chatterjee, P. A. Sreeram, G. Mukherjee and S. S. Manna, 'Small-world Properties of the Indian Railway Network,' *Phys. Rev. E* **67**, 036106 (2003).
- [44] W. Li and X. Cai, 'Statistical Analysis of a Airport Network of China,' *Phys. Rev. E* **69**, 046106 (2004).
- [45] P. Erdős, A. Rényi, *Publ. Math. Inst. Hungar. Acad. Sci.* **5**, 17 (1960).
- [46] S. Milgram, *Psychol. Today* **2**, 60 (1967).
- [47] C. Huygens, *Oeuvres Complètes de Christiaan Huygens*, Martinus Nijhoff, The Hague, 1888-1950.
- [48] L. Glass and M. C. Mackey, *From Clocks to Chaos : The Rhythms of Life* (Princeton Univ. Press, Princeton, 1988).
- [49] M. Bennelt, M. F. Schatz, H. Rockwood, K. Wiesenfeld, 'Huygens' Clocks,' *Proc. R. Soc. Lond. A* **458**, 563-579 (2002).
- [50] M. G. Rosenblum, A. S. Pikovsky, and J. Kurth, 'Phase Synchronization of Chaotic Oscillators,' *Phys. Rev. Lett.* **76**, 1804 (1996).
- [51] W. Wang, Z. Liu, Bambi Hu, 'Phase Order in Chaotic Maps and in Coupled Map Lattices,' *Phys. rev. Lett.* **84**, 2610 (2000).

- [52] S. C. Manrubia and A. S. Mikhailov, 'Globally coupled logistic maps as dynamical glasses,' *Europhys. Lett.* **53**, 451 (2001).
- [53] N. B. Janson, A. G. Balanov, V. S. Anishchenko and P. V. E. McClintock, 'Phase Synchronization between Several Interacting Processes from Univariate Data,' *Phys. Rev. Lett.* **86**, 1749 (2001).
- [54] H. L. Yang, 'Phase Synchronization of Diffusively Coupled Rössler Oscillators with Funnel Attractors,' *Phys. Rev. Lett.* **64**, 026206 (2001).
- [55] A. T. Winfree, *J. Theoret. Biol.* **16**, 15 (1967).
- [56] N. Nakagawa and Y. Kuramoto, 'Collective Chaos in Population of Globally Coupled Oscillators,' *Prog. Theor. Phys.* **89**, 313 (1983).
- [57] R. Kapral, 'Pattern Formation in Two-dimensional Arrays of Coupled, Discrete-time Oscillators,' *Phys. Rev. A* **31**, 3868
- [58] J. D. Crawford, 'Scaling and Singularities in the Entrainment of Globally Coupled Oscillators,' *Phys. Rev. Lett.*, **74**, 4341 (1995).
- [59] M. Timme, F. Wolf and T. Geisel, 'Coexistence of Regular and Irregular Dynamics in Complex Networks of Pulse-Coupled Oscillators,' *Phys. Rev. Lett.* **89**, 2587011 (2002).
- [60] A. Vilfan and T. Duke, 'Synchronization of active mechanical oscillators by an inertial load,' to be appeared in PRL.
- [61] J. Pantaleone, 'Stability of Incoherence in an Isotropic Gas of Oscillating Neutrons,' *Phys. Rev. D* **58**, 3002 (1998).
- [62] K. Wiesenfeld, P. Colet, S. H. Strogatz, 'Frequency Locking in Josephson Arrays: Connection with the Kuramoto model,' *Phys. Rev. E* **57**, 1563 (1998).
- [63] G. Kozyreff, A. G. Vladimirov and P. Mandal, 'Global coupling with time delay in an array of semiconductor lasers,' *Phys. Rev. Lett.* **85**, 3809 (2000).
- [64] P. A. Robinson, J. J. Wright and C. J. Rennie, 'Synchronous Oscillations in the Cerebral Cortex,' *Phys. Rev. Lett.* **57**, 4578, (1998).

- [65] C. S. Peskin, *Mathematical Aspects of Heart Physiology* (Courant Institute of Mathematical Science Publication, New York, 1975, pp. 268).
- [66] L. Glass, 'Synchronization and Rhythmic Processes in Physiology,' *Nature* **410**, 277 (2001).
- [67] J. Aldridge, E. K. Pye, 'Cell Density Dependence of Oscillatory Metabolism,' *Nature* **259**, 670 (1976).
- [68] J. Buck, E. Buck, *Scientific Am.* **234**, 74 (1996).
- [69] T. J. Walker, 'Acoustic Synchrony : Two Mechanisms in the Smowy Tree Cricket,' *Science* **166**, 891 (1969).
- [70] Z. Jiang, M. McCall, 'Numerical Simulation of a Large Number of Coupled Lasers,' *J. Opt. Soc. Am.* **10**, 155 (1993).
- [71] I. Farkas, D. Helbing and T. Vicsek, 'Social Behaviour : Mexican Wave in an Excitable Medium,' *Nature* **419** 131 (2002).
- [72] G. Benettin, L. Galgani and J. M. Strelcyn, 'Kolmogorov Entropy and Numerical Experiments,' *Phys. Rev. A*, **14**, 2338 (1976).
- [73] J. -P. Eckmann, D. Ruelle, 'Ergodic Theory of Chaos and Strange Attractors,' *Rev. Mod. Phys.* **57**, 617-656 (1985).
- [74] K. Kaneko and I. Tsuda, *Chap 4 of Complex Systems : Chaos and Beyond — A Constructive Approach with Application in Life Sciences*, (Springer, 2000).
- [75] Workshop on *Chaos and Complexity*, Torino, (World Scientific, 1987), edited by R. Livi et. all.
- [76] R. E. Devaney, *An Introduction to Chaotic Dynamical Systems* (Addison-Wesley Publishing Company, Inc., 1948)
- [77] A. J. Lichtenberg and M. A. Lieberman, *Regular and Chaotic Dynamics* (Springer-Verlag, 1983).
- [78] Michael Tabor, *Chaos and Integrability in Nonlinear Dynamics: An Introduction* (John Wiley & Sons, Inc., 1989).

- [79] E. Ott, *Chaos in Dynamical Systems* (Cambridge University Press, 1993).
- [80] R. C. Hilborn, *Chaos and Nonlinear Dynamics : An Introduction for Scientists and Engineers* (Oxford University Press, 1994).
- [81] D. L. Turcotte, *Fractals and Chaos in Geology and Geophysics* (Cambridge Univ. Press, Cambridge, 2nd edn, 1997).
- [82] S. A. Levin, B. T. Grenfell, A. Hastings, and A. S. Perelson, 'Mathematical and Computational Challenges in Population Biology and Ecosystems,' *Science* **275**, 334 (1997)
- [83] A. T. Winfree, *The Geometry of Biological Time* (Springer, New York, 1980).
- [84] J. -P. Eckmann, S. O. Kamphorst, D. Ruelle, S. Ciliberto, 'Liapunov Exponents From Time Series,' *Phys. Rev. A* **34**, 4971 (1986).
- [85] J. P. Gollub and H. L. Swinney, 'Many Routes to Turbulent Convection,' *J. Fluid Mech.* **100**, 449 (1980); A. Brandstater and H. L. Swinney, 'Strange Attractor in Weakly Turbulent Couette-Taylor Flow,' *Phys. Rev. A* **35**, 2207 (1987); K. R. Sreenivasan, 'Chaos in Open Flow Systems,' in *Dimensions and Entropies in Chaotic systems*, edited by G. Mayer-Kress (Springer-Verlag, New York, 1986).
- [86] Application of chaos to plasma as well as many other topics are dealt with in the book by R. Z. Sagdeev, D. A. Usikov and G. M. Zaslavsky, *Nonlinear Physics* (Harwood Academic Publishers, New York, 1990).
- [87] T. L. Carroll, L. M. Pecora and F. J. Rachford, 'Chaotic Transients and Multiple Attractors in Spin Wave Experiments,' *Phys. Rev. Lett.* **59**, 2891 (1987); W. L. Ditto, M. L. Spano, H. T. Savage, S. N. Rauseo and E. Ott, 'Experimental Observation of a Strange Nonchaotic Attractor,' *Phys. Rev. Lett.* **65**, 533 (1990).
- [88] P. S. Linsay, 'Period Doubling and Chaotic Behaviour in a Driven Anharmonic Oscillator,' *Phys. Rev. Lett.* **47**, 1349 (1981); R. W. Rollins and E. R. Hunt, 'Intermittent Transient Chaos at Interior Crises in the Diode Resonator,' *Phys. Rev. A* **29**, 3327 (1984).
- [89] F. T. Arecchi, R. Meucci, G. Puccioni and J. Tredicce, 'Experimental evidence of subharmonic bifurcations, multistability and turbulence in a Q-Switched Gas Laser,' *Phys. Rev. Lett.* **49**, 1217 (1982); J. Mork, J. Mark and B. Tromberg, 'Route to Chaos

- and Competition Between Relaxation Oscillations for a Semiconductor Laser with Optical Feedback,' *Phys. Rev. Lett.* **65**, 1999 (1990).
- [90] F. C. Moon, *Chaotic Vibrations* (John Wiley, New York, 1987).
- [91] O. E. RöSSLer, 'An Equation for Continuous Chaos,' *Phys. Lett. A* **57**, 397 (1976); R. H. Simoyi, A. Wolf and H. L. Swinney, 'One dimensional dynamics in a multicomponent chemical reaction,' *Phys. Rev. Lett.* **49**, 245 (1982).
- [92] W. Lauterborn, 'Subharmonic Route to Chaos in Acoustics,' *Phys. Rev. Lett.* **47**, 1445 (1981).
- [93] J. M. Petit and M. Hénon, 'Satellite Encounter,' *Icarus* **60**, 536 (1986); J. Wisdom, 'Rotational Dynamics of Irregularly Shaped Natural Satellites,' *Astron. J.* **94**, 1350 (1987).
- [94] *Exploring Chaos* (N. Hall, Ed. p. 96, Norton, New York, 1993); E. Lorenz, *Global Analysis* (J. Marsden, Ed., p.55, Springer, New York, 1979); First publication: E. Lorenz, *J. Atmospheric Science* **20**, 130, (1963).
- [95] R. M. May, 'Simple Mathematical Model With Very Complicated Dynamics,' *Nature* **261**, 459 (1976).
- [96] K. Kaneko, 'Transition from Torus to Chaos..,' *Prog. Theo. Phys.* **69**, 1427 (1983).
- [97] H. Fujisaka and T. Yamada, 'Stability Theory of Synchronized Motion in Coupled-Oscillator Systems,' *Prog. Theo. Phys.* **69**, 32 (1983).
- [98] H. Aref, *Ann. Rev. Fluid Mech.* **15**, 345 (1983).
- [99] G. Perez, C. Pando-Lambruschini, S. Sinha and H. A. Cerderia, 'Nonstatistical Behavior of Coupled Optical Systems,' *Phys. Rev. A* **45**, 5469 (1992).
- [100] E. A. Jackson and A. Kodogeorgiou, 'A Coupled Lorenz-Cell Model of Rayleigh-Bénard Turbulence,' *Phys. Lett. A* **168**, 270 (1992).
- [101] T. Yanagita and K. Kaneko, 'Coupled Map Lattice Model for Convection,' *Phys. Lett. A* **175**, 415 (1993).
- [102] C. Tsallis, A. M. C. de Souza and E. M. F. Curado, *Chaos, Solitons and Fractals* **6**, 561 (1995).

- [103] R. J. Hendry, J. M. McGlade and J. Weiner, *Ecological Modeling* **84**, 81 (1996).
- [104] S. Sinha and W. L. Ditto, 'Dynamics Based Computation,' *Phys. Rev. Lett.* **81**, 2156 (1998).
- [105] K. Aoki and N. Mugibayashi, 'Onset of Turbulent Pattern in a Coupled Map Lattice. Case for Soliton-like Behavior,' *Phys. Lett. A* **128**, 349 (1998).
- [106] F. A. Bignone, *Theor. Comp. Sci.* **217**, 157 (1999).
- [107] K. Kaneko, '....Spatial Intermittency in Coupled Logistic Lattice,' *Prog. Theo. Phys.* **72**, 480 (1984).
- [108] I. Waller and R. Kapral, 'Spatial and Temporal Structure in systems of coupled non-linear oscillations,' *Phys. Rev. A* **30**, 2047 (1984).
- [109] K. Kaneko, 'Lyapunov Analysis and Information Flow in Coupled Map Lattices,' *Physica D* **23**, 436 (1986).
- [110] K. Kaneko, 'Pattern Dynamics in Spatiotemporal Chaos : Pattern Selection, Diffusion of Defect and Pattern Competition Intermittency,' *Physica D* **34**, 1-41 (1989), and references therein.
- [111] K. Kaneko, 'Chaotic but Regular Posi-Nega Switch among Coded Attractors by Cluster-Size Variation,' *Phys. Rev. Lett.* **63**, 219 (1989).
- [112] K. Kaneko, 'Globally Coupled Chaos Violates the Law of Large Numbers but not the Central-Limit Theorem,' *Phys. Rev. Lett.* **65**, 1391 (1990).
- [113] K. Kaneko, 'Clustering, Coding, Switching, Hierarchical Ordering, and Control in a Network of Chaotic Elements,' *Physica D* **41**, 137-172 (1990).
- [114] K. Kaneko, 'On the Strength of Attractors in a High-dimensional System: Milnor Attractor Network, Robust Global Attraction and Noise-induced Selection,' *Physica D* **124**, 322 (1998).
- [115] D. H. Zanette and A. S. Mikhailov, 'Condensation in Globally Coupled Populations of Chaotic Dynamical Systems,' *Phys. Rev. E* **57**, 276 (1998).

- [116] N. J. Balmforth, A. Jacobson and A. Provenzale, 'Synchronized Family Dynamics in Globally Coupled Maps,' *CHAOS*, **9**, 738 (1999).
- [117] Y. Zhang, G. Hu, H. A. Cerdeira, S. Chen, T. Braun and Y. Yao, 'Partial Synchronization and Spontaneous Spatial Ordering in Coupled Chaotic Systems,' *Phys. Rev. E* **63**, 026211 (2001).
- [118] O. Popovych, Y. Maistenko and E. Mosekilde, 'Role of Asymmetric Clusters in Desynchronization of Coherent Motion,' *Phys. Lett. A* **302**, 171 (2002).
- [119] G. I. Menon, S. Sinha, P. Ray, 'Persistence at the Onset of Spatio-Temporal Intermittency in Coupled Map Lattices,' *Europhy. Let.* **61**, 27 (2003).
- [120] O. Popovych, A. Pikovsky and Y. Maistrenko, 'Cluster-splitting Bifurcation in a System of Coupled Maps,' *Physica D* **168**, 106 (2002).
- [121] G. Abramson and D. H. Zanette, 'Globally Coupled Maps with Asynchronous Updating,' *Phys. Rev. E* **58**, 4454 (1998).
- [122] Q. Zhilin and G. Hu, 'Spatiotemporally Periodic States, Periodic Windows, and Intermittency in Coupled Map Lattice,' *Phys. Rev. E* **49**, 1099 (1994).
- [123] M. Ding and W. Yang, 'Stability of Synchronous Chaos and on-off Intermittency in Coupled Map Lattices,' *Phys. Rev. E* **56**, 4009 (1997).
- [124] M. Soins and S. Zhou, 'Stability and Transverse Manifolds of Periodic Points for Coupled Maps,' *Physica D* **165**, 12 (2002).
- [125] Y. Chen, G. Rangarajan and M. Ding, 'General Stability Analysis of Synchronized Dynamics in Coupled Systems,' *Phys. Rev. E* **67**, 026209 (2003).
- [126] L. A. Bunimovich and E. A. Carlen, 'On the Problem of Stability in Lattice Dynamical Systems,' *Journal of differential Equation* **123**, 213 (1995).
- [127] A. Lemâitre and H. Chate, 'Phase Ordering and Onset of Collective Behavior in Chaotic Coupled Map Lattices,' *Phys. Rev. Lett.* **82**, 1140 (1999).
- [128] R. E. Amritkar, P. M. Gade, A. D. Gangal and V. M. Nandkumaran , 'Stability of Periodic Orbits of Coupled Map

- [129] R. E. Amritkar, 'Structures in Coupled Map Lattices,' *Physica A* **224**, 382 (1996).
- [130] E. Olbrich, R. Hegger and H. Kantz, 'Local Estimates for Entropy Densities in Coupled Map Lattices,' *Phys. Rev. Lett.* **84**, 2132 (2000).
- [131] P. García, A. Parravano, M. G. Cosenza, J. Jiménez and A. Marciano, 'Coupled Map Networks as Communication Schemes,' *Phys. Rev. E* **65**, 045201 (2002).
- [132] L. Cisneros, J. Jiménez, M. G. Cosenza and A. Parravano, 'Information Transfer and Nontrivial Collective Behavior in Chaotic Coupled Map Networks,' *Phys. Rev. E* **65**, 045204 (2002).
- [133] N. B. Ouchi and K Kaneko, 'Coupled Maps with Local and Global Interactions,' *CHAOS* **10**, 359 (2000).
- [134] H. Chaté and P. Manneville, *Europhys. Lett.* **17**, 291 (1992); 'Collective Behaviors in Coupled Map Lattices with Local and Nonlocal Connections,' *Chaos* **2**, 307 (1992).
- [135] P. M. Gade, 'Synchronization of Oscillators with Random Nonlocal Connectivity,' *Phys. Rev. E* **54**, 64 (1996).
- [136] M. G. Cosenza and K. Tucci, 'Pattern Formation on Trees,' *Phys. Rev. E* **64**, 026208 (2001)
- [137] C. S. Manrubia and A. S. Mikhailov, 'Mutual Synchronization and Clustering in Randomly Coupled Chaotic Dynamical Networks,' *Phys. Rev. E* **60**, 1579 (1999).
- [138] Y Zhang, G. Hu, H. A. Cerderia, S. Chen, T. Barun and Y. Yao, 'Partial Synchronization and Spontaneous Spatial Ordering in Coupled Chaotic Systems,' *Phys. Rev. E* **63**, 63 (2001).
- [139] S. Sinha, 'Random Coupling of Chaotic Maps Leads to Spatiotemporal Synchronization,' *Phys. Rev. E* **66**, 016209 (2002).
- [140] P. M. Gade and H. A. Cerderia, R. Ramaswamy, 'Coupled Maps on Trees,' *Phys. Rev. E* **52**, 2478 (1995).
- [141] P. M. Gade and C.-K. Hu, 'Synchronous Chaos in Coupled Map Lattices with Small-world Interactions,' *Phys. Rev. E* **62**, 6409 (2000);

- [142] H. Hong, M. Y. Choi and B. J. Kim, 'Synchronization on Small-world Networks,' *Phys. Rev. E* **65**, 026139 (2002); 'Phase Ordering on Small-world Networks with Nearest-neighbor Edges,' *Phys. Rev. E* **65**, 047104 (2002).
- [143] T. Nishikawa, A. E. Motter, Y. C. Lai and F. C. Hoppensteadt, 'Heterogeneity in Oscillator Networks: Are Smaller Worlds Easier to Synchronize?,' *Phys. Rev. Lett.* **91**, 014101 (2003).
- [144] N. J. Balmforth, A. Provenzale and R. Sassi, 'A Hierarchy of Coupled Maps,' *Chaos* **12**, 719 (2002).
- [145] K. Tucci, M. G. Cosenza and O. Alvarez-Llamoza, 'Phase Separation in Coupled Chaotic Maps on Fractal Networks,' *Phys. Rev. E* **68**, 027202 (2003).
- [146] F. S. de San Roman, S. Boccaletti, D. Maza and H. Mancini, 'Weak Synchronization of Chaotic Coupled Map Lattices,' *Phys. Rev. Lett.* **81**, 3639 (1998).
- [147] S. C. Manrubia and A. S. Mikhailov, 'Very Long Transients in Globally Coupled Maps,' *Europhys. Lett.* **50**, 580 (2000).
- [148] S. Sinha, D. Biswas, M. Azam and S. V. Lawande, 'Local-to-global Coupling in Chaotic Maps,' *Phys. Rev. A* **46**, 6242 (1992).
- [149] V. Ahlers and A. Pikovsky, 'Critical Properties of the Synchronization Transition in Space-Time Chaos,' *Phys. Rev. Lett.* **88**, 254101 (2002).
- [150] S. E. de S. Pinto and R. L. Viana, 'Synchronization Plateaus in a Lattice of Coupled Sine-circle Maps,' *Phys. Rev. E* **61**, 5154 (2000).
- [151] Y. L. Maistrenko, V. L. Maistrenko, O. Popovych and E. Mosekilde, 'Desynchronization of Chaos in Coupled Logistic Maps,' *Phys. Rev. E* **60**, 2817 (1999).
- [152] S. Wiggins, *Introduction to Applied Nonlinear Dynamical Systems and Chaos* (Springer-Verlag, 1990).
- [153] R. He and P. G. Vaidya, 'Analysis and Synthesis of Synchronous Periodic and Chaotic Systems,' *Phys. Rev. A*, **46**, 7387 (1992); 'Implementation of Chaotic Cryptography with Chaotic Synchronization,' *Phys. Rev. E* **57**, 1532 (1998).

## List of Publications

### I. Papers in Journals and Books:

1. *Self-organized and driven phase synchronization in coupled maps*, S. Jalan and R. E. Amritkar, Phys. Rev. Lett. **90**, 014101 (2003).
2. *Self-organized and driven phase synchronization in coupled map networks*, R. E. Amritkar and Sarika Jalan, Physica A **321**, 220, (2003)
3. *Synchronized clusters in coupled map networks: Self-organized and driven synchronization*, Sarika Jalan and R. E. Amritkar, arXiv:nlin.CD/0307029 and references therein (communicated to PRE)
4. *Synchronized clusters in coupled map networks: Stability analysis* Sarika Jalan, R. E. Amritkar and C. K. Hu, arXiv:nlin.CD/0307037 (communicated to PRE)

### II. In Proceedings/Abstracts of International and National Conferences:

1. *Controlling Chaos and Its Applications*, S. Jalan and R. E. Amritkar, "Inter-disciplinary Workshop on Probability and Statistical Physics," held at S. N. Bose National Center for Basic Sciences, Kolkata, India 19-23 Feb., 2001.
2. *Self-organized and Driven behaviour in scale-free networks*, S. Jalan and R. E. Amritkar, "Joint International Workshop on Dynamics of Networks and Spatially Extended Systems," held at Saha Institute of Nuclear Physics, Kolkata, India, 21-23 Jan., 2002.
3. *Stability Analysis of S- and D-Synchronized Clusters in Coupled Map Networks*, S. Jalan and R. E. Amritkar, "First National Conference on Nonlinear Systems and Dynamics," held at Indian Institute of Technology, Kharagpur, India, 28-30 Jan, 2003.